Ultra-Narrow Laser Linewidth Measurement

Xiaopei Chen

Dissertation submitted to the Faculty of the
Virginia Polytechnic Institute and State University
in partial fulfillment of the requirements for the degree of

Doctor of Philosophy
in
Electrical Engineering

Dr. Anbo Wang, Chair
Dr. Ira Jacobs
Dr. Yong Xu
Dr. Gary Pickrell
Dr. Randy Heflin

July 06, 2006
Blacksburg, Virginia

Keywords: Ultra-narrow linewidth laser, heterodyne detection, Lorentzian linewidth

Ultra-Narrow Laser Linewidth Measurement

Xiaopei Chen

(ABSTRACT)

In this report, we give a deeper investigation of the loss-compensated recirculating delayed self-heterodyne interferometer (LC-RDSHI) for ultra-narrow linewidth measurement, including the theoretical analysis, experimental implementation, further modification on the system and more applications.

Recently, less than 1kHz linewidth fiber lasers have been commercialized. But even the manufacturers face a challenge on accurately measuring the linewidth of such lasers. There is a need to develop more accurate methods to characterize ultra-narrow laser linewidth and frequency noises.

Compared with other currently available linewidth measurement techniques, the loss-compensated recirculating delayed-heterodyne interferometer (LC-RDSHI) technique is the most promising one. It overcomes the bottle-neck of the high resolution requirement on the delayed self-heterodyne interferometer (DSHI) by using a short length of fiber delay line. This method does not need another narrower and more stable laser as the reference which is the necessary component in heterodyne detection. The laser spectral lineshape can be observed directly instead of complicated interpretation in frequency discriminator techniques.

The theoretical analysis of a LC-RDSHI gives us a guidance on choosing the optimal parameters of the system and assists us to interpret the recorded spectral lineshape. Laser linewidth as narrow as 700Hz has been proved to be measurable by using the LC-RDSHI method.

The non-linear curve fitting of Voigt lineshape to separate Lorentzian and Gaussian components was investigated. Voigt curve fitting results give us a clear view on laser frequency noises and laser linewidth nature. It is also shown that for a ultra-narrow linewidth laser, simply taking 20dB down from the maximum value of the beat spectrum and dividing by $2\sqrt{99}$ will over estimate the laser linewidth and coherent length.

Besides laser linewidth measurement in the frequency domain, we also implemented time-domain frequency noise measurement by using a LC-RDSHI. The long fiber delay obtained by a fiber recirculating loop provides a higher resolution of frequency noise measurement.

However, spectral width broadening due to fiber nonlinearity, environmental perturbations and laser intrinsic 1/f frequency noises are still potential problems in the LC-RDSHI method. A new method by adding a transmitter switch and a loop switch is proposed to minimize the Kerr effect caused by multiple recirculation.

Acknowledgments

I would like to take this chance to express my sincere appreciations to people who offered me tremendous help and support in the past several years, especially, my adviser, Professor Anbo Wang. He provided me a great opportunity to do the research in an excellent group and he gave me a large space to think freely on each project. He always encouraged me and gave me suggestions and guidance. I was benefited from his advises before and I will be benefited in the future.

My thanks also go to all my colleagues and friends at Center for Photonics Technologies (CPT) for their kindness and help. Special thanks is given to Dr. Ming Han who provided a very good theoretical foundation for this project.

I also appreciate the advice of the committee members: Professor Ira Jacobs, Professor Yong Xu, Professor Gary Pickrell, and Professor Randy Heflin for their supports and for a good discussion with Professor Yong Xu about this project.

Contents

List of Figures

List of Tables

Chapter 1

Introduction

Lasers are unique sources of light and come in a variety of forms. The inside processes are greatly different from one type to another. But common features of lasers are the same. They have a pump source to provide energy to the laser system; they have an active medium to establish population inversion and transfer external energy into the laser beam; they possess an optical resonator (cavity) to introduce feedback. The properties of laser light can therefore be characterized by an extremely high degree of monochromaticity, coherence, directionality, brightness and short duration for some lasers[6].

Various types of lasers provide a wide range of physical and operating parameters[6]. The active medium of the lasers can be solid state, gas or semiconductor materials. The radiation wavelength of lasers can be varied from infrared, visible, ultraviolet (UV) to x-ray. The output waveform of lasers can be continuous-wave (CW) or femto-second pulses. The output power of the lasers can cover a range from a few milliwatts to several megawatts. The spectral bandwidth (linewidth) of lasers can be as broad as several hundreds of gigahertz and down to as narrow as several hundreds of hertz. This wide range of parameters offers enormous potential in fields of engineering, applied science and pure scientific research.

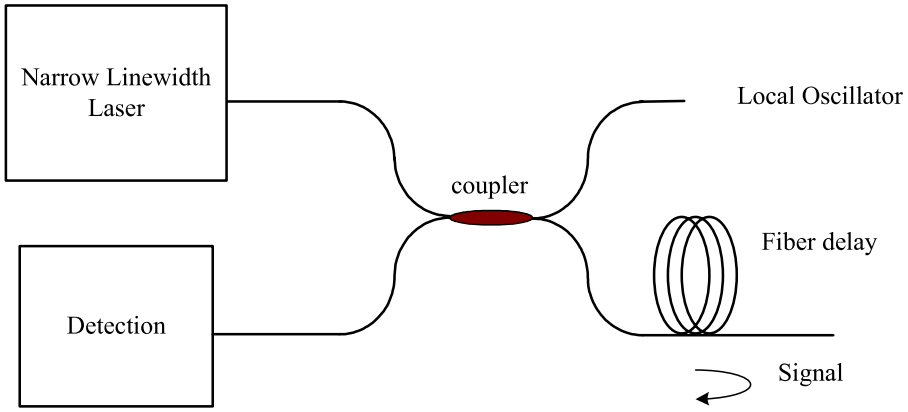

Figure 1.1: Schematic of FMCW technique[1]

Among all these different lasers, lasers with an ultra-long coherent length, or exceptionally low phase noise, have become a strong interest. Fiber optic sensing systems can take the advantage of the long coherent length to realize long distance coherent detection. Such long distance coherent detection techniques can be widely used for security or military, oil or gas wells, earthquake detection and high-voltage power lines.

One example of such coherent detection in fiber optic sensing systems is the frequency modulated continuous wave (FMCW) technique. In this technique, the light from laser source is modulated and is divided into two beams by a two by two coupler. One of the beams is reflected back and plays the role of the local oscillator (LO) in a heterodyne coherent detection scheme. The other beam propagates along a long sensing fiber and reflects back. It is mixed with the light from the LO generating a beat frequency, which is proportional to the difference in the time delay it experiences. This technique can detect return signals haveing power as small as 10^{-10} of the probe signals[1].

Fiber optic hydrophone sonar arrays based upon interferometric fiber optical sensors can also take the advantage of extremely low phase noise of the narrow linewidth laser. In such an interferometric fiber sensor system, frequency noise

can degrade the phase resolution, which determines the pressure resolution of hydrophones[1].

To meet these needs and to create new landscapes of laser applications, the development of lasers and laser systems with an extremely narrow linewidth accelerates very rapidly. Consequently, the needs to accurately measure their spectral linewidths and characterize frequency noises also arise. Unfortunately, currently available techniques for these measurements are either resolution limited or accuracy limited either because of the rather limited optical delay line involved or because of the lack of an analytical model for the thorough description of the laser linewidth as a function of key system parameters. As a result, today's manufactures of narrow line lasers can only provide estimated values of their laser linewidths. This situation suggests that methods that require only one laser and offer accurate measurement of extremely narrow laser linewidths be developed to meet not only today but also future needs.

This report presents a new theoretical analysis on a linewidth measurement technique- Loss Compensated Recirculating Delayed Self-heterodyne Interferometer (LC-RDSHI). Experiments are conducted to fully characterize the narrow linewidth lasers. The report is organized into following chapters:

Chapter 2 is a review of laser spectral width theory. Laser linewidth can be analyzed by either the phasor theory or the RCL circuit model in different conditions. In practice, laser linewidth is broader than the quantum limit linewidth. Thus, several linewidth enhancement factors are introduced.

Chapter 3 presents and compares the current linewidth measurement techniques, especially for narrow linewidth lasers. All the methods have their own advantages and disadvantages, but they seem difficult to fulfill the task to measure the laser linewidth as narrow as sub-kHz. Loss-compensated recirculating delayed self-heterodyne interferometer (LC-RDSHI), therefore, is proposed.

Chapter 4 presents the theoretical analysis of the LC-RDSHI system. The theories, related to power spectrum, amplitude fluctuations, polarization and frequency stability, offer guidance to the later experimental implementations. Also the analysis assists us to interpret the measurement results.

Chapter 5 describes the details of the experimental implementation of the laser linewidth measurement techniques.

Chapter 6 provides several methods to interpret the measurement results obtained from the LC-RDSHI. Not only the LC-RDSHI measures the linewidth in frequency domain, but also provides linewidth information in time domain.

Chapter 7 lists the existing problems in the experiment and a future work plan.

Chapter 2

Theory of Laser Linewidth

An ideal LASER (Light **A**mplication by **S**timulated **E**mission of **R**adiation) is an optical source that emits photons in a coherent, monochromatic and directional collimated beam. But in reality, due to quantum mechanical fluctuations, cavity length fluctuations, vibrational and temperature fluctuations, and other laser noises, the output of a laser is not perfectly monochromatic. Lasers have finite linewidths.

The linewidth of a single frequency laser is the full width at half maximum (FWHM) of the optical spectrum. For simple cases, the laser linewidth only arises from quantum fluctuations. The laser thus has the Schawlow-Townes linewidth. One of the causes of the quantum noise is spontaneous emission of excited atoms and ions. Compared with stimulated emission, the spontaneous photons have random directions and random phases. Each spontaneous emission event adds a random phase to the optical field. Some radiation caused by the spontaneous emission will propagate very nearly along the same direction as that of the stimulated emission and cannot be separated from it. The main consequence of the spontaneous emission noise is to make the laser output have a finite spectral width[7].

2.1 Schawlow-Townes linewidth

Even before the first laser was experimentally demonstrated, A. L. Schawlow and C. H. Townes calculated the fundamental (quantum) limit for the linewidth of a laser. This lead to the famous Schawlow-Townes formula and the spectral lineshape is Lorentzian:

$$\Delta\nu_{laser} = \pi h\nu(\Delta\nu_c)^2/P_{out}, \tag{2.1}$$

where $h\nu$ is the photon energy, $\Delta\nu_c$ is the cavity bandwidth (full width at half maximum), and P_{out} is the laser output power. The Schawlow-Townes linewidth is proportional to the square of the cavity bandwidth divided by the output power.

Another form of the equation is [8]

$$\Delta\omega_{ST} = \frac{P_2}{P_2 - P_1}\left[\frac{\bar{h}\omega}{P_{out}}\right]\gamma_c^2, \tag{2.2}$$

where P_2 and P_1 are the steady-state lower-level and upper-level population, respectively. $\gamma_c \equiv -(c/2d)\ln(R_1R_2)$ is the cavity power damping rate. c is light speed and d is the cavity length of the laser. R_1 and R_2 are mirror reflectivities.

In general, laser linewidth can be derived from both the phasor theory[9, 8, 10, 11, 12] and the RLC circuit model[7, 13, 14, 15].

2.1.1 Phasor theory

Phasor theory is used when the laser oscillates above its threshold. In this regime, the amplitude of the optical field is nearly fixed, but the phase may take any value. In the phasor theory, laser radiation is thought as a classical wave field described by a complex amplitude. Electric field of spontaneous and stimulated photons can be described by 'phasor' as shown in Figure 2.1[11]. The light generated through stimulated emission is in-phase with the intra cavity optical field and compensates for out coupling losses at the mirrors. The light generated through spontaneous emission has no phase relation with the intra cavity optical

field and disturbs both its amplitude and phase. In-phase spontaneous emission, in radial direction, leads to amplitude variations. These variations induce changes in the population inversion that bring the amplitude back to equilibrium. Out-of-phase events, in the tangential direction, are not corrected for and disturb the phase $\phi(t)$ of optical field. Theoretically, it is impossible to introduce "phase of one spontaneously emitted photon", but by adding many spontaneous emission events, we can form a combined electric-field vector with a well-defined (random) phase. The accumulated disturbances lead to a random walk of the phase[12]. The wandering of phase can be described as Brownian motion or phase diffusion. In this way, quantum problem can be transformed into a classical problem of calculating the statistical properties of a fluctuating wave field. The linewidth of the laser arises from a stochastic process in the laser's phase, which is assumed to obey a langevin equation[16]:

$$\frac{d^2\phi}{dt^2} + \beta\frac{d\phi}{dt} = \beta F(t), \tag{2.3}$$

where F(t) is a zero mean Gaussian white noise process so that

$$< F(t) >= 0, \tag{2.4}$$

$$< F(t_1)F(t_2) >= 2\Gamma\delta(t_1 - t_2), \tag{2.5}$$

where Γ is called the diffusion coefficient.

In the limit $\beta \to \infty$, a laser with field $E = E_0\cos(\omega t + \phi(t))$ has a Lorentzian bandwidth with full width half maximum of 2Γ.

$$\phi(t) = \int_0^t F(t)dt, \tag{2.6}$$

For the purpose of analysis and simulation, here we use a discrete time random walk (also called Wiener-Levy) process to represent the phase noise[17]:

$$\phi_n = \phi_{n-1} + \Delta\phi, \tag{2.7}$$

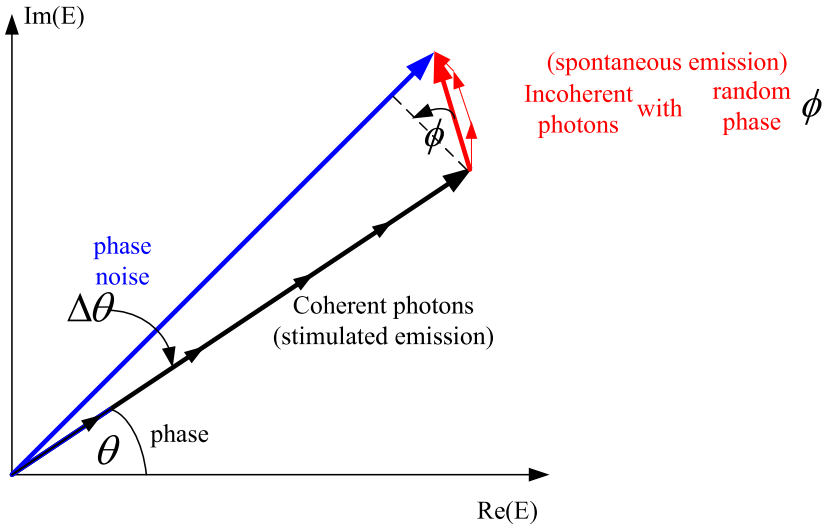

Figure 2.1: Phasor model

where Δn is referred as the step size of the walk and is a zero mean Gaussian random variable. And its variance equals to $\sigma_\Delta^2 = 2\pi t_s \Delta\nu$, where $t_s\Delta\nu$ is referred as the phase noise rate and t_s is the sampling time interval.

The simulation result is compared with a theoretical Lorentzian lineshape, shown in Figure 2.2. The blue thick curve is the simulation result and red curve is from the formula of Lorentzian lineshape with linewidth of 1kHz.

2.1.2 RLC circuit model

Phasor theory mainly deals with laser linewidth above the threshold of a laser oscillator. It explains the physical insight of spontaneous emission effects on the laser linewidth. But the spectral density of $\Delta\omega(t)$ obtained from the phasor theory is accurate for simple laser models at low frequencies[13]. But at high baseband frequencies agreement can only be reached if a phase-noise term is added *ad hoc* [14]. The phasor theory predicts rare but intense phase jumps for large photon lifetimes and large mean photon numbers. Because of this limitation and also for laser linewidth below the threshold, the RLC circuit model is thus used to derive

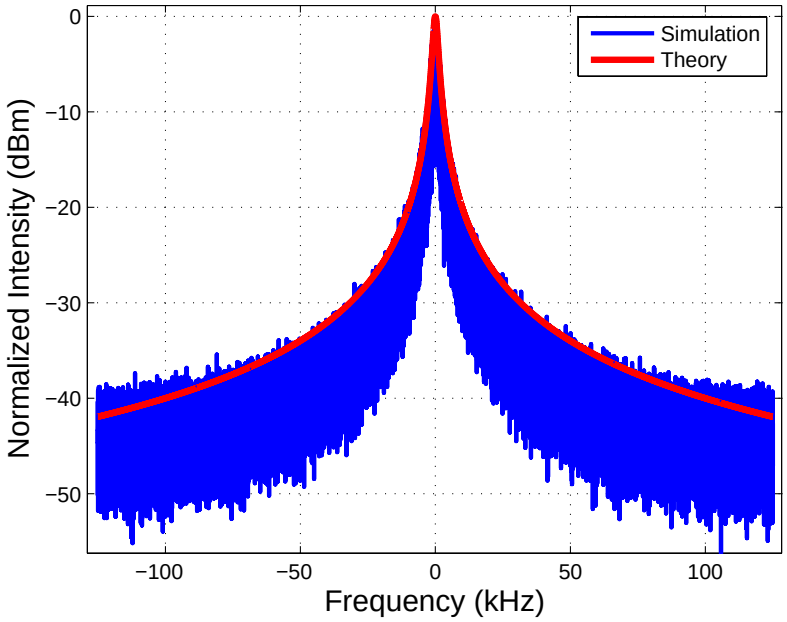

Figure 2.2: Simulation of Lorentzian Linewidth

the laser linewidth.

A *RLC* circuit, represents a laser oscillator is shown in Figure 2.3[13, 7, 15]. It consists of a single-mode cavity modeled by a parallel inductance-capacitance circuit containing non-interacting three-level atoms. The atoms may differ from each other by their transition frequencies, dipole strengths and relaxation times. Each atom is represented by a series of resistance-inductance-capacitance (RLC) circuits with a voltage noise source. The non-dispersive absorber is modeled by a current noise source[13]. For below-threshold light when the spontaneous emission is linearly amplified, the quantum limit laser spectral width in Equation (2.1) can be obtained from this circuit.

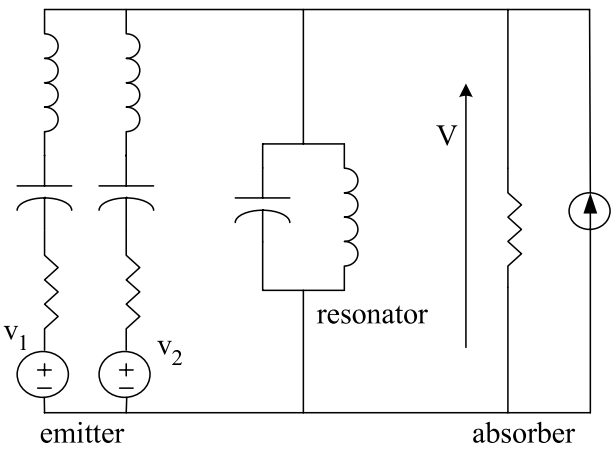

Figure 2.3: Schematic of the laser oscillator model led as RLC circuit

2.2 Beyond Schawlow-Townes linewidth

Laser linewidth is normally much larger than the Schawlow-Townes limit. The quantum limited linewidth can be only obtained when the output coupling is small (i.e.,laser mirror reflectivities near unity)[8, 10] so that the external vacuum field fluctuation coupled into the cavity is ignored; when the gain coefficient are approximately spatially uniform[8, 10]; when the active media are homogeneously broadened and when in the situation that the spontaneous emission is linearly-amplified (i.e.,below threshold light)[13, 8, 10].

The noise in the output of a laser will in many cases be well above the fundamental quantum noise limit, even if the laser is subject only to quantum noise. For example, intensity noise will always be above the shot noise level around the relaxation oscillation frequency[18].

2.2.1 K factor

Field noises in the laser cavity can be divided into vacuum field noise and source field noise. The atomic source noise within the cavity contributes mainly to Schawlow-Townes linewidth. The vacuum field noises are external noises entering the cavity from outside because of the

high output coupling. When laser mirror reflectivities are less than unity, the vacuum field leaks into the cavity and is amplified by the gain medium. The fundamental laser linewidth is attributable to both vacuum and source fields. This is not surprising in view of the fact that spontaneous emission itself may be regarded in part as stimulated emission due to the vacuum field[8].

In this situation, the laser linewidth may be expressed in the form[8]

$$\Delta\omega = K\Delta\omega_{ST}, \tag{2.8}$$

The K factor resulted from the amplification of vacuum field fluctuations entering from outside is an enhancement of spontaneous emission noise associated with an atom inside a gain medium. Therefore, it is usually referred to as the Petermann enhancement factor, or the "excess" spontaneous emission factor.

In the unsaturated regime, the K factor is given by [8]

$$K = \left[\frac{[(R_1)^{1/2} + (R_2)^{1/2}][1 - (R_1R_2)^{1/2}]}{(R_1R_2)^{1/2}\ln(R_1R_2)}\right]^2, \tag{2.9}$$

where R_1 and R_2 are mirror reflectivities. K is also called Petermann enhancement factor.

In the simplest possible terms we can conclude that the fundamental laser linewidth arises from spontaneous emission and the fluctuations of the vacuum field leaking into the laser cavity from the outside world. When there is large output coupling, and therefore high gain, the spontaneous emission generated both inside and outside of the cavity are amplified, and it is this amplification that is neglected in the standard theories and that gives rise to the K factor[8].

2.2.2 K' factor

When saturation and spatial-hole-burning effects are included, Equation(2.9) is no longer valid and the K factor will be modified. If we define the amplification of vacuum fluctuation

entering the cavity from outside as the "external" contribution(Γ_{ext}) then there is the "internal" contribution (Γ_{int}) due to atomic noise fields inside the cavity[8]. The "internal" contributions can be examined through three cases of interest:

(a) Exponential gain (linear) regime;

(b) Gain saturation regime-nonlinear regime;

(c) Gain saturation regime with interference between counter propagating intra cavity fields.

Considering both "internal" and "external" contributions, the laser linewidth, $\Delta\omega(d)$ obtained from the mirror at $z = d$, can be expressed by[8]

$$\Delta\omega(d) = \frac{1}{2}\left[\frac{c}{2d}\right]^2 \frac{\bar{h}\omega}{P_{out}(d)}\left[\Gamma_{ext} + \frac{1}{(P_2 - P_1)_t}\Gamma_{int}\right], \tag{2.10}$$

where P_1 and P_2 are the steady-state lower-level and upper-level population, respectively. $(P_2 - P_1)_t$ is the (z-independent) threshold population inversion.

It was shown in [8], that in linear regime, the internal and external contributions to the linewidth are exactly equal. The external contribution to the linewidth is unchanged regardless of how strongly the intra cavity field may saturate the gain, while the internal contribution will be modified by gain saturation. And the increase of internal contribution is more pronounced when the product of the reflectivities is small. Also, the saturated gain is modified when interference between the left- and right-propagating fields is properly taken into account. This interference produces spatial hole burning and a reduction in output power, therefore, increase the laser linewidth.

Based on these conclusions in [8], the modified K factor, K' can be expressed as:

$$K' = \frac{\Delta\omega}{\Delta\omega_{ST}} = \frac{\Gamma_{ext} + [1/(P_2 - P_1)^t]\Gamma_{int}}{2[P_2/(P_2 - P_1)]^t(\ln R_1 R_2)^2}, \tag{2.11}$$

or

$$\begin{aligned} K' &= \frac{1}{2}\left[(\Gamma_{int} + \Gamma_{ext}) + \left[\frac{P_1}{P_2}\right]_t (\Gamma_{int} - \Gamma_{ext})\right] \\ &\quad \times \frac{1}{(\ln R_1 R_2)^2}, \end{aligned} \tag{2.12}$$

2.2.3 α factor

In general, the laser linewidth is due to fluctuations in the phase of the optical field arising from spontaneous emission. However, spontaneous emission also induces intensity changes in the laser field. The restoration of the laser to its steady-state intensity results in changes in the imaginary part of the refractive index n'' and the real part of the refractive index n'. The ratio of these changes is

$$\alpha = \Delta n'/\Delta n'', \tag{2.13}$$

The change of $\Delta n'$ during a limited period of time broadens the laser linewidth by a factor of $(1+\alpha^2)$[9]. α is also called phase-amplitude coupling factor. The factor $(1+\alpha^2)$ is due to the increased phase changes brought by the intensity fluctuation suppression[9].

In the linear theory, amplitude and phase fluctuations each contribute half the linewidth. While above the threshold, the line broadening is primarily due to low frequency fluctuations. At low frequencies, the suppression of intensity fluctuations is extremely good[9]. Therefore, in the above threshold regime the stabilization of the amplitude eliminates the contribution from the amplitude fluctuations. The effect is to reduce the linewidth by a factor of $\frac{1}{2}$, with the phase fluctuations alone producing the linewidth[10]. Therefore the laser linewidth in the nonlinear above threshold regime becomes[10]:

$$\Delta\omega = \frac{(1+\alpha^2)}{2}\Delta\omega_{ST}, \tag{2.14}$$

which differs from the below threshold linewidth (Schawlow-Townes linewidth) by $(1+\alpha^2)/2$.

2.2.4 K'' factor

With increasing out coupling, the spatial variation in the intra cavity field has to be considered and we can no longer expect to obtain simply the $1+\alpha^2$ enhancement to the linewidth[10]. The laser linewidth should be modified by an additional factor $(1+\Omega^2)$ for a

detuned cavity:

$$\Delta\omega = K''\Delta\omega_{ST} = \frac{(1+\Omega^2)}{2}K'\Delta\omega_{ST}, \tag{2.15}$$

When $\Omega = 0$, K'' reduces to the linewidth enhancement factor K', due solely to "excess" spontaneous emission. In the linear approximation, K'' is simply K, the Petermann enhancement factor.

The linewidth enhancement factor K'', which multiplies the Schawlow-Townes linewidth, takes into account the effects of large output coupling, gain saturation, spatial hole burning and a correction to the $1+\alpha^2$ enhancement resulting from phase-amplitude coupling. As the value of α increases from zero, the linewidth is multiplied by the factor $1+\alpha^2$, and also by an enhancement factor that increases with increasing value of α[10]. Much of the increase in the enhancement factor is due to the effects of spatial hole burning, which are magnified at larger out coupling values[10].

2.2.5 Relaxation oscillation

Relaxation oscillations are small oscillations of the laser power and laser gain around their steady-state values. When a laser is disturbed during operation, e.g. by fluctuations of the pump power, both the phase and amplitude of the laser field undergo changes. The amplitude changes induce relaxation oscillations, which cause additional phase changes while restoring the field amplitude to the steady state value. It was previously shown that the additional phase change greatly enhance the linewidth. We show here that the additional phase changes also give rise to lineshape structure in the form of additional peaks separated from the main peak by multiples of the relaxation oscillation frequency[19].

The laser power spectrum can be calculated by finding the Fourier transform of the exponential of $-1/2 < \Delta\phi(t)^2 >$, the mean square phase change occurring during time t. In previous sections on laser linewidth, a simplifying assumption was made that the relaxation oscillations died out rapidly compared to the time interval contributing to the calculation

of the power spectrum. With this assumption, $< \Delta\phi(t)^2 >$ increases linearly in time and the line shape is Lorentzian. Without this approximation, $< \Delta\phi(t)^2 >$ exhibits damped oscillations which generate subsidiary peaks in the line shape when the power spectrum is calculated[19].

It is worth mentioning that such an oscillatory behavior is particularly pronounced for solid state lasers, where the relaxation oscillations are only weakly damped and have relatively low frequencies. On the other hand, semiconductor lasers exhibit strongly damped relaxation oscillations with rather high frequencies. For the fiber laser we are measuring, the relaxation oscillation frequency is at 800kHz. Therefore, when we transfer the beat-note frequency down to 1MHz by using the LC-RDSHI method, we can observe strong relaxation oscillation peaks in the power spectrum.

2.2.6 Inhomogeneous broadening

Laser linewidth can be broadened by both homogeneous and inhomogeneous broadening. A line-broadening mechanism is said to be inhomogeneous when it distributes the atomic resonance frequencies over some spectral range[18]. That means all atoms in an ensemble are perturbed by a different amount. Inhomogeneously broadened may be due to the Doppler effect in gas lasers, to the environment of rare-earth ions in glass-fiber lasers or to the presence of different isotopes[20].

Doppler broadening is one case of inhomogeneous broadening. Doppler broadening arises from atomic motion. The FWHM Gaussian linewidth for Doppler broadening is[18]

$$\Delta\nu = 2\nu_0\sqrt{\frac{2kT\ln 2}{Mc^2}}, \tag{2.16}$$

and the normalized lineshape can be:

$$g(\nu,\nu_0) = \frac{2}{\Delta\nu}sqrt\frac{\ln 2}{\pi}\exp[(-2(\nu-\nu_0)/\Delta\nu)^2\ln 2], \tag{2.17}$$

where M is particles mass at temperature T.

Environmental variations can also cause the inhomogeneous broadening. These environmental variations including composition or doping variation, variation of orientation with respect to the matrix, impurities and lattice imperfections. And lineshape is also Gaussian because of these variations.

When both homogeneous broadening and inhomogeneous broadening contribute to line broadening, the overall lineshape turns out to be Voigt which is the convolution of the Lorentzian and Gaussian.

Chapter 3

Linewidth Measurement Techniques

A fiber laser using trivalent rare earth as the active element has the potential for very narrow linewidth operation compared with other sources that oscillate in the same spectral regions (e.g., semiconductor lasers). First the wave guiding nature of a fiber allows the cavity length of a fiber laser to be many meters. The cavity linewidth scales inversely with the cavity length of the laser. Secondly, the coupling of amplified spontaneous emission to the oscillating mode is determined by the gain cross section of the transition. The cross section for most rare earth ions is of the order of $10^{-21}cm^2$, where for a semiconductor laser it is typically $10^{-6}cm^2$[21]. Thirdly, at least one fiber Bragg grating is usually used in a fiber laser. The reflection bandwidth of a fiber grating is typically well below 1 nm. Very narrow linewidths of a few kilohertz can be achieved[22].

Once the fiber laser output has been line-narrowed, the linewidth measurement becomes difficult. Typical grating-based optical spectrum analyzers (OSAs) do not offer the measurement resolution required for laser linewidth measurement. Scanning filter methods are not able to achieve the measurement resolution either. Therefore, heterodyne detection, frequency discriminator and self-heterodyne detection are possible techniques and are presented here for high resolution linewidth measurement.

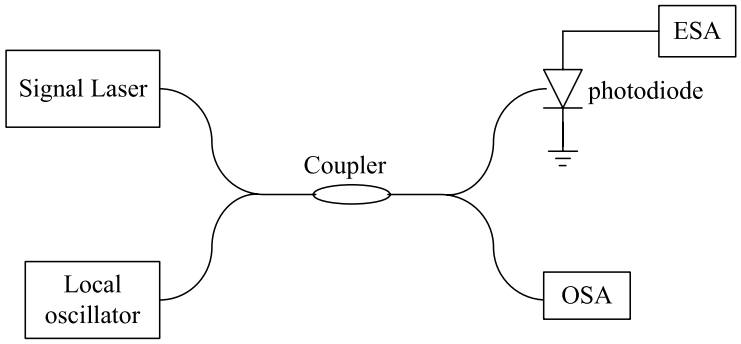

Figure 3.1: Schematic of the setup for optical heterodyne detection

3.1 Heterodyne Detection

Heterodyne detection can provide not only laser linewidth data, but also optical power spectrum. This method is the only technique that is capable of characterizing non symmetrical spectral lineshape. This method also offers high sensitivity and high resolution. The key component required for this method is a stable, narrow linewidth reference laser.

In heterodyne detection, two lasers have to be used. One is the signal laser, the other one is a reference laser and referred to as the local oscillator(LO). The central frequency of the LO laser must be tuned close to the signal laser frequency to allow the mixing product to fall within the bandwidth of typical detection electronics. In Figure 3.1, light from the LO is combined with the signal laser under test. The optical spectrum analyzer(OSA) can be used for course wavelength tuning. The coupler combines the two fields, delivering partial power to each output port. One port leads to a photodetector (PD) which detects the interference beat note, converting it to an electrical tone. The lower frequency term in the interference signal is described by:

$$i(t) = R[P_s(t) + P_{LO}(t) + 2\sqrt{P_s(t)P_{LO}(t)}\cos(2\pi(\nu_s - \nu_{LO})t + \Delta\phi(t))], \tag{3.1}$$

where $P_s(t)$ is the power of the laser under test, $P_{LO}(t)$ is the LO power, ν_s and ν_{LO} are the central frequencies of the laser under test and LO respectively, $\Delta\phi(t)$ is the instantaneous phase difference between the laser and LO, and R is the detector responsivity.

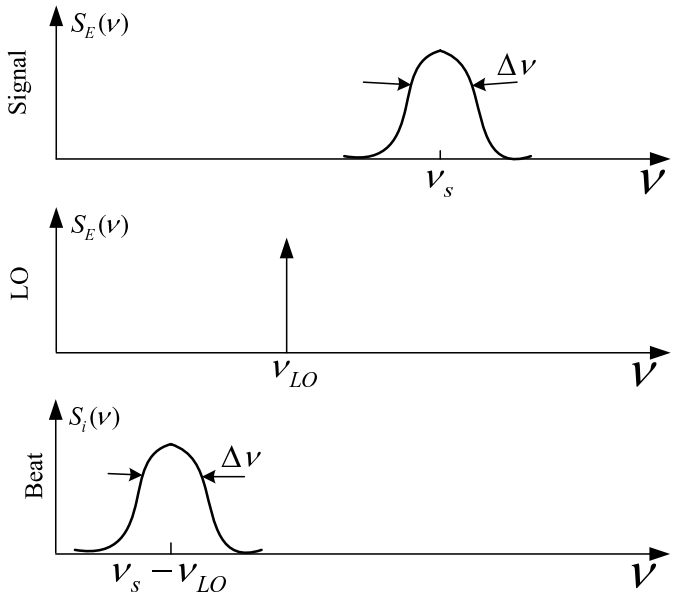

Figure 3.2: Convolution of narrow linewidth laser fof translation of signal spectrum to low frequencies

If the LO spectrum is much narrower than the signal laser linewidth, the spectrum of the LO can be treated as a δ function, as shown in Figure 3.2. Then the spectrum appears at the PD will be the same spectrum as that of the signal laser, but the central frequency is moved to a lower frequency.

The main difficulty to use heterodyne detection is that two lasers must be used. And the linewidth of the reference laser must be narrower than or at least comparable to that of the laser source to be measured in order to achieve reasonable measurement accuracy. For extremely narrow linewidth measurements, the characterization of the reference laser itself is very difficult. In addition, the limited bandwidth of the PD limits the measurement frequency range to at most tens of gigahertz vicinity of the reference laser central frequency, which greatly limits the applicability of this method to lasers with a wide range of different frequencies[5].

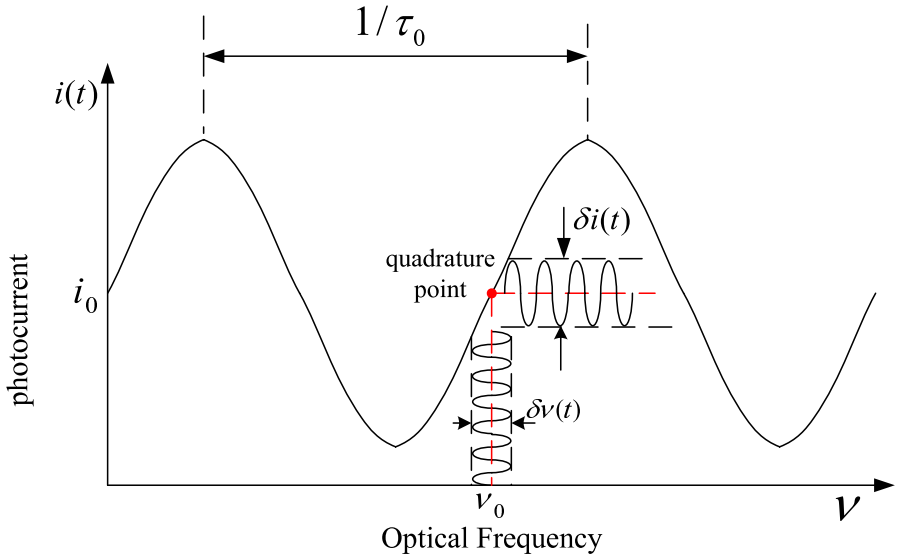

Figure 3.3: Optical frequency discriminator for linewidth measurement

3.2 Frequency Discriminator

Frequency discriminator is a direct measurement method to measure frequency noise. Frequency discriminators convert frequency fluctuation to intensity fluctuation, so that the frequency variations can be detected through the detection of the intensity variations. There are many interferometric configurations available to construct a discriminator, for example, a Michelson interferometer, a Mach-Zehnder interferometer or a Fabry-Perot interferometer in optical domain[23]. And electronic frequency discriminators in RF domain are also developed to improve the stability and resolution[24, 25].

In Figure 3.2, at the quadrature position, small current variations are linearly proportional to the optical frequency fluctuations. The variations on the laser frequency can be described by using the instantaneous frequency of the optical carrier as:

$$\nu(t) = \nu_0 + \delta\nu(t), \tag{3.2}$$

where ν_0 is the average optical frequency and $\delta\nu(t)$ describes the smaller frequency variations about the large average offset frequency. And the optical interference results in photo current

approximated by[5]

$$i(t) = i_0 + \Delta i \cos(2\pi\nu_0\tau_0 + 2\pi\delta\nu(t)\tau_0), \tag{3.3}$$

where τ_0 represents the differential time delay through the interferometer and Δi is equal to the maximum amplitude of the photo current variations due to optical interference. The discriminator slope then can be given as[5]:

$$\frac{\delta i}{\delta\nu} \approx 2\pi\tau_0\Delta i, \tag{3.4}$$

Equation (3.3) shows that we can get direct measurement of the optical frequency variations even though they are centered at several hundreds of teraherz. It also shows that only two experimental parameters are required to calibrate the FM discriminator.

In order to keep the phase variation small so that the approximation $\sin(\theta) \sim \theta$ is valid at the quadrature position, the optical frequency should not change much during the time delay τ_0. And this constraint can be stated mathematically as[5]

$$\Delta\phi(t) = 2\pi \int_t^{t+\tau_0} \delta\nu(t) \cong 2\pi\delta\nu(t)\tau_0 \ll 1, \tag{3.5}$$

Since the optical frequency variations for a cw laser tend to be somewhat random, it is convenient to measure the power spectral density (PSD), $S_\nu(f)$, of the optical frequency fluctuations. Using the linear relationship, the PSD of the measured photo current,$S_i(f)$, is related to the optical frequency variations by the relation

$$S_i(f) \cong (2\pi\tau_0\Delta i)^2 sinc(\tau_0 f) S_\nu(f), \tag{3.6}$$

which is valid for $2\pi\delta\nu(t)\tau_0 \ll 1$.

The fundamental laser linewidth can be determined from the PSD of the optical frequency. For a cw laser with a Lorentzian linewidth of $\Delta\nu$, the PSD of the optical frequency caused by the effects of spontaneous emission is given by[26]

$$S_\nu(f) = \frac{\Delta\nu}{\pi}, \tag{3.7}$$

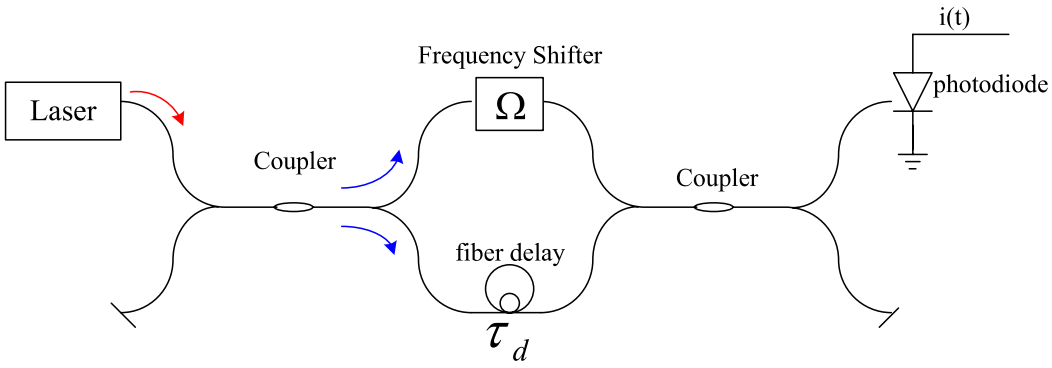

Figure 3.4: Schematic setup for optical delayed self-heterodyne detection

which states that the PSD is a constant, independent of frequency. For actual lasers experiencing external perturbations, this result will usually not be accurate at low frequencies. Depending on the specifics of the laser and the sensitivity of the measurement setup, it is often possible to find a frequency range where the flat spectral characteristics given by Equation (3.6) is valid.

The advantage of a frequency discriminator is that it can be used to measure extremely narrow laser linewidths and laser frequency jitter. But the frequency discriminator does not directly yield linewidth, therefore, interpretation of the data is more difficult. Also the frequency discriminator measurement is under the assumption that the laser runs cw, and its intensity will be constant and variations will occur only in its optical frequency or phase[5]. Usually, the experimental setup and calibration of a frequency discriminator is more complicated.

3.3 Delayed Self-heterodyne Detection

Compared with heterodyne detection, delayed self-heterodyne detection provides a simpler method to perform laser linewidth measurement without using a separate local oscillator. Instead, delayed self-heterodyne detection needs a large optical delay.

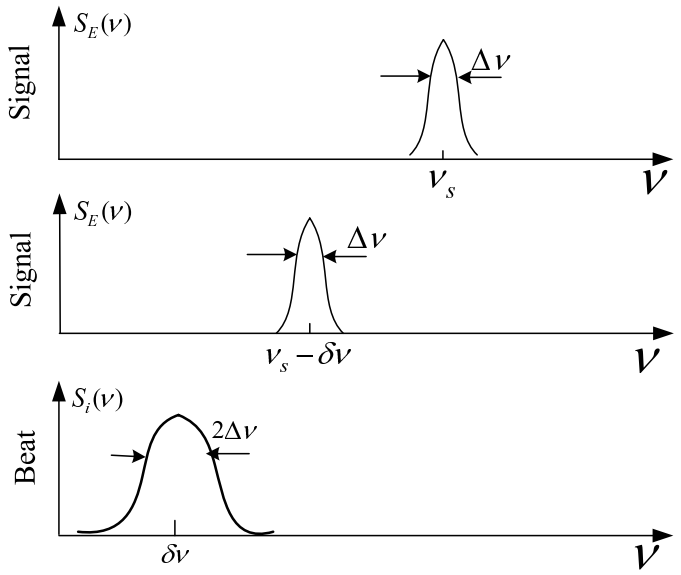

Figure 3.5: Delayed self-heterodyne mixing of the laser field

The delayed self-heterodyne interferometer (DSHI) concept is shown in Figure 3.4. Incident light is split into two paths by the interferometer. The optical frequency of one arm is offset with respect to the other. If the delay,τ_d, of one path exceeds the coherence time, τ_c of the source, the two combining beams interfere as if they originated from two independent lasers offset in frequency by $\delta\nu$. Thus the system performs similarly to optical heterodyne detection. The translation of linewidth information from optical frequencies to low frequencies where electronics instrumentation operates is shown in Figure 3.5.

3.3.1 Power Spectrum of DSHI

Theoretical analysis of the DSHI together with mathematical descriptions of the laser phase noise has been considered in [26, 27]. The analysis is simplified and more explicitly presented here by using the complex amplitude representation of a quasi-monochromatic wave[28]. The laser field is modeled as a sinusoidal wave with constant amplitude if the intensity noise is neglected.

$$E(t) = A\exp[j\phi(t)], \tag{3.8}$$

In Equation (3.8), the optical center angular frequency ω_0 has been ignored so $E(t)$ represents the complex amplitude of the laser field. From the Wiener-Khinchin theorem, the power spectral density can be obtained by the Fourier transform of the field autocorrelation function which is defined by

$$R_e(\tau) =< E(t)E(t-\tau)^* >= A^2 < \exp[j\Delta\phi(t,\tau)] >, \tag{3.9}$$

where $*$ denotes the complex conjugate, the angle brackets denote an ensemble average and

$$\Delta\phi(t,\tau) = \phi(t) - \phi(t-\tau), \tag{3.10}$$

is the phase jitter of the laser. Here we define the phase-noise spectrum S_ϕ is the power spectrum of the phase fluctuations and the frequency noise spectrum S_f is the power spectrum of the frequency fluctuations. The mean square phase fluctuations, $< \Delta\phi^2(t,\tau) >$ is related to the frequency noise spectrum by[26]

$$< \Delta\phi^2(t,\tau) >= \frac{2}{\pi}\int_{-\infty}^{\infty} \sin^2\left(\frac{\omega\tau}{2}\right) S_f(\omega)\frac{d\omega}{\omega^2}, \tag{3.11}$$

The line shape of most lasers has a Lorentzian profile. The corresponding frequency noise of such lasers has a constant spectral density (white noise) given by

$$S_f = S_0 = 2\pi\Delta\nu, \tag{3.12}$$

where $\Delta\nu$ is FWHM of the Lorentzian spectral line shape. Under these conditions, the phase jitter $\Delta\phi(t,\tau)$ is a zero-mean, stationary and Gaussian random process with variance

$$\left\langle \Delta\phi^2(t,\tau) \right\rangle = \left\langle \Delta\phi^2(\tau) \right\rangle = 2\pi\Delta\nu|\tau|, \tag{3.13}$$

Equation (3.13) is obtained by substituting Equation (3.12) into Equation (3.11). Using the well-known condition

$$< \exp[\pm j\Delta\phi(t,\tau)] >= \exp\left[- < \Delta\phi^2(t) > /2\right], \tag{3.14}$$

in Equation (3.13), and substituting Equation (3.13) into Equation (3.9), the Fourier transform of Equation (3.9) leads to the Lorentzian line shape of the laser

$$S_E(f) = 1/\left[(\Delta\nu/2)^2 + f^2\right], \tag{3.15}$$

where f is the frequency deviated from the optical center frequency. In a conventional DSHI as shown in Figure 3.4, the detected optical field is the sum of the laser beam and a time delayed and frequency shifted replica of itself

$$E_T(t) = E(t) + E(t - \tau_d)\exp(j\Omega t), \tag{3.16}$$

where τ_d and Ω are the time delay and angular frequency shift respectively. For simplicity, we have assumed the two beams have equal amplitudes. The photo current $I(t)$ is proportional to the optical intensity because of the square law of the photo detector (PD),

$$\begin{aligned} I(t) &\propto E_T(t)E_T^*(t) \\ &\propto 2 + \exp -j[\phi(t) - \phi(t - \tau_d)]\exp(j\Omega t) + c.c., \end{aligned} \tag{3.17}$$

where *c.c.* denotes the complex conjugate of the preceding term. In Equation (3.17) the constant coefficient related to the laser field intensity and the PD sensitivity has been ignored. The photo current contains a dc and a quasi-monochromatic signal centering at angular frequency Ω with a constant amplitude and random phase fluctuations equivalent to the laser field phase jitter. Here we are only interested in and consider the quasi-monochromatic term that contains the information of the laser phase noise. Similar to the case of the laser field, by ignoring the center angular frequency Ω, the complex amplitude of this term is given by

$$I_\Omega(t) = \exp -j[\phi(t) - \phi(t - \tau_d)], \tag{3.18}$$

The autocorrelation function of $I_\Omega(t)$ is thereby calculated by

$$\begin{aligned} R_\Omega(\tau) &= < I_\Omega(t)I_\Omega^*(t - \tau) > \\ &= < \exp -j[\phi(t) - \phi(t - \tau_d) - \phi(t - \tau) + \phi(t - \tau_d - \tau)] >, \end{aligned} \tag{3.19}$$

Using Equation (3.14) in Equation (3.19) and after some straightforward algebra, Equation (3.19) can be expressed as a function of phase jitter variance

$$R_\Omega(\tau) = \exp[B(\tau, \tau_d)], \tag{3.20}$$

where

$$B(\tau,\tau_d) = - < \Delta\phi^2(\tau_d) > - < \Delta\phi^2(\tau) > + \frac{1}{2} < \Delta\phi^2(\tau+\tau_d) > + \frac{1}{2} < \Delta\phi^2(\tau-\tau_d) >, \quad (3.21)$$

The spectrum of the corresponding photo current component is thus obtained by the Fourier transform of Equation(3.20)

$$S_0(\omega,\tau_d,\Omega) = F[R_\Omega(\tau)] = F\{\exp[B(\tau,\tau_d)]\}, \quad (3.22)$$

where F denotes the Fourier transform. In deriving Equation(3.22), the carrier angle frequency Ω has been implied, thus $\omega = 2\pi f$ is defined as the angular frequency deviated from the carrier angular frequency. For the Lorentzian spectral line shape of the laser, Equation (3.13) is satisfied and Equation(3.22) therefore leads to

$$\begin{aligned} S(\omega) &= \exp(-2\pi\Delta\nu\tau_d)\delta(f) + \frac{\delta\nu}{\delta\nu^2+f^2} \times \\ &\quad \{1 - \exp(-2\pi\Delta\nu\tau_d)[cos(2\pi f\tau_d) + \frac{\Delta\nu}{f} sin(2\pi f\tau_d)]\}, \end{aligned} \quad (3.23)$$

3.3.2 Linewidth interpretation

For the case of a Lorentzian-shaped laser field spectrum, the lineshapes retain their form during conversion from the optical spectrum to the electrical domain through the delay self-heterodyne process, except that the electrical lineshape has linewidth twice the actual optical linewidth. Let the laser lineshape be expressed as:

$$S_E(f) \sim \frac{1}{1+(\frac{f}{\Delta\nu/2})^2}, \quad (3.24)$$

It's autocorrelation is given by[29]

$$S(f) = S_E(f) \otimes S_E(f) \sim \frac{1}{1+(\frac{f}{\Delta\nu})^2} \quad (3.25)$$

The FWHM linewidth of $S(f)$ is twice as that of $S_E(f)$.

3.3.3 Effect of fiber delay in DSHI

From Figure 3.6, when τ/τ_c is below 1, the effects of phase between the two interfering waves becomes more significant and ripples appear in the spectrum. When τ/τ_c=1, the shape of the spectrum is approximately that of the original Lorentzian laser lineshape, but there is still small ripples appear, so a time delay of at least 5 times longer than the laser coherence time was suggested for a direct laser linewidth measurement from the spectrum.

In the delayed self-heterodyne detection, the delay line must be longer than the coherence length of the laser such that the beat signal is as if from two mutually incoherent sources. This technique is simple, inherently self-calibrated and capable of measuring a large range of laser frequencies where the fiber loss is tolerable. However, it is only suited for measurement of laser linewidths on the order of or above 10 kHz because otherwise the required fiber delay line would become impractically long. Compared with heterodyne detection, another advantage of the delayed self-heterodyne method is the auto wavelength tracing. Since the local oscillator signal in these measurements is provided by the laser under test, slow drift in wavelength is usually tolerable.

3.4 Loss-compensated Recirculating Delayed Self-heterodyne Detection

It is clearly shown that methods mentioned in the previous section do not allow accurate measurement of laser spectral linewidths below 1 kHz. We therefore use an improved DSHI in which a loss-compensated fiber recirculation loop is used as the delay line for ultra-narrow linewidth measurement. This method is called loss-compensated recirculating delayed self-heterodyne interferometer (LC-RDSHI). It was developed to improve the resolution of laser linewidth measurement by using a short fiber delay repeatedly.

In 1990, Hidemi Tsuchida[30] proposed the first recirculating delayed self-heterodyne con-

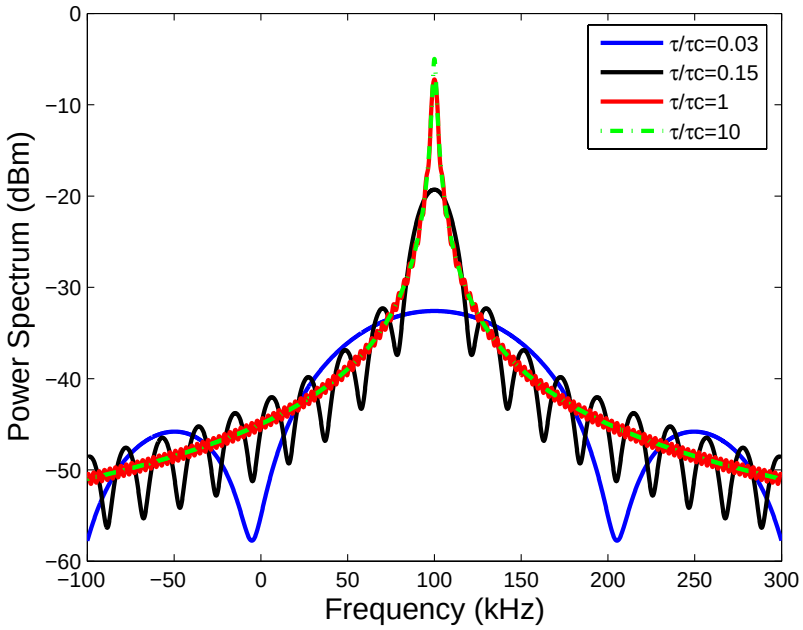

Figure 3.6: Power spectrum for various values of τ/τ_c

figuration for laser linewidth measurement, as shown in Figure 3.7. This method allows the same fiber delay to be used multiple times in order to further improve the resolution of conventional delayed self-heterodyne detection method. But the detectable highest-order beat signal is limited by the large transmission loss of the recirculating loop, especially by the insertion loss of the frequency shifter. Theoretical analysis can only give five orders of beat notes. That means the total fiber delay line is 20km if 4km fiber delay was used for each cycle.

In 1992, Jay W. Dawson, el.at. [31] reported the implementation of a loss-compensated recirculating delayed self-heterodyne detection by including an erbium-doped fiber amplifier (EDFA) in the loop. The schematic of a LC-DSHI is shown in Figure 3.8 in which a loss-compensated fiber loop is used as a fiber delay line. The fiber delay line contains a fiber coupler to couple the light into the loop, a span of single-mode fiber to provide the time delay to the field, an acousto-optic modulator (AOM) to introduce a frequency shift to the field and an erbium-doped fiber amplifier (EDFA) to partially compensate the loss of the

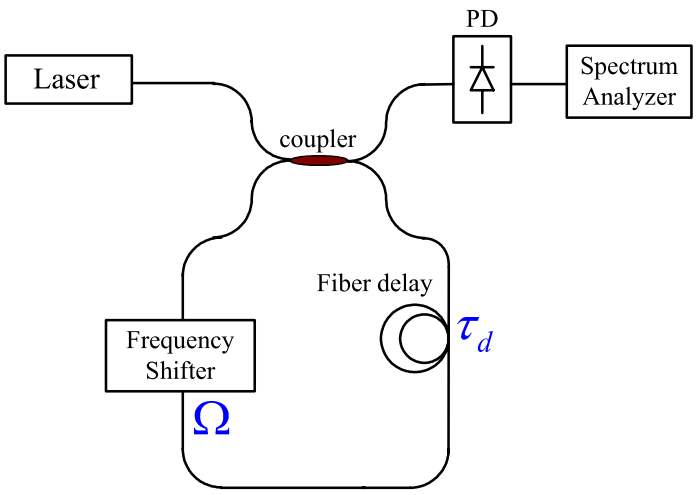

Figure 3.7: Schematic of recirculating delayed self-heterodyne interferometer

fiber span and other components involved in the loop. A fiber Raman amplifier can also be used if needed to replace the EDFA to significantly broaden the applicability of this method to a much broader spectral range. A practical fiber loop may also include a polarization controller which has been ignored here by assuming the field polarization is maintained during its propagation in the system. The maximum order of beat notes in[31] was increased to 30 with fiber delay of 11km.

Besides the linewidth measurement, we also perform the direct frequency noise measurement by using LC-RDSHI system. In the next chapter, we will further introduce this method by a theoretical analysis of the beat-note spectrum based on this method.

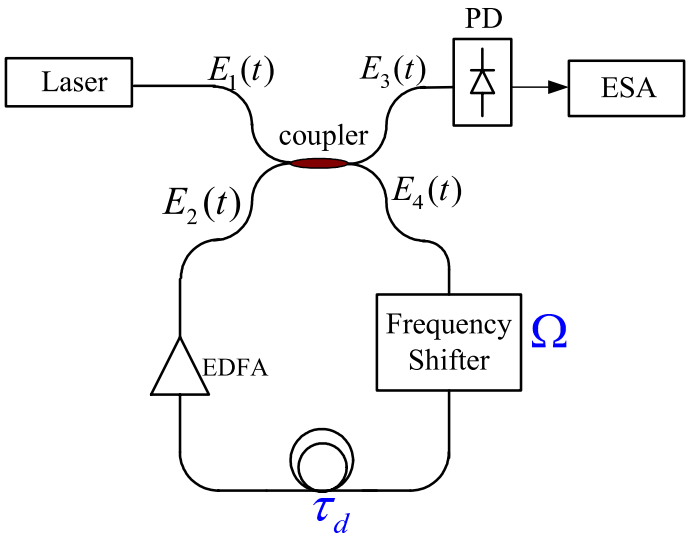

Figure 3.8: Schematic of loss-compensated recirculating delayed self-heterodyne interferometer

Chapter 4

Theoretical Analysis of LC-RDSHI

The theoretical analysis of LC-RDSHI was conducted based on the following assumptions:
1) The nonlinear effects are ignored;
2) ASE noise generated from the EDFA may accumulate as the light recirculate in the loop, but it has no effect on laser linewidth broadening;

4.1 Power Spectrum of LC-RDSHI

The spectrum from the LC-RDSHI can be analyzed with the equation that describes the relationship of the fields between the input and the output ports of the coupler, which is[28]:

$$\begin{bmatrix} E_3(t) \\ E_4(t) \end{bmatrix} = \begin{bmatrix} \sqrt{\alpha} & j\sqrt{1-\alpha} \\ j\sqrt{1-\alpha} & \sqrt{\alpha} \end{bmatrix} \begin{bmatrix} E_1(t) \\ E_2(t) \end{bmatrix} \tag{4.1}$$

where $E_1(t)$, $E_2(t)$, $E_3(t)$ and $E_4(t)$ are the optical fields at input ports 1 and 2 and output ports 3 and 4 of the coupler as shown in Figure 3.8. α is coupling coefficient of the coupler and α is a real number between 0 and 1. The laser output is directly connected to input port 1 of the coupler, therefore

$$E_1(t) = [A + \Delta A(t)]e^{j\phi(t)}, \tag{4.2}$$

Compared with Equation (3.8), $\Delta A(t)$ is added to represent the amplitude fluctuation. Part of the field output from the laser is coupled into the fiber loop by the coupler and recirculates inside the loop. Each pass of the loop introduces a time delay τ_d and an angular frequency shift Ω to the laser field.

When the recirculating number $n = 0$, the output field at four ports of the coupler are:

$$\begin{aligned} E_1(t) &= [A + \Delta A(t)]e^{j\phi(t)} \\ E_2(t) &= 0 \\ E_3(t) &= \sqrt{\alpha}E_1(t) \\ E_4(t) &= j\sqrt{1-\alpha}E_1(t), \end{aligned} \tag{4.3}$$

When the recirculating number $n = 1$, the output field at four ports of the coupler are:

$$\begin{aligned} E_1(t) &= [A + \Delta A(t)]e^{j\phi(t)} \\ E_2(t) &= \sqrt{\beta}E_4(1-\tau_d)e^{j\Omega t} = j\sqrt{1-\alpha}\sqrt{\beta}E_1(1-\tau_d) \\ E_3(t) &= \sqrt{\alpha}E_1(t) + j\sqrt{1-\alpha}E_2(t) \\ &= \sqrt{\alpha}E_1(t) + [j\sqrt{1-\alpha}]^2\sqrt{\beta}E_1(1-\tau_d)e^{j\Omega t} \\ E_4(t) &= j\sqrt{1-\alpha}E_1(t) + \sqrt{\alpha}E_2(t) \\ &= j\sqrt{1-\alpha}E_1(t) + j\sqrt{1-\alpha}\sqrt{\alpha}\sqrt{\beta}E_1(1-\tau_d)e^{j\Omega t}, \end{aligned} \tag{4.4}$$

The input signal field of PD after n passes of the loop can be given:

$$E_3(t) = \sqrt{\alpha}E_1(t) + C_0\sum_{n=0}^{\infty} C_n e^{j\Omega t}E_1(t - n\tau_d), \tag{4.5}$$

where[28]

$$\begin{aligned} C_0 &= \alpha/(\alpha - 1) \\ C_n &= \gamma^{n/2}\exp\{[\frac{n(n-1)}{2}]\Omega\tau_d\}, \quad n = 1, 2, \cdots \\ \gamma &= \alpha\beta, \end{aligned} \tag{4.6}$$

The first term in Equation (4.5) is the signal directly from the laser with $\sqrt{\alpha}$ attenuation. The second term is the sum of n components of $E_1(t-\tau_d)$, with each component having the amplitude modulated by $\sum_{n=0}^{\infty} C_n$, and frequency shifted by $n\Omega$. And $\sum_{n=0}^{\infty} C_n$ can be viewed as the result of interference of n multiple beams with amplitude attenuation $(\alpha/(\alpha-1))(\gamma^{n/2})$, and phase change $[\frac{n(n-1)}{2}]\Omega\tau_d$. The coefficient γ is the effective overall gain of the fiber loop including the coupling loss from port 2 to port 4 of the coupler.

Then the electrical current from the PD is proportional to the optical intensity at output port 3 of the coupler given by

$$\begin{aligned} I(t) = E_3(t)E_3^*(t) &\propto \sum_{n=0}^{\infty}\sum_{m=0}^{\infty} C_n C_m^* e^{j(\phi_n-\phi_m)}[E_1(t-n\tau_d)E_1^*(t-m\tau_d)]e^{j(n-m)\Omega t} \\ &= term\ 1(when\ m=n) + term\ 2(when\ m\neq n), \end{aligned} \tag{4.7}$$

where

$$term\ 1 = \sum_{l=0}^{\infty} C_l C_l^*[A + \Delta A(t-l\tau_d)], \tag{4.8}$$

$$term\ 2 = \sum_{k=1}^{\infty}\{\sum_{l=0}^{\infty} C_l^* C_{k+l}[A+\Delta A(t-l\tau_d)][A+\Delta A(t-(k+l)\tau_d)]e^{\Delta\phi(t,\tau_d,l,(l+k))}e^{jk\Omega t} + c.c.\}, \tag{4.9}$$

$$\Delta\phi(t,\tau_d,l,(l+k)) = \phi_{l+k}(t) - \phi_l(t), \tag{4.10}$$

And we further define

$$K(t,\tau_d,l,k+l) = [A+\Delta A(t-l\tau_d)][A+\Delta A(t-(k+l)\tau_d)], \tag{4.11}$$

Equations (4.7) to (4.11) indicate that the current contains a series of beat-notes at discrete angular frequencies. Without loss of generality, the current component with center angular frequency $k\Omega$ (the k^{th} order beat-note) is considered, and its complex amplitude is given by[28]

$$I_k(t) = \sum_{l=0}^{\infty} C_l^* C_{k+l} K(t,\tau_d,l,k+l)e^{\Delta\phi(t,\tau_d,l,(l+k))}, \tag{4.12}$$

The autocorrelation function of $I_k(t)$ is thus given by

$$\begin{aligned} R_k(\tau) &= < I_k(t) I_k^*(t-\tau) > \\ &= \sum_{p=0}^{\infty}\sum_{q=0}^{\infty} C_p^* C_{p+k} C_q C_{k+q}^* K(t,\tau_d,p,k+p) K(t-\tau,\tau_d,q,k+q) \\ &\quad < \exp\{-j[\Delta\phi(t,\tau_d,p,p+k) - \Delta\phi(t,\tau_d,q,q+k)]\} >, \end{aligned} \tag{4.13}$$

If we define[28]:

$$\begin{aligned} B(\tau+(p-q)\tau_d, k\tau_d) &= < -j[\Delta\phi(t,\tau_d,p,p+k) - \Delta\phi(t,\tau_d,q,q+k)] > \\ &= < \Delta\phi^2(k\tau_d) > - < \Delta\phi^2(\tau+(p-q)\tau_d) > \\ &\quad + \frac{1}{2} < \Delta\phi^2(\tau+(p-q+k)\tau_d) > \\ &\quad + \frac{1}{2} < \Delta\phi^2(\tau-(p-q-k)\tau_d) >, \end{aligned} \tag{4.14}$$

Then $R_k(\tau)$ becomes:

$$R_k(\tau) = \sum_{p=0}^{\infty}\sum_{q=0}^{\infty} C_p^* C_{p+k} C_q^* C_{k+q} K(t,\tau_d,p,k+p) K(t-\tau,\tau_d,q,k+q) \exp[B(\tau+(p-q)\tau_d, k\tau_d)], \tag{4.15}$$

The power spectrum is therefore calculated by the Fourier transform of Equation (4.15) and is expressed as:

$$\begin{aligned} S_k(\omega) &= F[R_k(\tau)] \\ &= \sum_{p=0}^{\infty}\sum_{q=0}^{\infty} C_p^* C_{p+k} C_q C_{k+q}^* \exp[j(p-q)\omega\tau_d] \\ &\quad F\{K(t,\tau_d,p,k+p) K(t-\tau,\tau_d,q,k+q) \exp[B(\tau,k\tau_d)]\} \\ &= \{S_0(\omega,k\tau_d,k\Omega)\} \otimes F[A^4 + R_{AA}(\tau)]\} \mid \sum_{p=0}^{\infty} C_p^* C_{p+k} \exp(jp\omega\tau_d)|^2, \end{aligned} \tag{4.16}$$

where we have used the relationship

$$F(\tau+\tau_d) = \exp(j\omega\tau_d) F(\tau), \tag{4.17}$$

and

$$\begin{aligned} K(t,\tau_d,p,k+p) K(t-\tau,\tau_d,q,k+q) &= A^4 + 2A^2 R_A(0) + 4A^2 R_A(\tau) + R_A^2(\tau) \\ &= A^4 + R_{AA}(\tau), \end{aligned} \tag{4.18}$$

Substituting Equation(4.6) into Equation(4.16) and after some algebra, we find that the lineshape of the k_{th} order beat-note ($k > 0$) from the LC-RDSHI becomes:

$$\begin{aligned} S_k(\omega) &= F[A^4 + R_{AA}(\tau)] \otimes \{\frac{\gamma^m}{1-\alpha^2} P(\omega) S_0(\omega, k\tau_d, k\Omega)\} \\ &= S_{nn}(\omega) \otimes S_{ff}(\omega), \end{aligned} \tag{4.19}$$

where[28]

$$P(\omega) = \alpha + \frac{(1-\alpha)(\gamma^2-\alpha)}{1+\gamma^2-2\gamma\cos[(\omega+k\Omega)\tau_d]}, \tag{4.20}$$

is a periodical function of angular frequency ω, resulting from the multi-interferences of the laser field after multi-passing through the loop[28]. $S_{nn}(\omega)$ and $S_{ff}(\omega)$ are amplitude noise spectrum and phase noise spectrum. It is worthy recalling that $S_0(\omega, k\tau_d, k\Omega)$ is the rf spectrum from a conventional DSHI with time delay $k\tau_d$ and angular frequency shift $k\Omega$. Noting that in Equation(4.19), the carrier frequency has been implied, thereby ω is the angular frequency deviated from center angular frequency $k\Omega$. Equation(4.19) shows that the spectral component at frequency $k\Omega$ of a LC-RDSHI is a modified version of the spectrum from a conventional DSHI with an equivalent time delay and frequency shift, which indicates that a direct measurement of the laser linewidth from the spectrum may not be appropriate especially when the laser linewidth is small.

In order to permit a direct measurement of the linewidth, the modification function, $P(\omega)$, must be invariant of angular frequency ω. From Equation(4.20) this is the case when the parameters α and γ satisfies[28]

$$\gamma = \alpha^{1/2}, \tag{4.21}$$

or γ is very small (such as 0.09) or very large (such as 3.6) so that $P(\omega)$ can be approximately equal to a constant.

4.2 RIN Effect

The intensity of lasers fluctuate during operation due to the quantum nature of the lasing process. The term Relative Intensity Noise (RIN) describes the amplitude fluctuations in the optical fields.

We assume that the amplitude fluctuation is statistically independent of the phase noise[32].And the amplitude noise spectrum is white, which is correct because the laser noise bandwidth is much larger than the frequency shift Ω (1MHz - 40MHz)[32].

The spectrum of k^{th} order of beat-note with consideration of amplitude noise should be:

$$\begin{aligned} S_k(\omega) &= F[R_k(\tau)] \\ &= A^4 S_{ff}(\omega) + S_{AA}(\omega) \otimes S_{ff}(\omega) \\ &= A^4 S_{ff}(\omega) + S_{AA}(\omega), \end{aligned} \tag{4.22}$$

It is shown from Equation(4.22) that the measured power spectrum consists of an amplitude noise spectrum and a phase noise spectrum. The phase spectrum exhibits a Lorentzian lineshape which can be found around integer multiplies of Ω. The amplitude noise spectrum is a flat noise spectrum. The phase noise spectrum is superimposed on the amplitude noise spectrum.

4.3 Fiber Birefringence Effect

Polarization analysis of the LC-RDSHI system is complex as the state of polarization (SOP) cannot be fully controlled and it may change anywhere at anytime within the system due to the birefringence of the single mode fiber delay line and the presence of the EDFA, AOM and other optical components in the system.

In a single channel amplified system, polarization dependent gain (PDG) plays a more important role than polarization dependent loss(PDL) and polarization mode dispersion(PMD)[33].

PDG causes the ASE to accumulate with length faster than expected which introduces additional noise on detection[34].

Light polarization also changes during the Bragg acousto-optic interaction. It is shown that the linearly polarized light wave, entering an acoustic field, becomes elliptically polarized because of an additional phase shift effect. The polarization state can be controlled by varying power or frequency of the ultrasound[35]. But in the following analysis, we only consider the fiber birefringence effect on the LC-RDSHI.

In ordinary circularly cylindrical fibers, there are two types of hybrid modes, $HE_{\nu\mu}$ and $EH_{\nu\mu}$ modes. The label ν refers to the azimuthal variation of the field while the label μ accounts for modes of different radial variation. The dominant mode of an ordinary optical fiber is designated as the HE_{11} mode. However, under weakly guiding condition, an approximate modal field description can be obtained by solving the scalar wave equation instead of the full set of Maxwell's equations. This dominant mode solution is designated as LP_{01} mode for which the electric field is linearly polarized[36]. In the framework of Cartesian coordinates, the electric field of the dominant mode has three components, E_x, E_y and E_z. One of the two transverse components, E_x or E_y predominates, while the E_z component, considered in the direction of the fiber axis, is much smaller than the transverse. If E_x is the dominant field component in an isotropic circularly symmetric fiber, the LP_{01} mode is said to be polarized in the x-direction, while for if E_y is the dominant component, the mode is y-polarized. Thus, single-mode fibers can, in fact, simultaneously support two identical modes which are mutually orthogonally polarized. In an ideal dielectric waveguide of circular cross section, these two modes are degenerate; that is, there is no difference between their propagation constants, and thus propagate with the same phase-velocity. In practical situations, an actual optical fiber is not absolutely perfect. It is neither completely axially-symmetric nor perfectly straight. In addition, the fiber material is often assumed to be nominally isotropic, in which the refractive index is the same regardless of the direction of the polarization of the electric field. This is also not strictly true in practical fibers. Small departures from perfect circularity and fluctuations of the anisotropy of the fiber material,

couple the x-polarized mode to the y-polarized mode since both modes are very nearly degenerate. These conditions lead to a complete mixing of the two polarization states so that the initially linearly polarized light field quickly reaches a state of arbitrary polarization[36]. Polarization states in the optical fibers are extremely sensitive to the environment, such as external stress, bending, tension, electric field, twist or magnetic field[37].

From the interferometer point of view, it is well known that the polarization of the two interfering beams may drift randomly due to alterations in residual birefringence of the single mode fiber delay line[38]. Normally, circular fibers do not maintain the input state of polarization for more than a few meters, because of polarization-coupling perturbations that are randomly distributed along the length of the fiber. Any device that depends upon the interference of two coherent optical beams, as in homodyne or heterodyne detection, requires that the interacting beams have identical polarizations for efficient operation. If the polarizations of the two beams are 90° apart, complete fading can result[36]. Though an ideal polarization controller can transform the state of polarization of highly polarized light between any two given states, with no change in light intensity, in our application, the SOP setting time of polarization controller is about 1ms (recirculating time = $125\mu s$ in our application) for $< 1°$ deviation. The polarization state from the loop cannot be adjusted to be the same with the laser. Therefore, polarization effect must be examined in the LC-RDSHI system.

If we only consider single mode fiber, we can decompose the input field of laser into[39]

$$E_1(t) = gE_a(t) + hE_b(t) \tag{4.23}$$

where $E_a(t)$ and $E_b(t)$ represent two orthogonal modes a and b respectively. If $E_a(t)$ and $E_b(t)$ have equal intensities, and $E_1(t)$ has a unit power,then

$$|h|^2 + |g|^2 = 1, \tag{4.24}$$

because $E_a(t)$ and $E_b(t)$ are orthogonal. The autocovariance of $I(t)$ is

$$R_I(t_1, t_2) = |g|^4 R_{aa}(t_1, t_2) + 2|g|^2|h|^2 R_{ab}(t_1, t_2) + |h|^4 R_{bb}(t_1, t_2), \tag{4.25}$$

In the LC-RDSHI system, for N recirculations without considering amplitude fluctuation, Equation(4.7) becomes:

$$\begin{aligned} I(t) \propto E_3(t)E_3^*(t) &= \sum_{n=0}^{N}\sum_{m=0}^{N} C_n C_m^* [E_1(t-n\tau_d)E_1^*(t-m\tau_d)] \\ &\quad \exp\{j(\phi_n(t-n\tau_d)-\phi_m(t-m\tau_d))\}\exp\{j(n-m)\Omega t\}, \end{aligned} \quad (4.26)$$

When $m \neq n$, the intensity can be represented by[28]:

$$I(t) = \sum_{m=0}^{N}\{\sum_{l=0}^{N} C_l^* C_{m+l} \exp[-j(m\omega_0\tau_d + \phi(t-l\tau_d) - \phi(t-(l+m)\tau_d))]e^{jm\Omega t} + c.c.\}, \quad (4.27)$$

The cross-correlation function of I_a and I_b is thus given by

$$\begin{aligned} R_{ab}(t_1,t_2) &= < I_a(t_1)I_b^*(t_2) > \\ &= < \sum_{m_1=0}^{N}\{\sum_{l_1=0}^{N} C_{l_1}^* C_{m_1+l_1} \exp[-j(m_1\omega_0\tau_a + \phi(t-l_1\tau_a) \\ &\quad -\phi(t-(l_1+m_1)\tau_a))]e^{jm_1\Omega t}\} \\ &\quad \sum_{m_2=0}^{N}\{\sum_{l_2=0}^{N} C_{l_2} C_{m_2+l_2}^* \exp[-j(m_2\omega_0\tau_b + \phi(t-l_2\tau_b) \\ &\quad -\phi(t-(l_2+m_2)\tau_b))]e^{jm_2\Omega t}\} > \\ &= \sum_{m_1=0}^{N}\sum_{l_1=0}^{N}\sum_{m_2=0}^{N}\sum_{l_2=0}^{N} C_{l_1}^* C_{m_1+l_1} C_{l_2} C_{m_2+l_2}^* \exp[j(m_1-m_2)\Omega t] \\ &\quad < \exp[-j\omega_0(m_1\tau_a - m_2\tau_b)] \\ &\quad \exp\{-j[\phi(t_1-l_1\tau_a) - \phi(t_1-(l_1+m_1)\tau_a) \\ &\quad -\phi(t_2-l_2\tau_b) + \phi(t_2-(l_2+m_2)\tau_b)]\} >, \end{aligned} \quad (4.28)$$

We further transfer the time average term in Equation (4.30) to:

$$\begin{aligned}
& < \exp\{-j[\phi(t_1 - l_1\tau_a) - \phi(t_1 - (l_1 + m_1)\tau_a) - \phi(t_2 - l_2\tau_b) + \phi(t_2 - (l_2 + m_2)\tau_b)]\} > \\
= \; & \exp\{-j\frac{1}{2} < [\phi(t_1 - l_1\tau_a) - \phi(t_1 - (l_1 + m_1)\tau_a) \\
& -\phi(t_2 - l_2\tau_b) + \phi(t_2 - (l_2 + m_2)\tau_b)]^2 >\} \\
= \; & \exp\{-j\frac{1}{2}[\phi(t_1 - (l_1 + m_1)\tau_a)]^2\} \exp\{-j\frac{1}{2}[\phi(t_2 - (l_2 + m_2)\tau_b)]^2\} \\
& \exp\{j[\phi(t_1 - (l_1 + m_1)\tau_a)][\phi(t_2 - (l_2 + m_2)\tau_b)]\}
\end{aligned} \tag{4.29}$$

where

$$\begin{aligned}
& \exp\{j[\phi(t_1 - (l_1 + m_1)\tau_a)][\phi(t_2 - (l_2 + m_2)\tau_b)]\} \\
= \; & \exp\{\frac{1}{2}[\phi(t_1 - l_1)\tau_a - \phi(t_2 - l_2\tau_b)]^2 + \frac{1}{2}[\phi(t_1 - (l_1 + m_1)\tau_a - \phi(t_2 - (l_2 + m_2)\tau_b)]^2\} \\
& \exp\{\frac{1}{2}[\psi(t_1 - l_1\tau_a) - \phi(t_2 - (l_2 + m_2)\tau_b]^2 - \frac{1}{2}[\phi(t_1 - (l_1 + m_1)\tau_a - \phi(t_2 - l_2\tau_b]^2\},
\end{aligned} \tag{4.30}$$

For a Wiener process, we define $D(t_1, t_2) =< [\phi(t_1) - \phi(t_2)]^2 >= \frac{t_1 - t_2}{\tau_c}$, where τ_c is the coherence time of the laser. So (4.29) can be expressed as

$$\begin{aligned}
& < \exp\{-j[\phi(t_1 - l_1\tau_a) - \phi(t_1 - (l_1 + m_1)\tau_a) - \phi(t_2 - l_2\tau_b) + \phi(t_2 - (l_2 + m_2)\tau_b)]\} > \\
= \; & \exp\{-j\frac{1}{2}D(|m_1\tau_a|)\} \exp\{-j\frac{1}{2}D(|m_2\tau_b|)\} \\
& \exp\{-j\frac{1}{2}[D(|t_1 - t_2 - l_1\tau_a + l_2\tau_b|) + D(|t_1 - t_2 - (l_1 + m_1)\tau_a + (l_2 + m_2)\tau_b|)\} \\
& \exp\{j\frac{1}{2}[D(|t_1 - t_2 - l_1\tau_a + (l_2 + m_2)\tau_b|) + D(|t_1 - t_2 - (l_1 + m_1)\tau_a + m_2\tau_b|)\} \\
= \; & \exp\{-j\frac{1}{2}[\frac{|m_1\tau_a| + |m_2\tau_b| + |t_1 - t_2 - l_1\tau_a + l_2\tau_b|}{\tau_c} \\
& \frac{+|t_1 - t_2 - (l_1 + m_1)\tau_a + (l_2 + m_2)\tau_b|}{\tau_c}]\} \\
& \exp\{+j\frac{1}{2}[\frac{|t_1 - t_2 - l_1\tau_a + (l_2 + m_2)\tau_b| + |t_1 - t_2 - (l_1 + m_1)\tau_a + l_2\tau_b|}{\tau_c}]\}
\end{aligned} \tag{4.31}$$

Then Equation(4.28) can be rewritten as:

$$\begin{aligned} & R_{ab}(t_1,t_2) =< I_a(t_1)I_b^*(t_2) > \\ = & \sum_{m_1=0}^{N}\sum_{l_1=0}^{N}\sum_{m_2=0}^{N}\sum_{l_2=0}^{N} C_{l_1}^* C_{m_1+l_1} C_{l_2} C_{m_2+l_2}^* \exp[j(m_1-m_2)\Omega t] < \exp[-j\omega_0(m_1\tau_a - m_2\tau_b)] \\ & \exp\{-j\frac{1}{2}[\frac{|m_1\tau_a| + |m_2\tau_b| + |t_1 - t_2 - l_1\tau_a + l_2\tau_b|}{\tau_c} \\ & \frac{+|t_1 - t_2 - (l_1+m_1)\tau_a + (l_2+m_2)\tau_b|}{\tau_c}]\} \\ & \exp\{+j\frac{1}{2}[\frac{|t_1 - t_2 - l_1\tau_a + (l_2+m_2)\tau_b| + |t_1 - t_2 - (l_1+m_1)\tau_a + l_2\tau_b|}{\tau_c}]\} > \end{aligned} \tag{4.32}$$

Assuming the average loop delay $\tau = \frac{\tau_a+\tau_b}{2}$[39], so τ_a and τ_a in (4.32) can be replaced by τ, Equation (4.32) can be changed to

$$\begin{aligned} R_{ab}(t_1,t_2) &= < I_a(t_1)I_b^*(t_2) > \\ &= \sum_{m_1=0}^{N}\sum_{l_1=0}^{N}\sum_{m_2=0}^{N}\sum_{l_2=0}^{N} C_{l_1}^* C_{m_1+l_1} C_{l_2} C_{m_2+l_2}^* \exp[j(m_1-m_2)\Omega t] \\ &\quad < \exp[-j\omega_0(m_1\tau_a - m_2\tau_b)] \exp\{-j\frac{1}{2}F(m_1,m_2,L)(\frac{\tau}{\tau_c}) - j\frac{1}{2}[|m_1| + |m_2|(\frac{\tau}{\tau_c})]\} > \end{aligned} \tag{4.33}$$

where[39]

$\Delta = (t_1 - t_2)/\tau_c$,

$L = \Delta - l_1 + l_2$,

$F(m_1, m_2, L) = |L| + |L - (m_1 - m_2)| - |L + m_2| - |L + m_1|$.

If $\tau \gg \tau_c$, $\exp\{-j\frac{1}{2}[|m_1| + |m_2|(\frac{\tau}{\tau_c})]\}$ in Equation (4.33) can be ignored. Then Equation (4.33) can be simplified to:

$$\begin{aligned} R_{ab}(t_1,t_2) &= < I_a(t_1)I_b^*(t_2) > \\ &= \sum_{m_1=0}^{N}\sum_{l_1=0}^{N}\sum_{m_2=0}^{N}\sum_{l_2=0}^{N} C_{l_1}^* C_{m_1+l_1} C_{l_2} C_{m_2+l_2}^* \\ &\quad \exp[j(m_1-m_2)\Omega t] < \exp[-j\omega_0(m_1\tau_a - m_2\tau_b)] \exp\{-j\frac{1}{2}F(m_1,m_2,L)(\frac{\tau}{\tau_c})\} >, \end{aligned} \tag{4.34}$$

The effect of $R_{ab}(t_1, t_2)$ is significant only when $(t_1 - t_2)$ is very close to an integer multiple M of τ [39]. At the central frequency of $(m_1 - m_2)\Omega$, Equation (4.34) can be rewritten as a convolution[39]:

$$R_{ab}(t_1, t_2) = R_{ab,\delta}(t_1, t_2) \otimes \exp[-|t_1 - t_2|/\tau_c], \tag{4.35}$$

$$R_{ab,\delta}(t_1, t_2) = \sum_{m_1=0}^{N} \sum_{l_1=0}^{N} \sum_{m_2=0}^{N} \sum_{l_2=0}^{N} C_{l_1}^* C_{m_1+l_1} C_{l_2} C_{m_2+l_2}^* \exp[-j\omega_0(\tau_a - \tau_b)]\delta[(t_1 - t_2) - M\tau], \tag{4.36}$$

Therefore, by setting $\tau_a = \tau_b$, and substitute Equation (4.35) to Equation (4.25), we can obtain[39]:

$$R_I(t_1, t_2) = TR_\delta(t_1, t_2) \otimes \exp[-|t_1 - t_2|/\tau_c], \tag{4.37}$$

where

$$T = |g|^4 + 2|g|^2|h|^2P + |g|^4, \tag{4.38}$$

$$P = |\sum_{m_1=0}^{\infty} \exp[jm_1\omega(\tau_a - \tau_b)]|^2,$$

The power spectrum at the central frequency of $k = (m_1 - m_2)\Omega$ is expressed by:

$$S_k(\omega) = TS_{ff}(\omega), \tag{4.39}$$

Thus $S_k(\omega)$ depends on a frequency independent factor T, and T is a function of the SOP of the fiber delay. Small value of T compresses the output spectrum, and cuases the signal fading.

4.4 Frequency Stability Effect

In order to analyze the frequency stability effect on laser linewidth, we tried to treat the LC-RDSHI as an optical mixing system. Electric fields $E_1(t)$ and $E_3(t)$ are both incident on

the PD. Expressed in terms of the analytic signals and complex envelopes, $E_1(t)$ and $E_3(t)$ are[29]:

$$E_1(t) = Re\{\mathbf{E}_1(t)\} = Re\{\tilde{E}_1(t)e^{j2\pi\nu_1 t}\}, \tag{4.40}$$

$$E_3(t) = Re\{\mathbf{E}_3(t)\} = Re\{\tilde{E}_3(t)e^{j2\pi\nu_3 t}\}, \tag{4.41}$$

The optical intensity incident upon the PD is:

$$I(t) = [E_1(t) + E_3(t)]^2 = I_1(t) + I_3(t) + I_x(t), \tag{4.42}$$

where

$$I_i(t) = E_i^2(t), \quad i = 1, 3 \tag{4.43}$$

are the direct detection intensity components, and

$$I_x(t) = 2E_1(t)E_3(t), \tag{4.44}$$

is the mixing cross-term. If we use ν_i to represent the frequency of $E_i(t)$,the cross-term of intensity can be further expressed as:

$$I_x(t) = 2E_1(t)E_3(t) = Re\{\tilde{E}_1(t)\tilde{E}_3^*(t)e^{j2\pi\Delta\nu t} + \tilde{E}_1^*(t)\tilde{E}_3(t)e^{j2\pi(\nu_1+\nu_3)t}\}, \tag{4.45}$$

Assuming the detector bandwidth is greater than $\Delta\nu = \nu_1 - \nu_3$ but less than $\nu_1 + \nu_3$, the detected intensity can be written as:

$$I_x^D(t) = Re\{\tilde{E}_1(t)\tilde{E}_3^*(t)e^{j2\pi\Delta\nu t}\}, \tag{4.46}$$

The autocorrelation of $I_x^D(t)$ is:

$$\begin{aligned} C_{I_x^D}(\tau, t) &= < I_x^D(t+\tau)I_x^D(t) > \\ &= \frac{1}{2}Re\{< \tilde{E}_1(t+\tau)\tilde{E}_3^*(t+\tau)\tilde{E}_1^*(t)\tilde{E}_3(t)e^{j2\pi\Delta\nu\tau} >\} \\ &\quad + \frac{1}{2}Re\{< \tilde{E}_1(t+\tau)\tilde{E}_3^*(t+\tau)\tilde{E}_1^*(t)\tilde{E}_3(t)e^{j2\pi\Delta\nu(2t+\tau)} >\}, \end{aligned} \tag{4.47}$$

Since $\tilde{E}_1(t)$ and $\tilde{E}_3(t)$ are wide-sense stationary, the second term in Equation (4.47) is zero. And assuming that $\tilde{E}_1(t)$ and $\tilde{E}_3(t)$ are statistically independent, Equation (4.47) yields:

$$\begin{aligned} C_{I_x^D}(\tau,t) &= \frac{1}{2}Re\{<\tilde{E}_1(t+\tau)\tilde{E}_1^*(t)><[\tilde{E}_3(t+\tau)\tilde{E}_3^*(t)]^*>e^{j2\pi\Delta\nu\tau}\} \\ &= \frac{1}{2}Re\{(\tilde{C}_{E_1}(\tau)e^{j2\pi\nu_1\tau})(\tilde{C}_{E_3}(\tau)e^{-j2\pi\nu_3\tau})\} \\ &= \frac{1}{2}Re\{C_{E_1}(\tau)C_{E_3}^*(\tau)\} \end{aligned} \tag{4.48}$$

Assuming that the spectrum $\tilde{S}_{E_1}$ and $\tilde{S}_{E_3}$ are symmetric, by using $F\{Rexy^*\} = X(f) \otimes Y(f) + Y(f) \otimes X(f)$[29], the spectrum of the detected current can be obtained by:

$$S_{I_x^D}(f) = \frac{1}{4}[\tilde{S}_{E_1} \otimes \tilde{S}_{E_3}](f-\Delta\nu) + \frac{1}{4}[\tilde{S}_{E_3} \otimes \tilde{S}_{E_1}](-f-\Delta\nu), \tag{4.49}$$

where $\tilde{S}_{E_1}$ and $\tilde{S}_{E_3}$ are referred to as laser lineshape.

In the LC-RDSHI system, $\tilde{E}_1(t)$ and $\tilde{E}_3(t)$ can be rewritten from Equation (4.5) as:

$$\begin{aligned} \tilde{E}_1(t) &= \sqrt{\alpha}e^{j\omega_1 t}e^{j\phi t}, \\ \tilde{E}_3(t) &= \sum_{m=0}^{N} C_m e^{j(\omega_3 t+m\Omega)t}e^{j\phi(t-m\tau_d)}, \end{aligned} \tag{4.50}$$

The spectrum of the LC-RDSHI system is $\frac{1}{4}[\tilde{S}_{E_1} \otimes \tilde{S}_{E_3}](\omega-(\omega_3+m\Omega-\omega_1))$ with central frequency at $(\omega_3+m\Omega-\omega_1) = m\Omega+\Delta\omega$.

The autocorrelation of $\tilde{E}_3(t)$ can be derived without considering the amplitude fluctuations as:

$$\begin{aligned} C_{I_3}(\tau) &= <I_3(t+\tau)I_3(t)> \\ &= <\sum_{m_1=1}^{N}\sum_{n_1=1}^{N} C_{m_1}^* C_{n_1} e^{j[\phi(t+\tau-m_1\tau_d)+\phi(t+\tau-n_1\tau_d]} \\ &\quad \sum_{m_2=1}^{N}\sum_{n_2=1}^{N} C_{m_2}^* C_{n_2} e^{j[\phi(t+\tau-m_2\tau_d)+\phi(t+\tau-n_2\tau_d]} > \\ &= \sum_{m_1=1}^{N}\sum_{n_1=1}^{N}\sum_{m_2=1}^{N}\sum_{n_2=1}^{N} C_{m_1}^* C_{n_1} C_{m_2}^* C_{n_2} \\ &\quad < e^{j[\phi(t+\tau-m_1\tau_d)+\phi(t+\tau-n_1\tau_d+\phi(t-m_2\tau_d)+\phi(t-n_2\tau_d]} > \\ &= C_\delta(\tau) \otimes < e^{j[\phi(t+\tau-m_1\tau_d)+\phi(t+\tau-n_1\tau_d+\phi(t-m_2\tau_d)+\phi(t-n_2\tau_d]} >, \end{aligned} \tag{4.51}$$

where

$$C_\delta(\tau) = \sum_{m_1=1}^{N}\sum_{n_1=1}^{N}\sum_{m_2=1}^{N}\sum_{n_2=1}^{N} C^*_{m_1}C_{n_1}C^*_{m_2}C_{n_2}\delta(\tau - m_1\tau_d - \tau + n_1\tau_d - m_2\tau_d + n_2\tau_d) \tag{4.52}$$

The Fourier transform of $C_{I_3}(\tau)$ can be written as:

$$\tilde{S}_{E_3}(\omega) = S_{E_3}(\omega + m\Omega) = S_\delta(\omega + m\Omega)\cdot S_{E_1}(\omega + m\Omega), \tag{4.53}$$

From $S_{E_3}(\omega) = S_\delta(\omega)\cdot S_{E_1}(\omega)$, we can see that $E_1(\omega)$ is source dependent and $S_\delta(\omega)$ is determined by the optical mixing system. Then the spectrum of the whole system can be expressed as:

$$\begin{aligned} S(\omega) &= \frac{1}{4}[\tilde{S}_{E_1}\otimes\tilde{S}_{E_3}](\omega - (\omega_3 + m\Omega - \omega_1)) \\ &= \frac{1}{4}[\tilde{S}_\delta\otimes(\tilde{S}_{E_1}\cdot\tilde{S}_{E_1})](\omega - (\omega_3 + m\Omega - \omega_1)) \\ &= \frac{1}{4}[\tilde{S}_{E_1}\otimes\tilde{S}_{E_1}\cdot\tilde{S}_\delta](\omega - (\omega_3 + m\Omega - \omega_1)) \end{aligned} \tag{4.54}$$

In the experiment, we collected data through an oscilloscope (OSC) and took Fourier transform of the time domain data to get the spectrum of each order of beat-note, as shown in Figure 4.1. It was noticed that the signal to noise ratio is not good enough for high accuracy measurement. So we tried to do 100 times average. 100 data must be collected, summed and divided by 100. Due to all types of frequency noises in the system, $\omega_3 - \omega_1$ has different values for different sets of data, so the central frequency of a beat-note varied as calculated in Equation(4.54). The averaged linewidth may broaden after summation of the spectra with different central frequencies though the signal to noise ratio was improved. The averaged spectrum is shown in Figure 4.1. In Chapter 5, we will show that actions have been taken to minimize the frequency fluctuations.

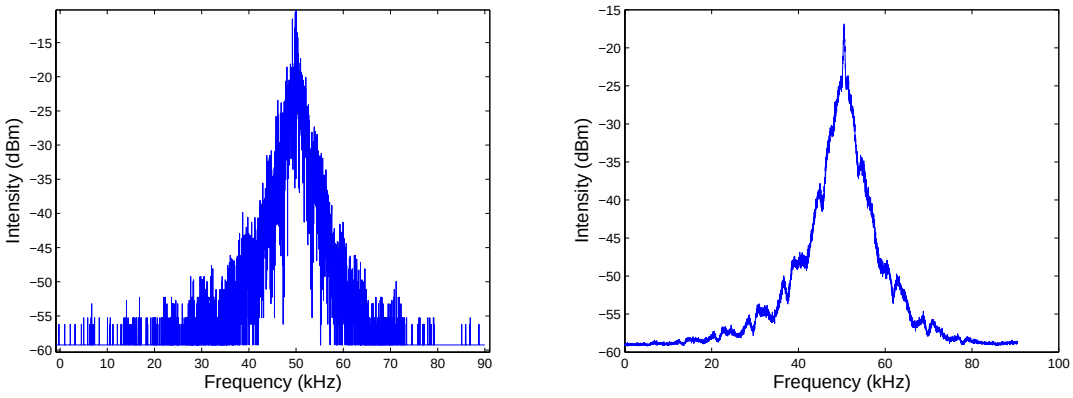

Figure 4.1: 100-time average to improve signal-to-noise ratio

4.5 Effect of $1/f$ Frequency Noise

It is well known that the frequency noise spectrum of a laser with both white and $1/f$ frequency noise components can be modeled as[26]:

$$S_f(\omega) = S_0 + k_f/|\omega|, \tag{4.55}$$

More complicated algorithms are necessary to derive the white frequency noise component,S_0, and $1/f$ frequency noise component, k, from the spectra of the various orders of beat notes. In this case, the autocorrelation function corresponding to a specific beat note is derived in [26] and is given by

$$R_\Omega(\tau) = LG, \tag{4.56}$$

where

$$L = \exp\left\{ \begin{array}{ll} -S_0|\tau| & for|\tau| \le \tau_d \\ -S_0\tau_d & for|\tau| \ge \tau_d \end{array} \right\} \tag{4.57}$$

and

$$G = |\tau+\tau_d|^{\{-k_f(\tau+\tau_d)^2/2\pi\}}|\tau-\tau_d|^{\{-k_f(\tau-\tau_d)^2/2\pi\}}|\tau|^{(-k_f\tau^2/2\pi)}\tau_d^{(-k_f\tau_d^2/2\pi)}, \tag{4.58}$$

L and G are the autocorrelation functions corresponding to the white and $1/f$ frequency noise components, respectively. The power spectral density for the combined white and $1/f$

frequency noises can be evaluated by finding the Fourier transform of Equation (4.56). A Gaussian approximation for the autocorrelation Equation (4.58), can be derived empirically [26]. When $k\tau_0^2 \gg 1$, we have

$$G = \exp[-\tau^2 \frac{k_f}{2\pi}(4.3 + \ln \frac{4.3\tau_d^{2.1} k_f}{\pi})], \tag{4.59}$$

The corresponding spectrum from the autocorrelation function G is also expected to be Gaussian so the linewidth is given as

$$G_{lw} = \frac{1}{\pi}[\frac{2k_f \ln 2}{\pi}(4.3 + \ln \frac{4.3\tau_d^{2.1} k_f}{\pi})]^{\frac{1}{2}} \quad (FWHM \quad in \quad hertz), \tag{4.60}$$

It is worth noting that the linewidth predicted is not independent of the delay time even for large delays. This is due to the very low frequencies presented in the $1/f$ noise. The resulting heterodyne spectrum for the combined white and $1/f$ frequency noise is also dependent on the delay time and is known as the Voigt spectrum which is defined by the convolution of a Lorentzian spectrum and a Gaussian spectrum. In order to illustrate the different effects of white and $1/f$ frequency noises on heterodyne line shapes, the line shapes caused by them are plotted in Figure 4.2. $S_0/2\pi$ =3.74 kHz is chosen for the white frequency noise and k_f =108 Hz for $1/f$ frequency noise, leading to the same FWHM of 3.74 kHz for both the line shapes. It is shown that the line shape due to the white frequency noise is Lorentzian and the $1/f$ line shape is very close to the Gaussian profile near the center and has much less power at the wings than a Lorentzian. The effect of the $1/f$ frequency noise on the self-heterodyne line shapes is further illustrated in Figure 4.3, in which line shapes due to different levels of $1/f$ frequency noise are plotted. The extra linewidth broadening due to $1/f$ frequency noise is evident.

Parameters S_0 and k_f in Equation (4.60) can be estimated by fitting the measured self-heterodyne line shape with a Voigt profile, so the frequency noise of a laser can be characterized. Efficient and accurate algorithms are available for estimating the Voigt line shape for any combination of Lorentzian and Gaussian contributions. Some of the approximations for the Voigt profile also provide derivatives with respect to all of the parameters allowing the

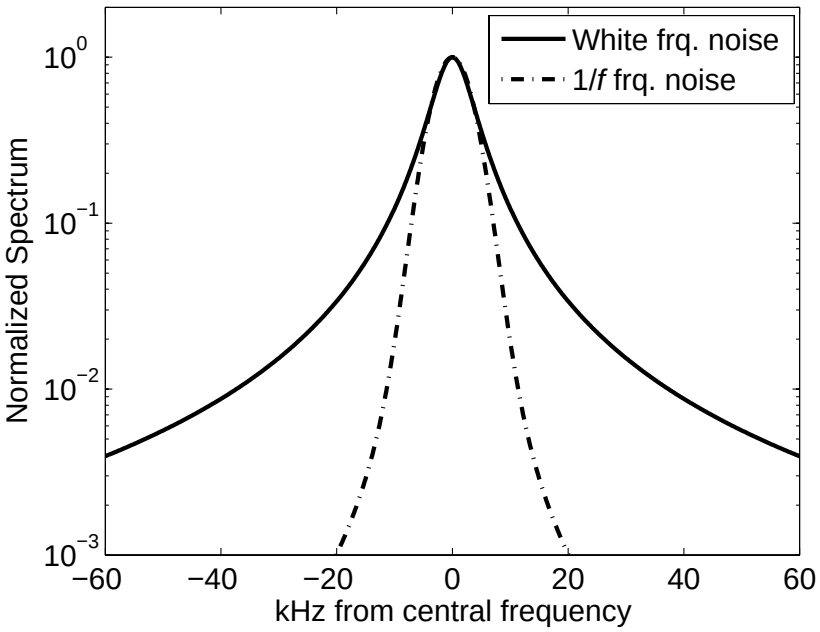

Figure 4.2: Comparison of normalized self-heterodyne lineshape due to white noise and $1/f$ frequency noise.

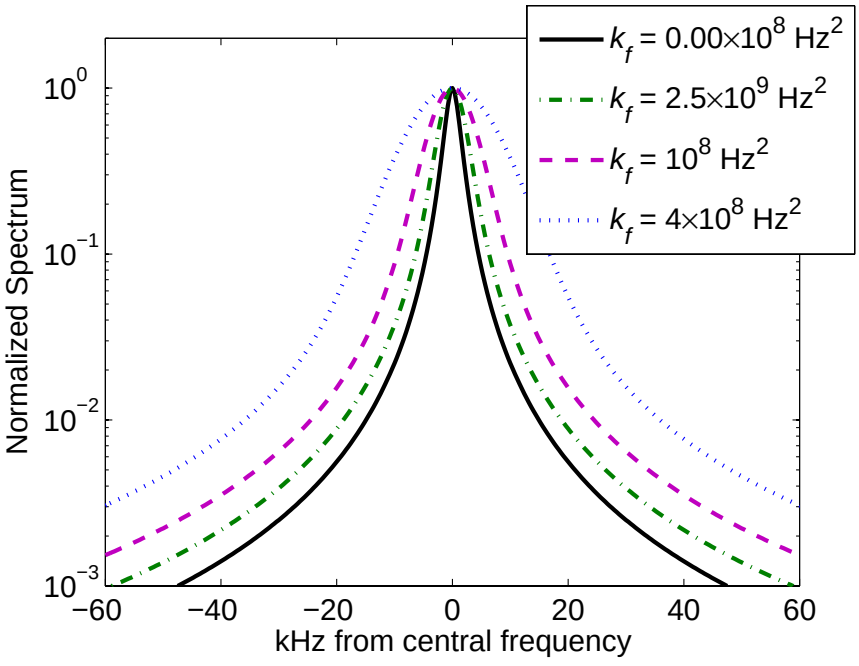

Figure 4.3: Normalized self-heterodyne lineshape due to different $1/f$ frequency noise

application of nonlinear least squares fitting procedures. These fitting procedures use the Voigt function and derivatives for each point in the line shape and iterate until a minimum error is obtained. We will show how to use the Voigt curve fitting to interpret the Lorentzian linewidth in Chapter 6.

Chapter 5

Experimental Implementation of LC-RDSHI

The loss-compensated recirculating DSHI (LC-RDSHI) was first proposed by Tsuchida[30] and Park et al. [31] and was used to measure the linewidth of semiconductor lasers. However, as our theoretical analysis revealed, the model used by these researchers no longer provides an accurate description of the laser linewidth as a function of key system parameters, especially when the laser linewidth is narrowed down to the order of kilohertz. We propose here an improved configuration that includes two frequency shifters and an electronic mixer. Both laser spectral width and laser frequency noises can be measured from this improved configuration.

5.1 System Configuration and Key Components

Based on the discussions in Chapter 4, the schematic of the proposed system is shown in Figure 5.1. The system essentially consists of three parts. The first part is the fiber delay loop consisting of a fiber coupler, 25 kilometer SMF, two acousto-optic modulators

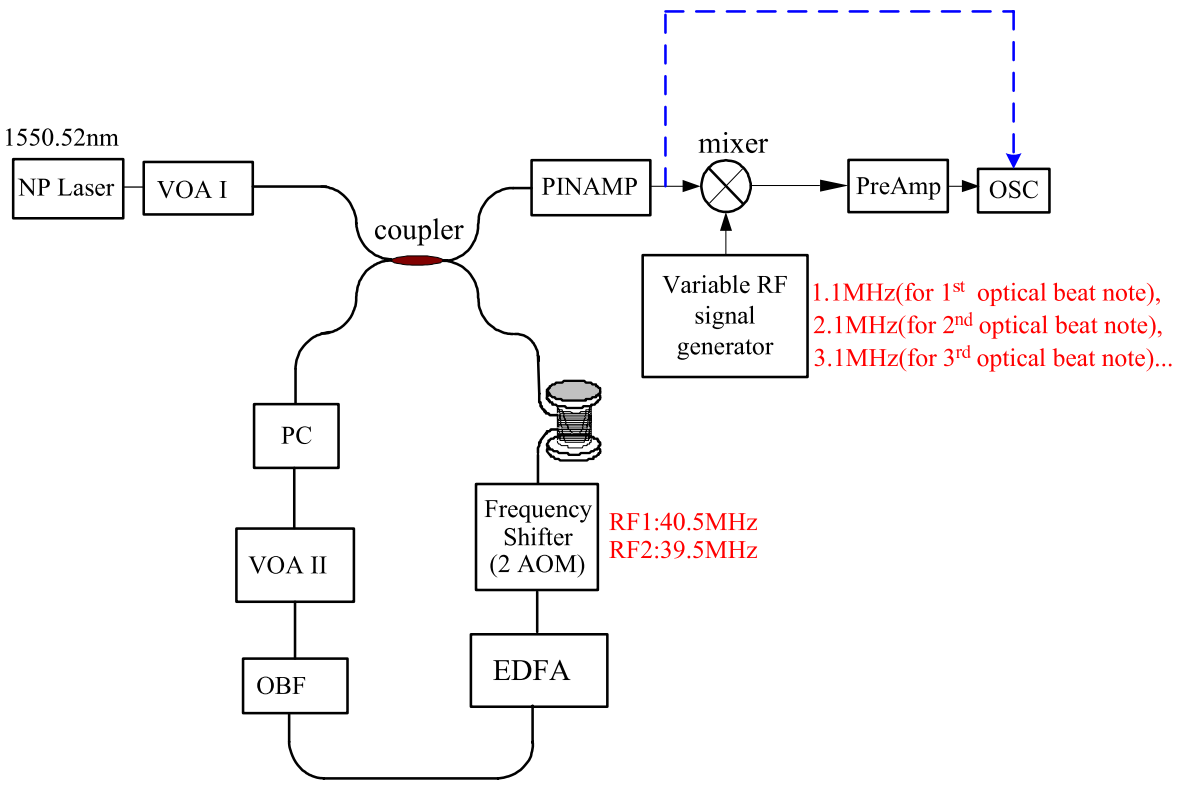

Figure 5.1: Schematic of experimental setup

(AOMs) to introduce the appropriate frequency shift, an EDFA to compensate the losses from the fiber span, the coupler and the other components involved in the fiber delay loop, an optical band-pass filter (OBF) to suppress the amplified spontaneous emission (ASE) noise, and a polarization controller (PC) to maintain the beam polarization. A variable optical attenuator (VOA) is placed right before the loop to obtain appropriate optical power input to the delay loop. The second part is signal detection and acquisition which consists of a PINAMP to detect the optical beat signal, and amplify the photo current from the detector. An electronic mixer circuit is added to further translate the beat signal to even lower frequencies. The last part is signal processing and interpretation in which the acquired data will be analyzed using an appropriate signal processing algorithm to determine the linewidth and the frequency noise of the measured laser.

NP Laser

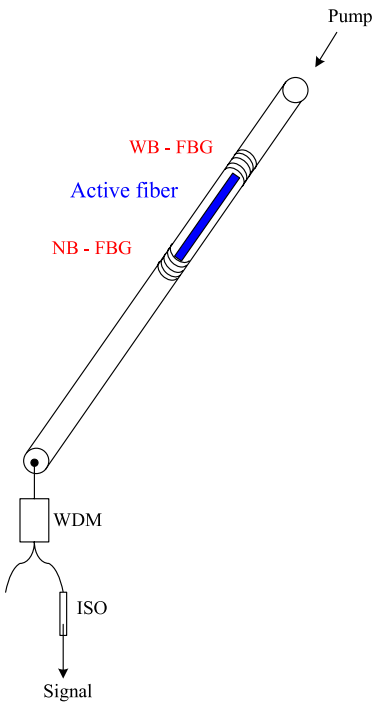

Figure 5.2: Schematic of the laser[2]

The laser we examined is a Benchtop Erbium Micro Fiber Laser Module manufactured by NP Photonics, Inc. In this laser, a cavity is established by two fiber Bragg gratings (FBGs) that are fusion spliced to a very short piece of active material. A spectrally narrow grating (NB-FBG) acts as the output coupler for the laser signal. The laser is excited through the second, spectrally much wider, high reflector grating (WB-FBG) using the output of a single mode pump diode. Both grating temperatures are well controlled. Wavelength tuning is achieved by changing the temperature of the two FBG's (T_{NB} and T_{WB})[2]. Within the spectral width of the NB-FBG, the laser cavity mode can be thermally tuned by changing the laser cavity (through T_{WB}). But the output power of the laser cannot be changed and keeps a value around 19.5mW. So a variable optical attenuator (VOA) is put before the coupler to control the power injected into the recirculating loop.

Frequency Shifter

The frequency shift in LC-RDSHI linewidth measurements can be obtained with a vari-

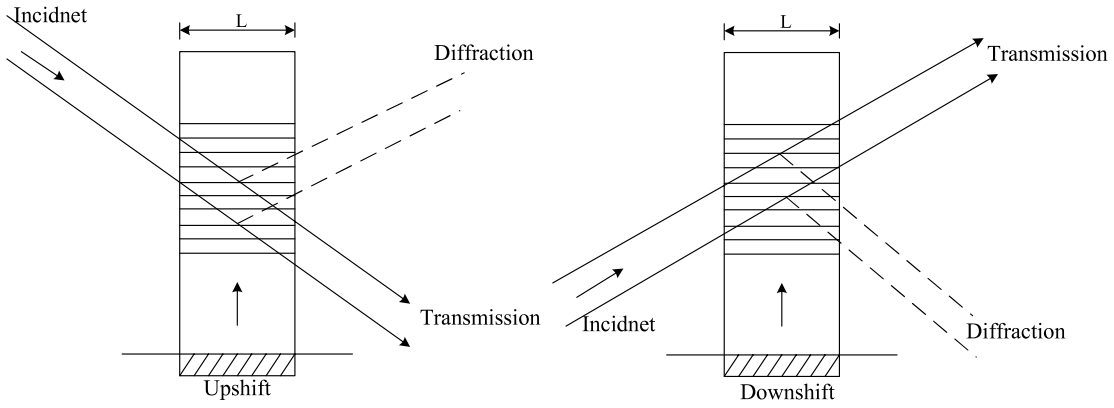

(a) Positive frequency shifter (b) Negative frequency shifter

Figure 5.3: Orientation of wavefronts

ety of devices including acousto-optic frequency shifters, phase modulators, and intensity modulators. Model FCM-401E5A Fiber Pigtailed Acousto-optic Modulator (AOM) manufactured by IntraAction Corp. is used to shift the frequency of a laser (ω_0) by a precise and stable amount (Ω). When a radio frequency (RF) acoustic wave propagates inside an optically transparent medium, a periodic change occurs in the refractive index due to the compressions and refractions of the sound wave. This periodic variation produces a grating capable of diffracting an incident laser beam[40].

AOM can generate both positive and negative frequency shift. If the light diffracted away from the direction of the incident acoustic wave, there is a positive frequency shift. After the positive frequency shift, the output frequency turns out to be $\omega_0 + \Omega$. If the light diffracted toward to the direction of the acoustic wave, there is a negative frequency shift. After the negative frequency shift, the output frequency is: $\omega_0 - \Omega$

Optical Amplifiers (EDFA) and Optical Bandpass Filter (OBF)

In the system, Bookham Technology's MultiWavelength Gain Module (MGMFP-1AOC28) is used. This amplifier module is specified for use in 1530-1563nm (C-band) optical transmission systems. The module is designed for integration with a control system, which includes appropriate power supplies, serial communications, alarm monitoring and thermal control.

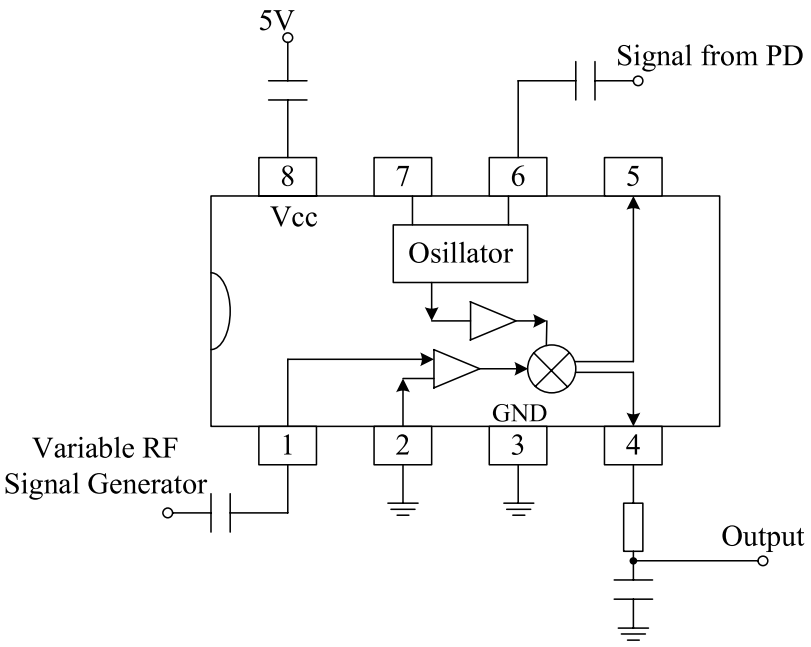

Figure 5.4: Blockdiagram of the mixer

The maximum input power of the EDFA is -10dBm and the maximum gain is 23dB. The maximum noise figure is 5.0dB.

An optical bandpass fiber with 50GHz bandwidth is placed after the EDFA and to filter out the ASE noise generated by the EDFA.

Mixer

The electronic mixer is a SA612A double-balanced mixer and oscillator manufactured by Philips. It is intended for low power communication systems with signal frequency up to 500MHz. The SA612A is a Gilbert cell mixer that generates both sum and difference frequencies. One of the inputs of the mixer is variable for different orders of beat-notes. The differential frequencies of the mixer outputs were used to further move down the frequencies of the beat-notes from the order of megahertz to 100 kHz.

5.2 System Design and Optimization

Design and implementation of the recirculation delay loop is the most critical task for a successful execution of the research because the maximum recirculation length determines the final spectral linewidth measurement resolution. Several issues need to be considered in this task.

5.2.1 Selection of parameter: α

The coupling coefficient α of commercially available 2×2 fiber optic couplers ranges from 0.5 to 0.99, providing a large freedom of the coupler selection for the designed system. If we define the peak intensity (PI) to be

$$PI = S_k(\omega)/S_0(\omega, k\tau_d, k\Omega), \tag{5.1}$$

From Equation (4.20), PI can be expressed by:

$$PI = \frac{\gamma^k}{1-\alpha^2}\left[\alpha + \frac{(1-\alpha)(\gamma^2-\alpha)}{1+\gamma^2-2\gamma\cos[(\omega+k\Omega)\tau_0]}\right], \tag{5.2}$$

Figure 5.5 shows the peak intensity of beat notes as a function of their order numbers for different values of α, when we set the net gain of the loop to be 0.23dB. For $\alpha = 0.9$, the relative spectral power is decreased by about 45 dB for the order of beat-note (k) as large as 200.

In Figure 5.7, we compare the peak intensity of each beat-note between the calculation and the experiment. We show the curve from the calculation in the left column, and the spectral of the beat notes captured by the oscilloscope in the right column. The value of frequency shifter ($\Omega = \Omega_1 - \Omega_2$) is 1MHz, so that the first order beat occurs at 1MHz and the second order beat occurs at 2MHz and so on. When the coupling coefficient $\alpha = 0.1$, 90% power from the laser goes into the loop, as shown in Figure 5.6. The coupler output port $E_3 = 9E_1 + E_2$. The maximum interference efficiency can only occur if $E_2 = 9E_1$. Even

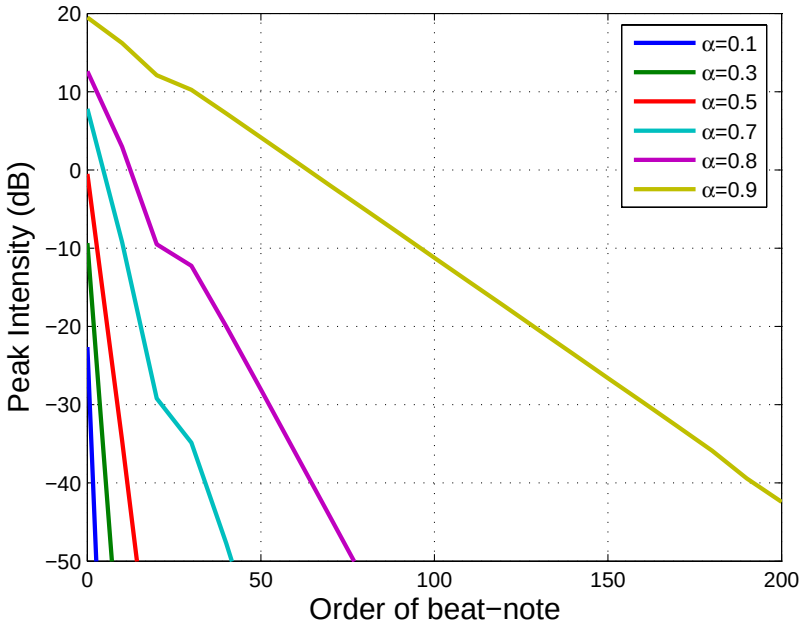

Figure 5.5: Peak intensity (PI) varies with the coupler coefficient α

we use an EDFA in the loop, this condition is hard to realize. The relative intensity drops by 45dB only after 15 orders of beat notes. But when the coupling coefficient $\alpha = 0.1$, 10% power from the laser goes into the loop, the relative intensity drops by 50dB after 160 orders of beat-notes. The maximum interference efficiency can only occur if $E_2 = (1/9)E_1$.

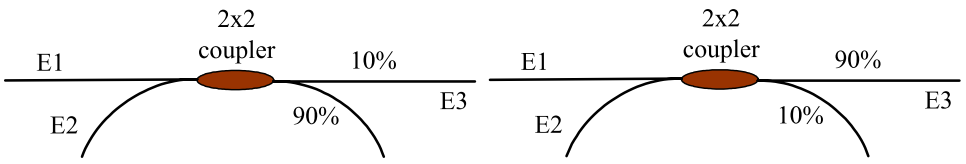

(a) $\alpha = 0.1$ (b) $\alpha = 0.1$

Figure 5.6: Coupler coefficient of a 2x2 coupler

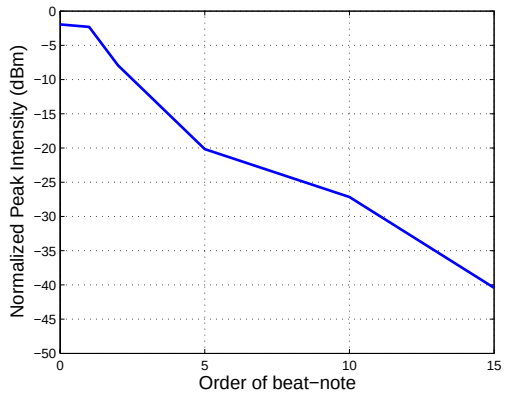

(a) $\alpha = 0.1$, $\beta = 7.5dB$

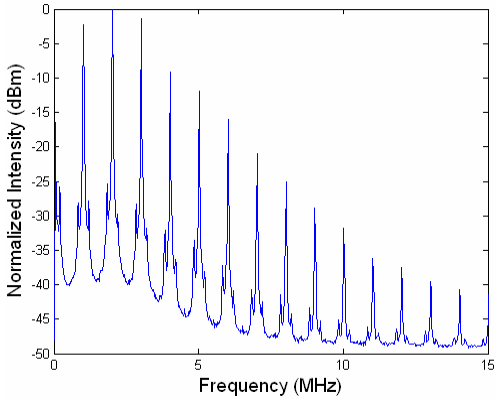

(b) $\alpha = 0.1$, EDFA gain=23dB

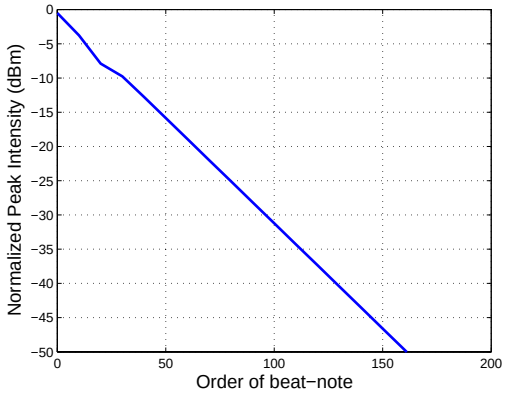

(c) $\alpha = 0.9$, $\beta = 0.15dB$

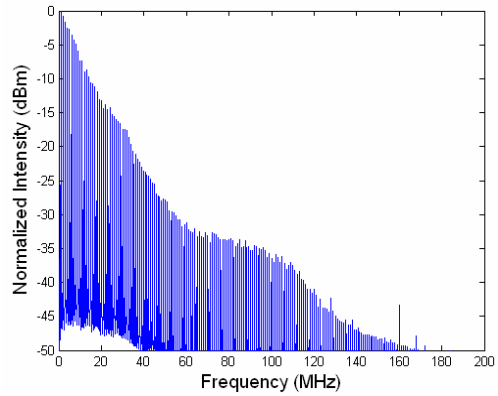

(d) $\alpha = 0.9$, EDFA gain=18dB

Figure 5.7: Selection of α

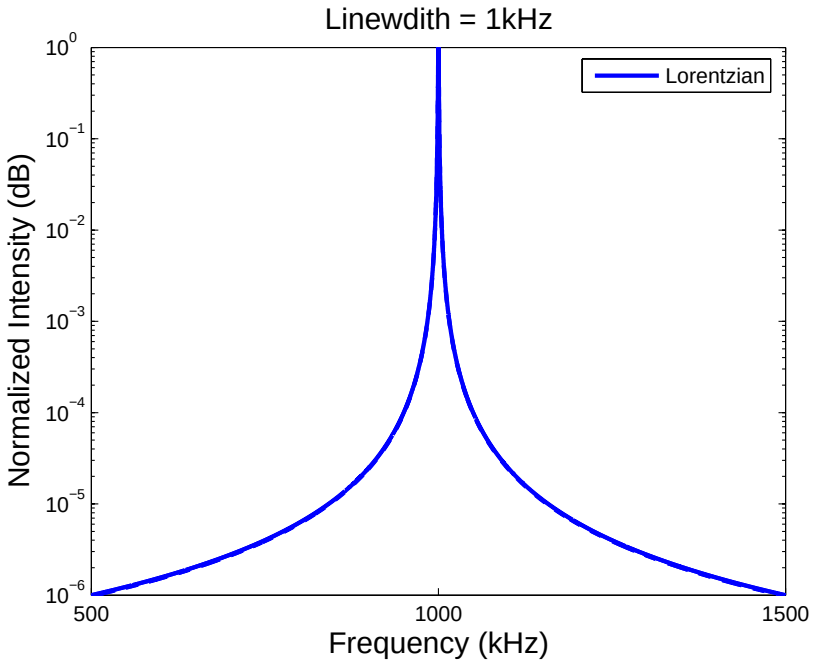

Figure 5.8: Lorentzian Spectrum of a 1kHz-linewidth Laser

5.2.2 Selection of parameter: Ω

Four issues need to be considered in the selection of the frequency shift Ω introduced by the AOM. First, the frequency shift of the beat-note with maximum measurement order number must be within the bandwidth of the photo-detector(PD) because the frequency shift increases linearly as the number of the light recirculations in the fiber delay loop increases. In addition, a too high frequency shift puts more stringent requirements on the electronic parts of the detection system, namely the amplifier, the data acquisition, and the spectrum analyzer and may thus not be economical in future practical use.

Secondly, Ω must be much larger than the linewidth of the laser source to be measured so two neighboring beat notes can avoid an overlap. The Lorentzian spectrum in Figure 5.8 shows the 60dB down bandwidth of a 1kHz-linewidth laser extended to 1MHz. Frequency shift of each loop should not be less than 1MHz for a 1kHz-linewidth laser.

Thirdly, Ω must be large enough to avoid the overlap between relaxation oscillation side-

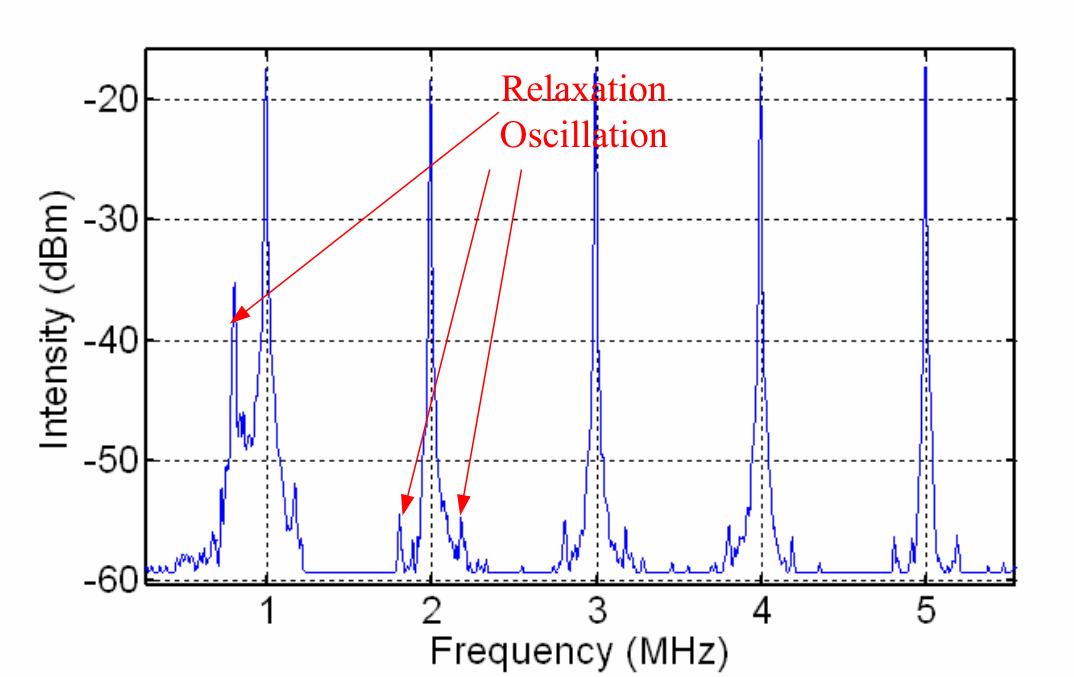

Figure 5.9: Relaxation Oscillation

bands and their neighboring beat notes. Relaxation oscillation (RO), which results from the interplay between the intra cavity optical intensity and the population inversion[8, 41], is another issue. The resulted spectral lineshape of the laser consists of a central line and two sidebands from the relaxation oscillation for each order of beat-note, as shown in Figure 5.9. The sidebands may have some effect on the tails of the beat-note spectrum. But through detailed calculation[41], it is proved that RO has no noticeable effect on the laser linewidth measurement. Therefore, only the frequency shift Ω is a concern related to RO.

The last issue we considered is how to effectively use the AOM. Although the frequency shift by the AOM is known to be the most precise technique, it is still sensitive to environmental vibrations. The crystal (AMTIR-1 Chalcogenide Glass for Model FCM-401E5A AOM) in the AOM vibrates with the environmental vibrations. Therefore, the velocity of the ultrasonic wave to the laser beam is varied due to the mechanical vibration of the AOM[42]. Hence the frequency of the first order beam is shifted by $\pm f_v$, where f_v is the frequency shift

due to the environmental vibration. Then the frequency shift induced by the AOM becomes $\Omega \pm f_v$, instead of Ω.

To overcome the vibration sensitivity of the AOM, one up-shift AOM (40.5MHz) and one down-shift AOM (39.5MHz) are used in series. When two such AOMs are used for measurement in the LC-RDSHI, the frequency fluctuation $\pm f_v$ can be canceled. For the system, the frequency shift is still Ω:

$$[\Omega_1(40.5MHz) \pm f_v] - [\Omega_2(39.5MHz) \pm f_v] = \Omega(1MHz), \tag{5.3}$$

even if there is environmental vibration [42].

The other advantage to use two AOMs is to realize a frequency shift less than 1MHz. The commercially available AOMs usually have a frequency shift higher than tens of megahertz with a very limited adjustable frequency range. This will lead to a frequency shift at least on the order of gigahertz for $k > 100$ beat notes, requiring a very costly high speed detection system. Therefore,using two AOMs in series with one upshifting a frequency Ω_1 and the other downshifting a frequency Ω_2 can generate a much smaller combined frequency shift $\Omega_1 - \Omega_2$, which can be on the order of megahertz, as shown in Equation (5.3).

5.2.3 Selection of parameter: γ

The overall optical gain of the fiber delay loop, γ, must be properly chosen to remove the interferometric effect from multi-recirculations of the laser beam in the fiber loop because otherwise, the spectrum of the photo current is modified by the periodical function to cause a measurement error.

In the loop, when the coupler coefficient is fixed to be $\alpha = 0.9$ and the fiber delay is fixed to be 25km ($\tau_d = 125\mu m$), the multi-recirculation effect only depends on the total gain of the loop γ. Different multi-recirculation patterns correspond to different values of γ, as shown in Figure 5.10. The corresponding spectrum from a conventional DSHI is also plotted (dash line) for comparison. And in order to remove the effect on multi-recirculation, the loop net

gain γ should be either smaller than -6dB (when $\alpha = 0.9$), also proved in [30] or larger than 3.5dB (when $\alpha = 0.9$) to make $P(\omega) \approx constant$ or close to 0.23dB (when $\alpha = 0.9$) to make $P(\omega) = 0$.

In the operation of the LC-RDSHI system, parameter γ can be easily changed by adjusting the power gain of the EDFA.

In Figure 5.11, three spectra of 10th order beat-notes captured by the oscilloscope under various EDFA gains are given. Peaks and notches are observed due to the multi-recirculation effect from the LC-RDSHI and agree with theoretical calculations. But in practice, controlling the EDFA gain precisely to be a fixed value is difficult. Polarization and environmental perturbations also contribute to the performance of the system. However, it is still possible to find an optimum point where the multi-recirculating effects are small enough to be observed through the oscilloscope, such as the first spectrum.

5.2.4 System intensity control

The NP laser is designed to have a constant output power and the power fluctuation is smaller than 0.05% over 14 hours. In our measurement, we put a VOA after the laser to change the system input power. From the analysis in Section 4.2, the intensity change has no effect on laser linewidth. In order to demonstrate this conclusion by experiment, we recorded several orders of beat-notes under different power levels, as shown in Figure 5.12.

Based on this assumption, we can change the value of VOA to avoid nonlinear effects in the optical fiber loop and maintain a high signal to noise ratio (SNR) of the system without broadening the laser linewidth.

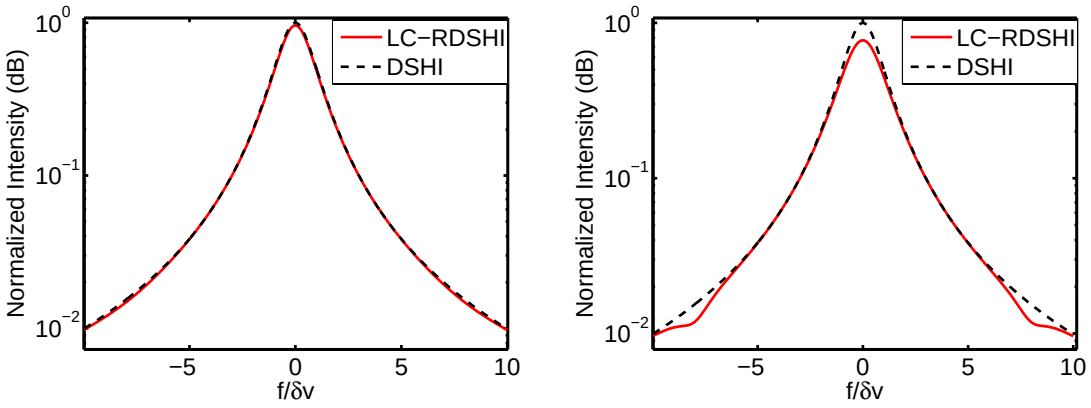

(a) $\gamma = 0.09$ (b) $\gamma = 0.45$

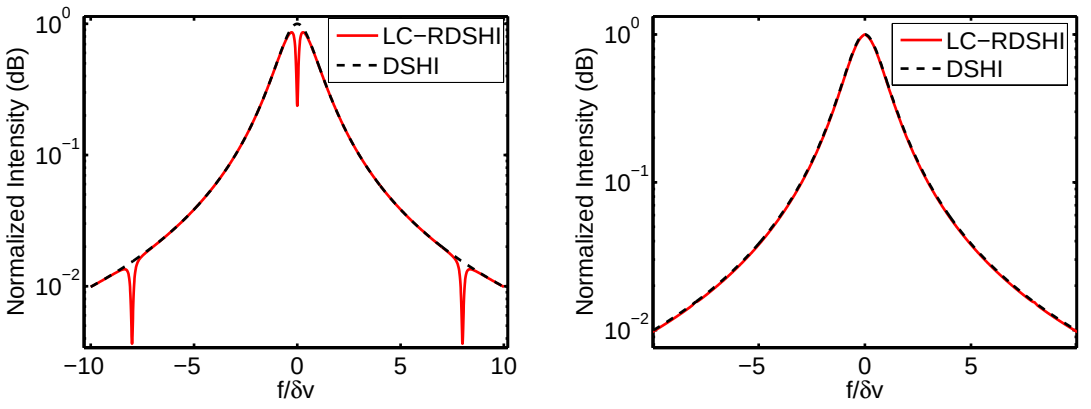

(c) $\gamma = 0.93$ (d) $\gamma = 0.95$

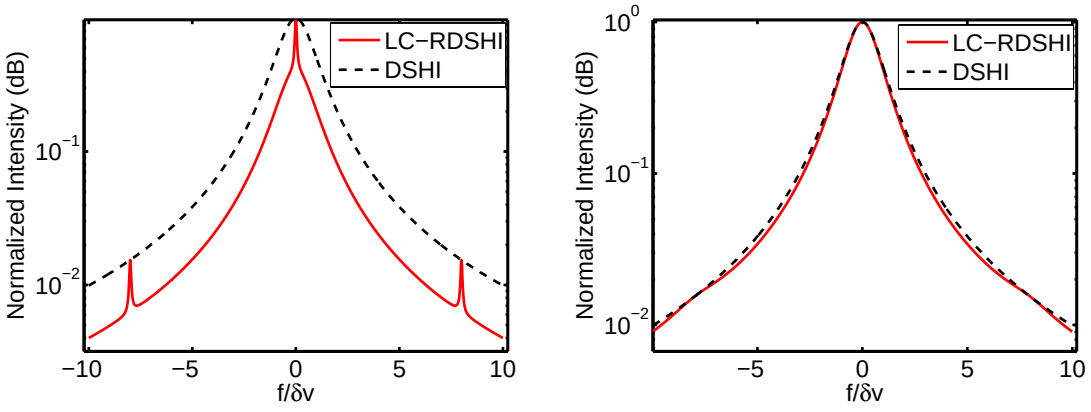

(e) $\gamma = 0.96$ (f) $\gamma = 3.5$

Figure 5.10: Normalized spectrum intensity from a LC-RDSHI with different values of γ

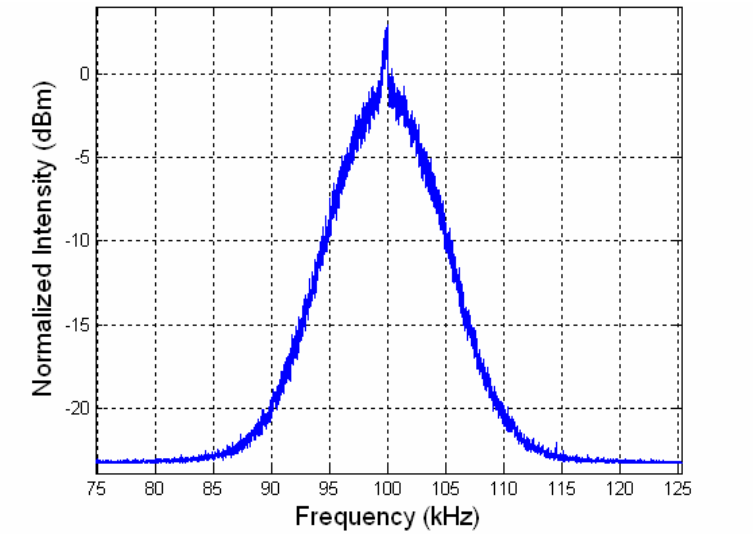

(a) $VOAI = 12dB$, $EDFA \quad gain = 15dB$

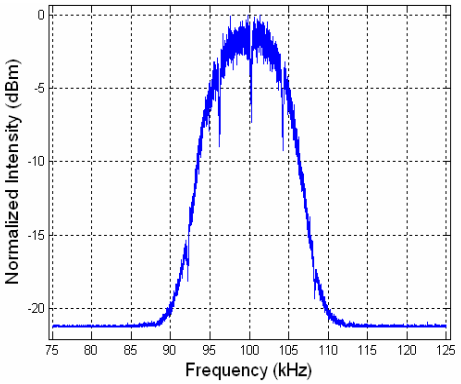

(b) $VOAI = 8dB$, $EDFA \quad gain = 20dB$

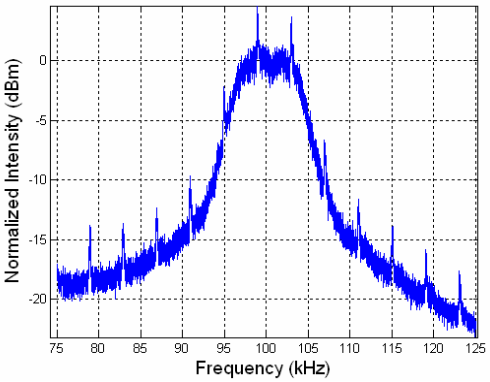

(c) $VOAI = 8dB$, $EDFA \quad gain = 21dB$

Figure 5.11: Experiment results from LC-RDSHI with different values of γ

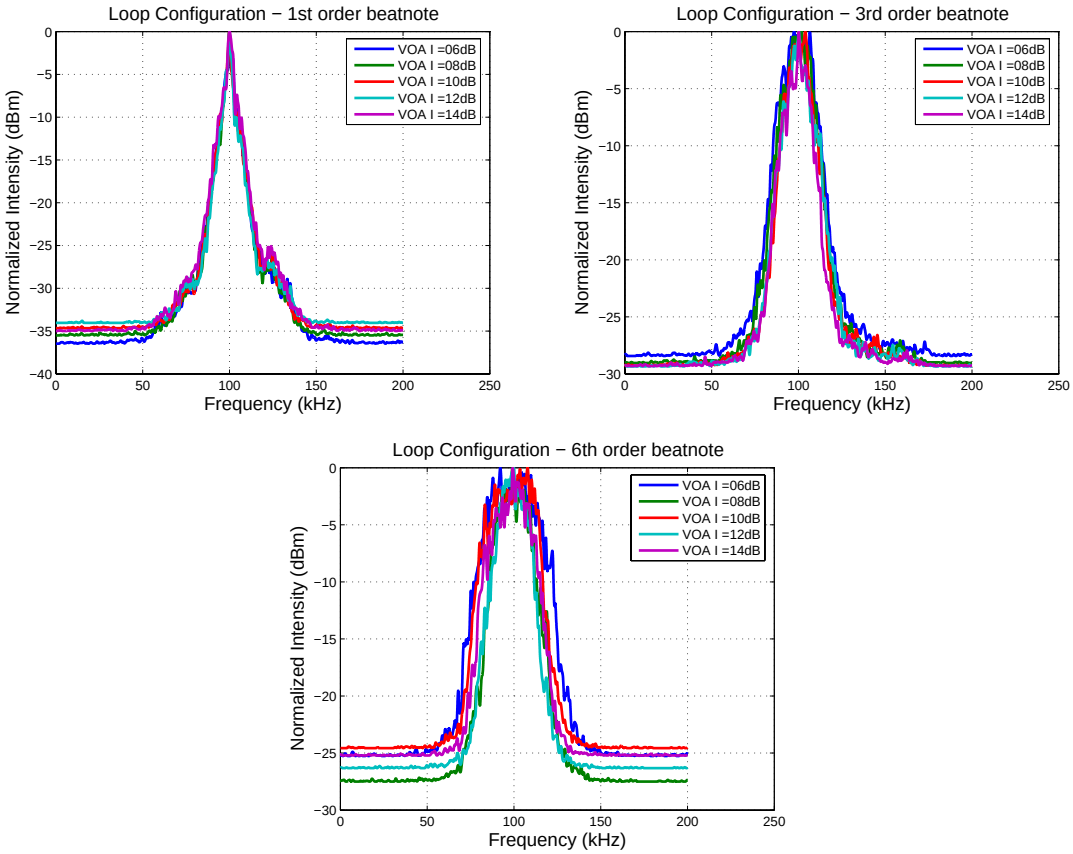

Figure 5.12: Experimental examination of the relationship between laser linewidth and system intensity

Nonlinear effect

The spectrum of the recirculated light in the fiber loop may also be affected by the optical nonlinearities of the fiber. Special care needs to be taken to minimize this effect to obtain desirable measurement accuracy. The main nonlinearity effects in a communication grade silica fiber include stimulated Brillouin scattering (SBS), stimulated Raman scattering (SRS) and Kerr effect[43].

SBS and SRS are similar in a sense because both manifest through the generation of a Stokes wave downshifted from the frequency of the incident or pump light wave by an amount determined by the nonlinear medium. Consequently, part of the energy from the pump wave is transferred to the Stokes wave. However, for both the SBS and SRS, this energy transfer only happens when the pump power exceeds a threshold level. The Brillouin and Raman thresholds are $P_{SBS}^{th} \approx 2mW$ and $P_{SRS}^{th} \approx 800mW$ for a standard single mode fiber. Since the laser power needed in the measurement is much less than the Raman threshold, only the SBS needs to be considered. The SBS can affect the system in two ways. First, the signal power can be lost significantly due to the power transfer to the Stokes wave; secondly, the first order Stokes wave could generate high order Stokes waves co-propagating with the signal light at different light frequencies, thus degrading the SNR and causing a measurement error; In order to avoid the SBS effect, the power P4 of the light at the output port 4 of the fiber coupler, which is the power injected into the fiber loop, must be controlled to be lower than the SBS threshold (See Figure 5.1). Assuming the power from the laser source is P0, we have $P_4 = P_0(1-\alpha)/(1-\gamma)$. Letting $P_4 < P_{SBS}^{th}$, the maximum power input to the coupler is given by

$$P_0 < P_{SBS}^{th}(1-\gamma)/(1-\alpha), \tag{5.4}$$

Choosing typical numbers of $\alpha = 0.9$ and $\gamma = 0.95$ and $P_{SBS}^{th} \approx 2mW$, Equation (5.4) gives $P_0 = 1mW$. For laser sources with greater output power, an optical attenuator can be used before the fiber coupler to control the power to avoid the SBS occurrence.

The nonlinear Kerr effect is discussed in Chapter 6.

EDFA ASE noise

One concern with having the EDFA in the fiber loop is that the signal spectrum is broadened as the EDFA introduces extra phase noise into the signal every time when it passes through the EDFA, which had been a well-accepted assumption[44, 45, 46, 47, 48]. However, recent experimental and theoretical analysis indicates that this is not true and an EDFA only adds an additive white noise (ASE noise) on the signal[49, 50]. Without considering the nonlinear Kerr effect caused by the power fluctuation of the fiber delay loop, this additive white noise does not change the linewidth of the signal rather only elevates the background noise level, which does not impose a threat to the linewidth measurement. Assuming n_0 is the ASE power added to the signal after one pass of the EDFA, the total ASE power in the fiber loop, n_T, is thus obtained by the summation of the ASE power introduced at each recirculation round, and is given by[51, 52]:

$$n_T = n_0 + \gamma n_0 + \ldots + \gamma^n n_0 = n_0/(1-\gamma)^n, \tag{5.5}$$

The ASE noise power of an EDFA is given by[51, 52]

$$\Delta S_0(\omega) = N_{sp} h f_0 (G-1), \tag{5.6}$$

where N_{sp} accounts for incomplete population inversion ($N_{sp} = 1$ for complete inversion), h is Planck's constant, f_0 is the central frequency of the light wave and G is the gain of the amplifier. A band-pass optical filter with a bandwidth of B_0 is placed after the EDFA to suppress the ASE noise. The noise added by one pass of the EDFA is therefore given by

$$n_0 = N_{sp} h f_0 (G-1) B_0, \tag{5.7}$$

The total ASE noise power is calculated using the following illustrative numbers: $\gamma = 0.95$, $B_0 = 0.4nm(50GHz)$, f_0 is the frequency of a light at wavelength of 1550nm and $Nsp = 2$. The gain of the EDFA is set to be $20dB$ to compensate for the 25 km fiber loss, the insertion loss of the AOMs, the coupling loss from the fiber optic coupler and other losses. The calculated total ASE power is 0.01 mW, which is less than the signal power by about two

orders of magnitude. Therefore ASE noise is negligible. When a different broadband fiber amplifier, such as a Raman amplifier, is used for a broader range of spectral capability, the same conclusion still holds. Therefore, there is a trade off between avoidance of nonlinear effect and keeping a high SNR by setting a proper value of the VOA.

5.2.5 Polarization control

It is well known that single-mode optical fiber (SMF) support two distinct orthogonal polarization modes[37, 53]. Without any perturbation, the attenuations of these two modes are identical. This means that the total attenuation of the fiber can be considered insensitive to the polarization state at the fiber input. But the polarization state of light in SMF is very sensitive to any perturbation which is not symmetric about the fiber axis[53]. At the same time, optical links are made up of more than simple fibers and usually different components are required, i.e., couplers, isolators, filters, multiplexers, and amplifiers. All these components present indeed a small anisotropy and are subject to polarization dependent losses (PDL) that eventually will affect the system's performances.

If we consider the LC-RDSHI an optical interferometer, the state of polarization (SOP) of the signals from the two arms of the interferometer becomes critical. Because SOP will directly affect the interference efficiency. The two light beams from the two arms cannot be orthogonal.

If we consider the LC-RDSHI a transmission system, PDL leads to more concerns. There are several conclusions regarding the PDL of a fiber optic system obtained by other researchers through experiments and theoretical calculations. First is that the total PDL of a series of concatenated elements is usually different from the sum of each single PDL-element contribution. The reason has to be ascribed to the fact that the polarization sensitive axes of the single components are not always necessarily aligned with each other. Therefore, the resulting total PDL depends on the relative orientations of the PDL axis at each connection[53, 54]. The second conclusion of system PDL is that the total accumulated PDL

is Maxwellian distributed (in decibels) with the accumulation of the mean PDL growing linearly with the system length[37, 55, 56]. The third conclusion is related to the recirculating loop. Due to the periodicity of the recirculating loop system, polarization phenomena are quite different from the one in optical straight-line systems. Studies reveal that the mean accumulated PDL is found to grow linearly with the number of circulations N in contraposition to a straight-line system. And the statistical distribution tends to become uniformly distributed as N is increasing[53].

A LC-RDSHI system involves both an optical interferometer and a recirculating loop. The SOP of the loop output and PDL of the loop seriously affect the beat signals. Especially the polarization fading effect caused by fiber birefringence, as analyzed in Section 4.3 has to be considered. Here we consider two extreme examples of the output of the LC-RDSHI as shown in Figure 5.13 to verify the conclusion in Section 4.3. The interference efficiency of the two optical beams decreased dramatically if the SOP of the two beams turned out to be orthogonal.

In a practical situation, various birefringence perturbations, both internal and external, can be introduced to the fiber. The output polarization will appear uncorrelated to the input polarization after only a few meters of propagation. Their numbers, strengths, orientations, and distributions are generally unknown and, moreover, they will usually vary with time as environmental conditions change. Therefore, mitigation of the polarization-related impairments must be dynamic and adaptive to random variations. Most polarization controllers can only stabilize the slow fluctuation of the polarization. However, it can be shown that unperturbed single-mode fiber can perform the same function as polarization-maintaining fiber in certain situations though the precautions must be taken to guard against perturbation of the SMF[57]. Therefore, during the experiment in lab, when the system connection is finished, moving, or twist of some portion of fiber, or patch cords will be helpful to find the best beat efficiency. As long as the best beat signal is obtained, environmental vibration, perturbation and moving should be avoided in order not to induce fast SOP changes.

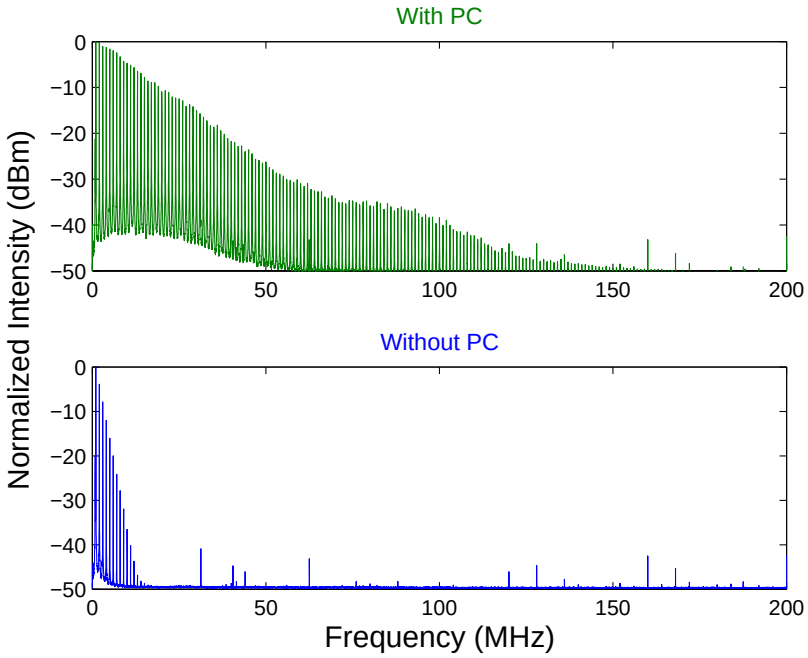

Figure 5.13: Effect of state of polarization

5.2.6 Environment perturbation control

Vibrations, acoustic noises and temperature fluctuations are potential factors to broaden the measured laser linewidth. And we found that the LC-RDSHI system is sensitive to environmental noises through a simple experiment. When a 6Hz mechanic pump was turn on besides the LC-RDSHI system, the SOP and the system power exhibits clear changes, as shown in Figure 5.14.

The isolation system is, therefore, set up to avoid the serious effects caused by the environmental noises. As shown in Figure 5.15, the fiber spools are put into a wood box with thick acoustic and thermal proof foam on the inner surfaces of the wall. The whole wood box is then placed on an optical table. We measured the temperature in the box. The temperature fluctuations at four randomly chosen points in the box are 2.87×10^{-6} $^{\circ}C/s$, 3.20×10^{-6} $^{\circ}C/s$, 3.30×10^{-6} $^{\circ}C/s$ and 3.27×10^{-6} $^{\circ}C/s$.

Though we carefully isolated the fiber delay line from environmental perturbation, the

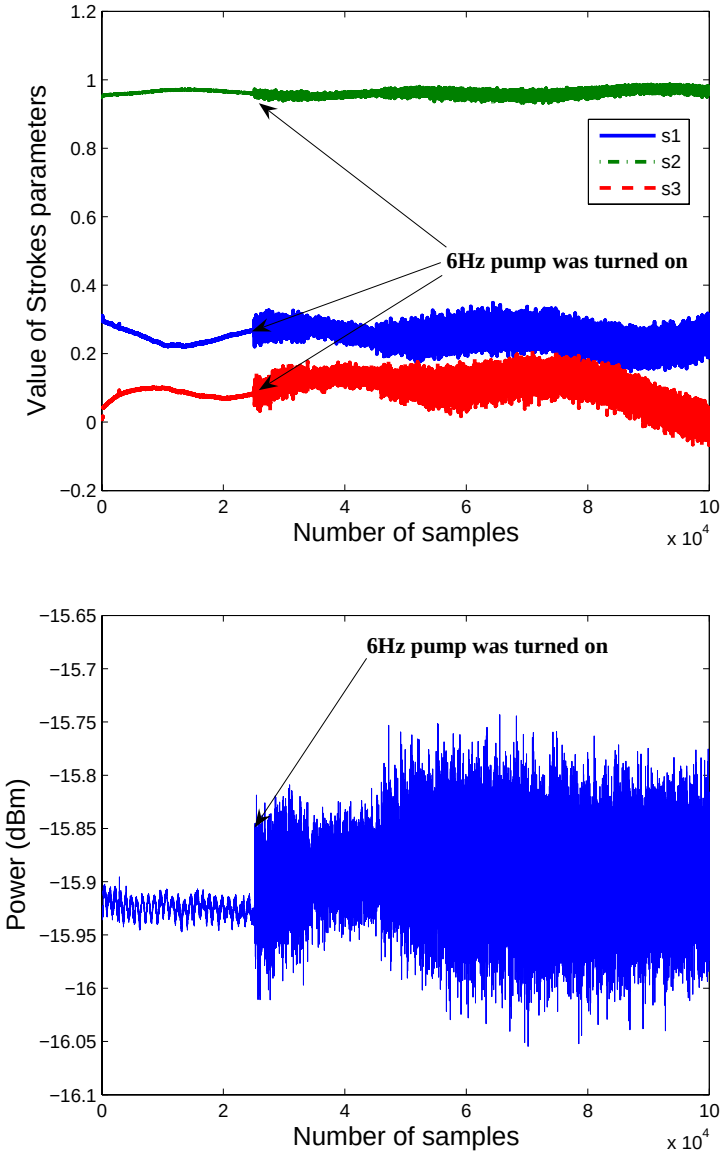

Figure 5.14: Environment sensitivity of LC-RDSHI

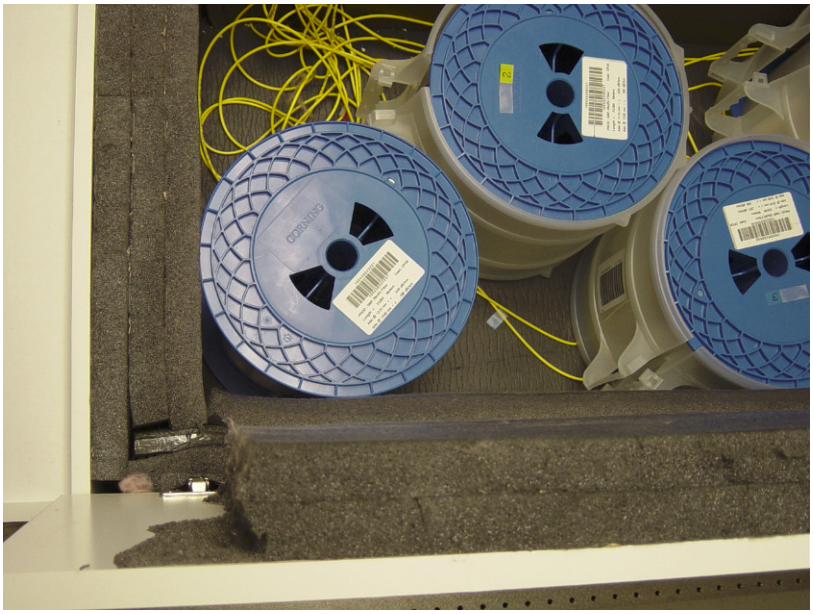

(a) Topview, inside

(b) Sideview, outside

Figure 5.15: Isolation system

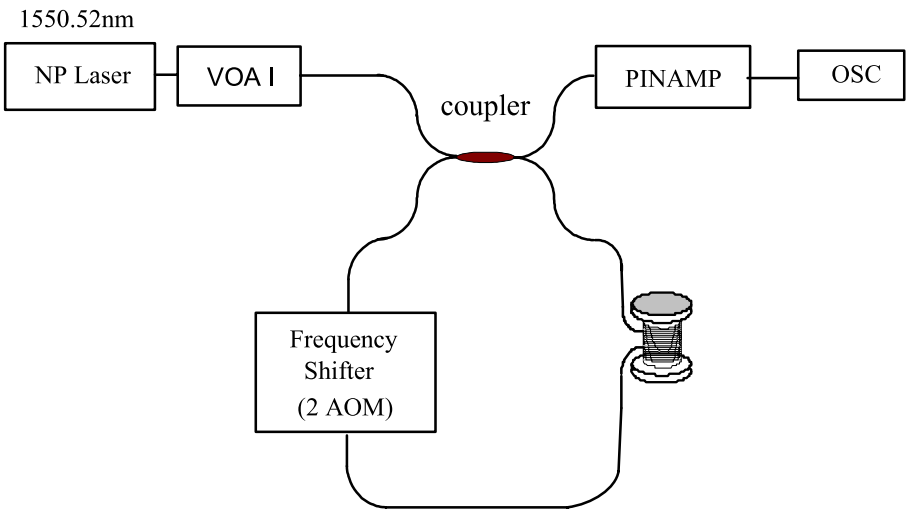

Figure 5.16: Schematic for identify environment induced noises

laser under test is also affected by the environment. We simplified the system to make it easy to identify environmental noise, as shown in Figure 5.16. Four orders of beat-notes can be obtained from this setup since there is no EDFA in the loop. We then measured the central frequency fluctuation of each order. In Table 5.1, standard deviation of the central frequencies recorded at different time slot are listed. In daytime (4:00pm), the environmental perturbations mainly due to the heavy traffic outside the building, a fitness center downstairs, and activities inside the lab. In midnight (1:00am), there is less traffic, less lab activities and the fitness center downstairs is closed. The frequency noise is reduced according to our experiment results shown in Table 5.1. Proper isolation is also helpful to further reduce the vibration, as shown in column (1:00am(2)) when we wrap the fiber spool with acoustic isolation polymer-fiber.

5.2.7 Effect induced by the mixer circuit

The mixer circuit used in the analysis of power spectrum of each order beat-note maybe another source of frequency noise. One input of the mixer,f_1, is generated by the frequency generator. Its standard deviation can be referred to $f_{1,std}$. The other input of the mixer is

Table 5.1: Effect of Environmental Conditions

Std (kHz)	4:00pm	1:00am	1:00am (2)
1st order	1.8	1.5	1.1
2nd order	4.8	2.2	1.5
3rd order	10.0	4.6	3.3
4rd order	14.6	8.4	4.6

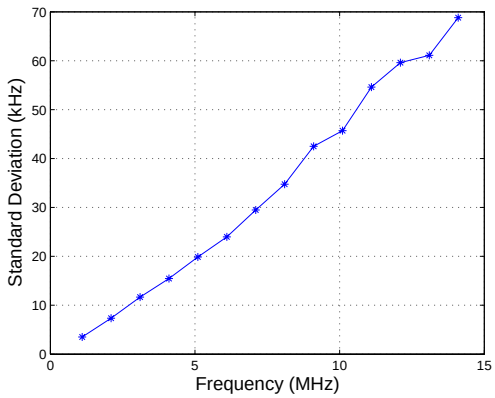

Figure 5.17: Stability of RF Frequency Source for mixer

from the photo detector (PD). We define the central frequency of each order of beat-note as f_2. The central frequency of the mixer output (after a low pass filter) then can be written as: $f_1 + f_{1,std} - f_2$. As we analyzed in Section 4.4, the central frequency jitter broadens the laser linewidth when we have to do 100 times average to obtain high quality spectrum by using an oscilloscope. In Figure 5.17, the standard deviation of the frequency generator was measured. The frequency noise increased with the increase of generated frequency, therefore, with the increase of the beat-note order. The best frequency source (Agilent 33120A with the stability of $\pm$1ppm) in lab was used in the experiment.

Chapter 6

Signal Processing and Result Interpretation

When laser linewidth gets narrower and its coherent length gets longer, the LC-RDSHI method becomes more powerful than other methods. Though we have not examined the ultimate limitation of this method from the experiment, we expect that the laser linewidth on the order of 100Hz can be measured. By using the LC-RDSHI, we can obtain more than 100 orders of beat-notes. If the fiber delay per loop is 25km, 100th order beat notes represent the coherent length of 2500 km, therefore, LC-RDSHI has the potential to measure the linewidth as narrow as 25Hz.

6.1 Frequency domain - spectrum

Since the maximum bandwidth of the oscilloscope used is 500MHz, the highest resolution for 100 orders of beat-notes with 1MHz frequency shift is 500kHz. This resolution cannot make us observe the details of the laser linewidth which is on the order of 100Hz. An electronic mixer is used to further move down the beat note frequencies to a much lower

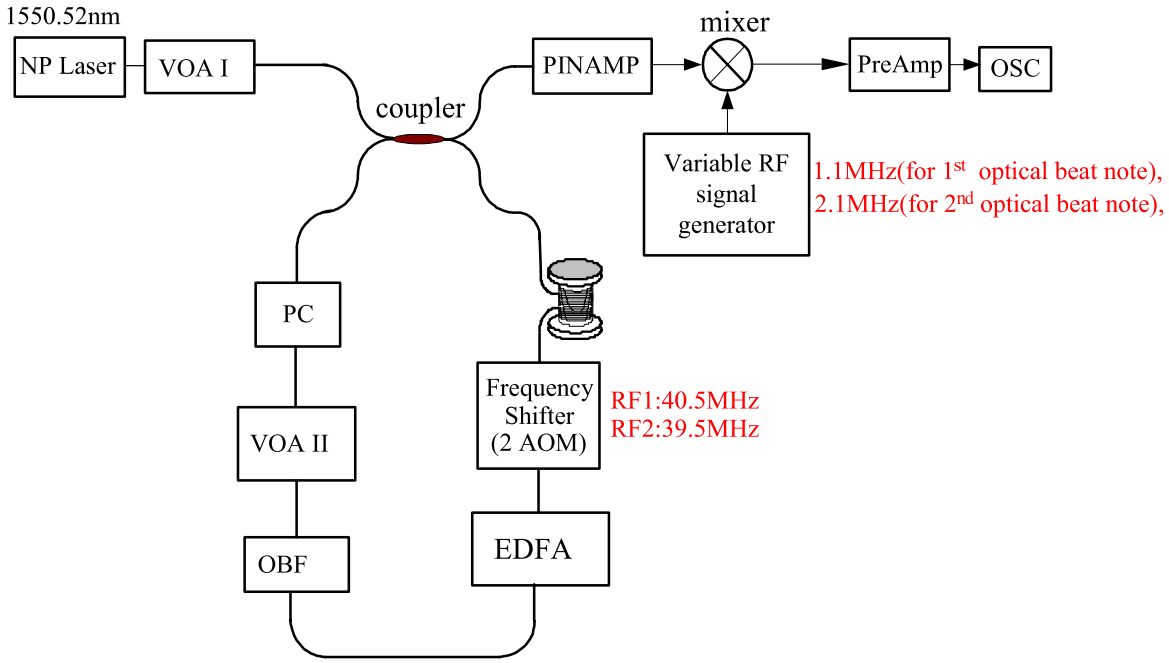

Figure 6.1: Schematic of LC-RDSHI with a mixer

frequency. One input of the mixer is the detected signal from the PINAMP containing all the orders of beat-notes at 1MHz, 2MHz, 3MHz and so on. When we observe the first order beat-note, the variable signal generator gives 1.1MHz sinusoidal signal to the other mixer input, the output of the mixer gives a downshifted signal at 100kHz (1.1MHz-1MHz) to the preamplifier. In order to observe the linewidth of the second order beat-note, the variable RF signal generator sends a 2.1MHz signal to the mixer, and so on. The highest resolution we can achieve by using the same oscilloscope is 0.001Hz. We show the complete system setup in Figure 6.1.

The first task we need to do after the setup of the system is to select proper parameters of the system. We here set the VOAI=12dB and EDFA working in the constant gain mode with its gain=15dB. The upshift AOM is set at 40.5MHz and the downshift AOM at 39.5MHz, therefore the frequency shift of the system is 1MHz for each revolution of light propagation. The next important task is to control the polarization. When the best beat-notes are achieved, the polarization controller (PC) is turned on and the whole system must be

Table 6.1: LC-RDSHI linewidth relations[5]

Measured Full-Width Point	**Displayed Width**
-3dB	$2\Delta\nu$
-10dB	$2\sqrt{9}\Delta\nu$
-20dB	$2\sqrt{99}\Delta\nu$

maintained stable. In Figure 6.2, 12 orders of beat-notes are demonstrated. The linewidth of beat-notes continue to broaden with increases in the time delay.

6.1.1 20dB down direct measurement

Considering the broadening effect of 1/f frequency noise, more accurate laser linewidth can be obtained 10dB or 20dB down from the maximum of the lineshape if the signal and noise levels permit. Because the broadening effect of the 1/f noise is most pronounced near the center of the spectral lineshape[26]. For Lorentzian lineshape, the 3dB linewidth can be inferred from the displayed lineshape by using the relationship shown in Table 6.1.

We obtain the laser linewidth from 20dB down from the maximum of the width of the displayed beat-notes and plot in Figure 6.3 for different orders of the beat-notes. The laser linewidth tends to be a constant (910Hz) after the 6th order of the beat-note. The coherence length of the laser therefore can be calculated from[26]:

$$L_c = v_g \tau_c = v_g \frac{1}{\pi \Delta\nu}, \tag{6.1}$$

where $v_g = c/n_g$ is the velocity of the light in the fiber, c is the light speed, and n_g is the refractive index of the fiber. Therefore, the coherence length of the NP laser is 69.9km.

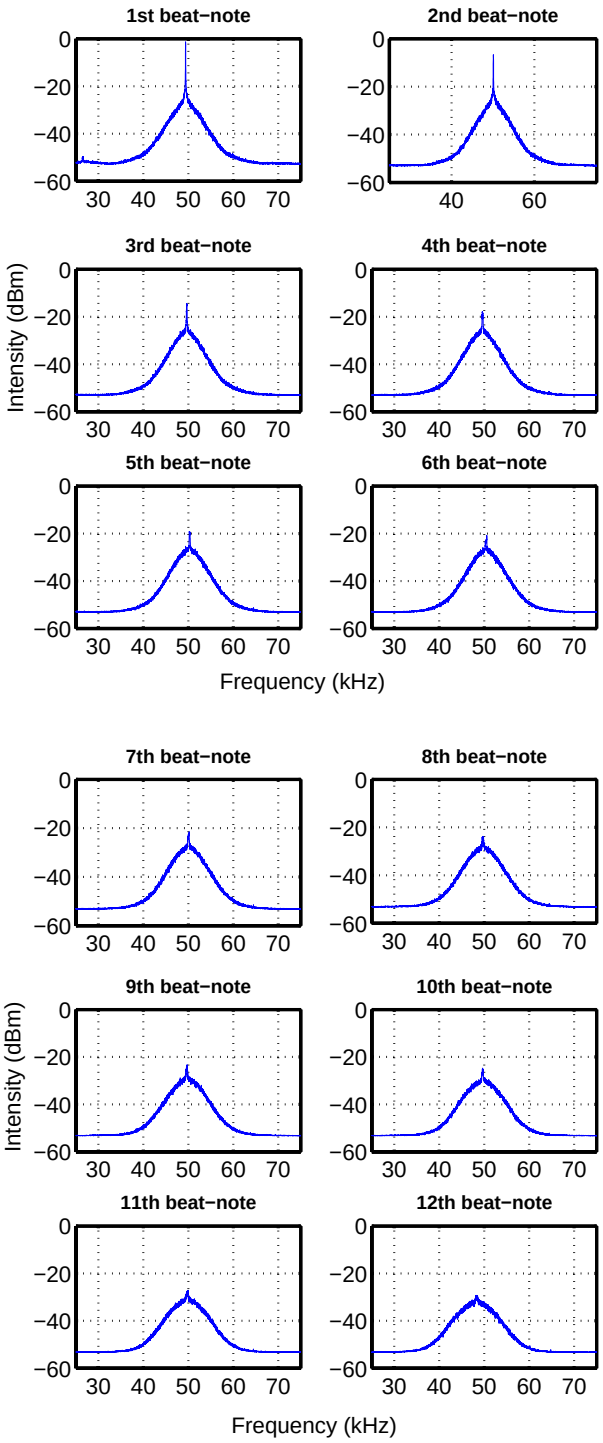

Figure 6.2: 12 orders of beat-notes obtained from LC-RDSHI

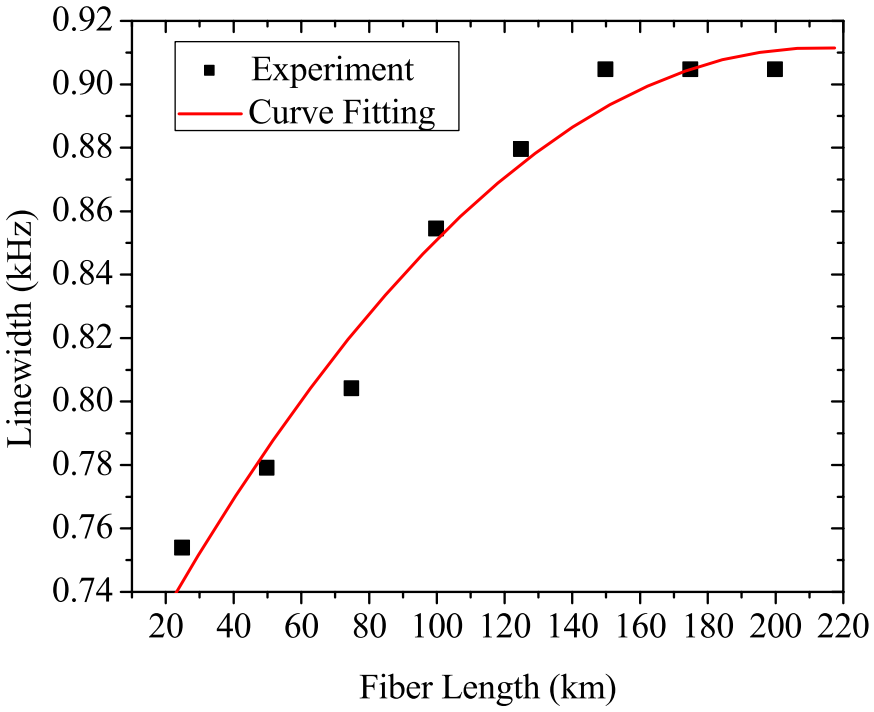

Figure 6.3: Dependence of laser linewidth on fiber delay

6.1.2 Voigt curve fitting method

In the LC-RDSHI system, the spectrum of each order of beat-note is Voigt profile, which is the convolution of the Lorentzian spectrum associated with the white frequency noise and the approximately Gaussian spectrum arising from the 1/f noise. The second method to extract Lorentzian linewidth is to use the curve fitting Voigt profile method. The Voigt spectrum can be expressed as[58]

$$I(\nu) = \int_{-\infty}^{\infty} G(\nu')L(\nu - \nu')d\nu', \tag{6.2}$$

where G is the normalized Gaussian lineshape centered at $\nu = 0$, and

$$G(\nu) = \frac{\sqrt{4\ln 2}}{\sqrt{2}\Delta\nu_{GF}} \exp[-(\nu\sqrt{4\ln 2})^2/\Delta\nu_{GF}^2], \tag{6.3}$$

where $\Delta\nu_{GF}$ is the full width at half-maximum (FWHM) of the Gaussian function. L is the normalized Lorentzian function centered at $\nu = 0$ as

$$L(\nu) = \frac{\Delta\nu_{LF}}{2\pi}\frac{1}{(\nu-\nu_0)^2 + \Delta\nu_{LF}^2/4}, \tag{6.4}$$

The Voigt profile function can be manipulated into an expression in terms of the complementary error function of complex argument, $erfc(z)$, as [58, 59]

$$V(u,a) = Re[\exp(z^2)erfc(z)], z = a + iu, \tag{6.5}$$

where

$$a = \sqrt{\ln 2}\Delta\nu_{LF}/\Delta\nu_{GF}, \tag{6.6}$$

$$u = 2\sqrt{\ln 2}(\nu-\nu_0)/\Delta\nu_{GF}, \tag{6.7}$$

Automatically fitting program is made to fit the captured data with 95% confidence. In Table 6.2, the Lorentzian linewidth and Gaussian linewidth are obtained by Voigt curve fitting the spectra shown in Figure 6.2. It is clearly shown that the noise spectrum of the laser under test is the white noise dominant. The Lorentzian linewidth is 680 Hz from this method. The broaden linewidth of the first three orders of beat-notes is due to strong relaxation oscillation (RO). RO, centered at 800kHz for the NP laser, raises the noise floor of the beat-notes and generates additional phase noise.

The 20dB direct measurement and the Voigt curve fitting method give different Lorentzian linewidth values can be explained through Figure 6.4. As shown in Figure 6.4, when the Lorentzian linewidth is 680Hz, if the laser noise spectrum contains a much greater Gaussian component (4.5kHz), 20dB down direct measurement infers a larger value of the linewidth. If the Gaussian linewidth is smaller than 680Hz, 20dB down direct measurement provides a simple way to infer the Lorentzian Linewidth. This is why the 20dB down method is widely used in linewidth measurement of semiconductor lasers which have their Lorentzian linewidth greater than the Gaussian linewidth. But for ultra-narrow linewidth lasers, the 20dB down method may over-estimate the Lorentzian linewidth.

Table 6.2: Lorentzian linewidth and Gaussian linewidth obtained from Voigt curve fitting

Order of beat note	$\Delta\nu_{LF}(kHz)$	$\Delta\nu_{GF}(kHz)$
1st	0.75	4.6
2nd	0.75	4.5
3rd	0.74	4.7
4th	0.68	4.8
5th	0.68	4.8
6th	0.68	5.1
7th	0.68	5.1
8th	0.68	5.1

As we mentioned in Chapter 5, the environmental perturbation isolation has its limitation. The Voigt curve fitting method provides an effective way to further isolate the environmental noises through the signal processing. This method is useful for all types of lasers.

6.1.3 Fiber non-linearity induced phase noise

The Kerr effect is a change in the refractive index of a material in response to an electric field of light. Its physical origin is a nonlinear polarization generated in the medium, which itself modifies the propagation of the light[22]. The refractive index for the high intensity light beam itself is modified according to

$$\Delta n = n_2 I, \tag{6.8}$$

with the nonlinear index n_2 and the optical intensity I. Fused silica, as used e.g. for optical fibers, has a nonlinear index of about $3 \times 10^{-16} cm^2/W$[22]. The description of the Kerr effect via an intensity-dependent refractive index is actually based on a certain approximation, valid for light with a small optical bandwidth[22]. Unlike the SBS and SRS, which exhibit

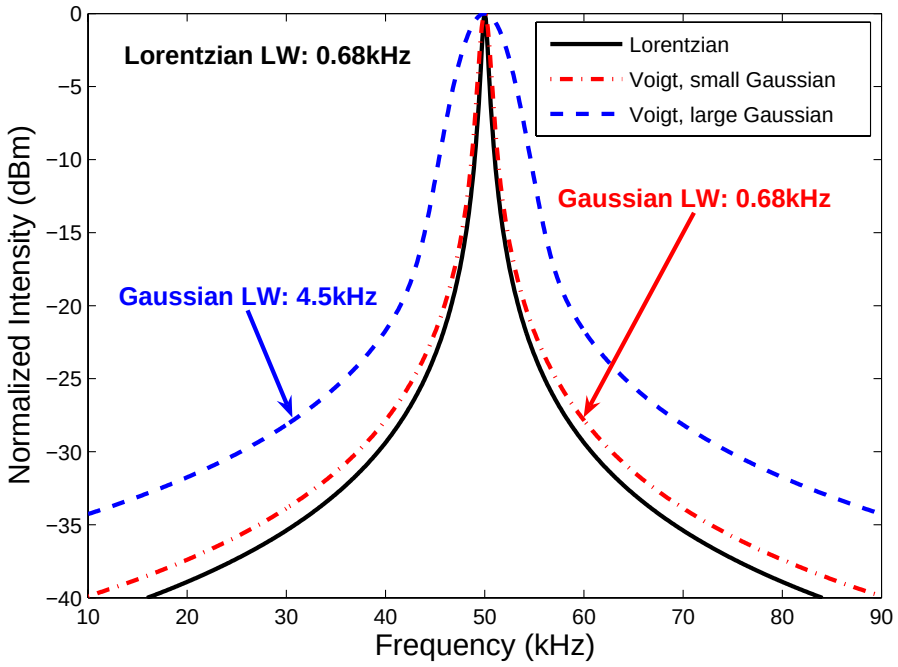

Figure 6.4: Voigt profile with different Lorentzian linewidth and Gaussian linewidth

a "threshold" property, the Kerr effect can accumulate during the light transmission along the fiber.

In the LC-RDSHI system, the electrical field passing through the fiber delay is the output from port 4 of the coupler, $E_4(t)$. Continuing the analysis in Section 4.1, $E_4(t)$ can be expressed as

$$\begin{aligned} E_4(t) &= j\sqrt{1-\alpha}E_1(t) + \sqrt{\alpha}E_2(t) \\ &= j\sqrt{1-\alpha}E_1(t) + j\sqrt{1-\alpha}\sum_{n=1}^{\infty}\gamma^n E_1(t-n\tau_d)e^{jn\Omega t}, \end{aligned} \tag{6.9}$$

It is clearly shown in Equation (6.9) that the fiber delay in the loop experiences amplitude fluctuations. The loop power measured by the polarization controller (Figure 6.5) gives the same conclusion. The amplitude fluctuation changes the refractive index of the fiber material due to the Kerr effect. Phase noise can be thus generated from the Kerr effect.

ASE noises generated by the EDFA are also accumulated and increase amplitude fluctuation to the transmission signal[44, 45, 46, 47, 48, 60, 61]. The amplitude fluctuation is caused by the in-phase components of spontaneous emission. Such noise directly increases the linewidth of the signal. The interaction between the Kerr effect and spontaneous emission increases the phase noise of the signal light[61]. Linewidth broadening, $\Delta\nu$ caused by such effects can be calculated from[60, 61]

$$\Delta\nu \simeq \frac{n_{sp}(G-1)^2\alpha L_{tot}h\nu B^2}{8\pi G[\ln(G)]^2}\left(\frac{1}{P_{ave}} + \frac{4}{3}k_2^2 L_{tot}^2 P_{ave}\right), \tag{6.10}$$

where n_{sp} and G are the spontaneous emission factor and gain of the optical amplifier, respectively, α is the attenuation factor of the fiber, L_{tot} the total system length, h the Planck constant, ν the optical carrier frequency, B the system data rate, P_{ave} the pass-averaged signal power over adjacent amplifiers, and k_2 the nonlinear coefficient.

In [62], the Kerr effect was considered by its classical and quantum nature separately. The intensity fluctuation induced the Kerr effect is referred to as a classical behavior. The Kerr effect caused by the spontaneous emission is referred to as the quantum behavior of Kerr

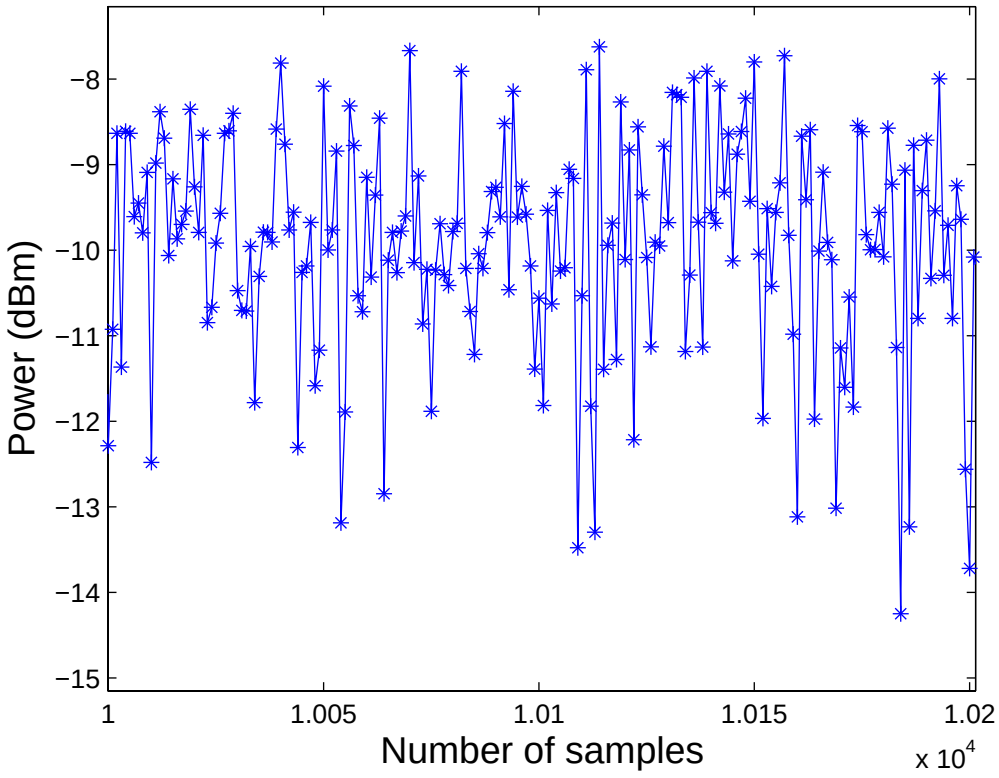

Figure 6.5: Power fluctuation in the loop - Zoomed in data

effect. Usually, the classical Kerr effect due to intensity fluctuation is larger effect than the quantum Kerr effect. Therefore, the phase noise caused by the classical effect is dominant in the LC-RDSHI system.

Linewidth broadening due to fiber non-linearity can be verified by two experiments. The first one is to use the setup shown in Figure 6.6(a,b). In Figure 6.6(a), we bypass the EDFA and other components in the loop to only keep the fiber delay and frequency shifter. Three orders of beat-note can be obtained and shown in Figure 6.7(a). Obvious broadening of the linewidth can be observed. In Figure 6.6(b), we replace the fiber delay with a VOA which only changes the signal intensity but does have the Kerr effect. The spectra of the three orders of the beat-note are shown in Figure 6.7(b). There is no phase noise generated from this setup. Experiments implemented by Makoto Murakami and Shigeru Saito[48] further proved that the classic Kerr effect of fiber either broadens or changes the laser spectral lineshape.

The other experiment to verify the broadening effect caused by fiber non-linearity is to compare the spectrum from a Mach-Zehnder interferometer with that of the recirculating delayed self-heterodyne interferometer. We tried to set up a Mach-Zehnder interferometer with the same fiber delay length, and almost same components in the LC-RDSHI system in order to fully compare the performance of the two system. The Mach-Zehnder interferometer is shown in Figure 6.8. In Figure 6.9, we show the spectrum obtained by both the Mach-Zehnder interferometer and the LC-RDSHI system with the same fiber delay length. It is shown that there is no obvious linewidth broadening in the Mach-Zehnder interferometer. We got the same result as [49, 50]. It is further proved that the quantum behavior of the Kerr effect caused by the ASE, is much smaller than the classical Kerr effect caused by multiple recirculation in the LC-RDSHI system. The phase noise will be significantly increased when the quantum Kerr effect and classical Kerr effects interact with each other.

Time dependence of laser linewidth is the third group of data that support our standpoint. It is well known that flicker frequency noise and environmental perturbation cause Gaussian

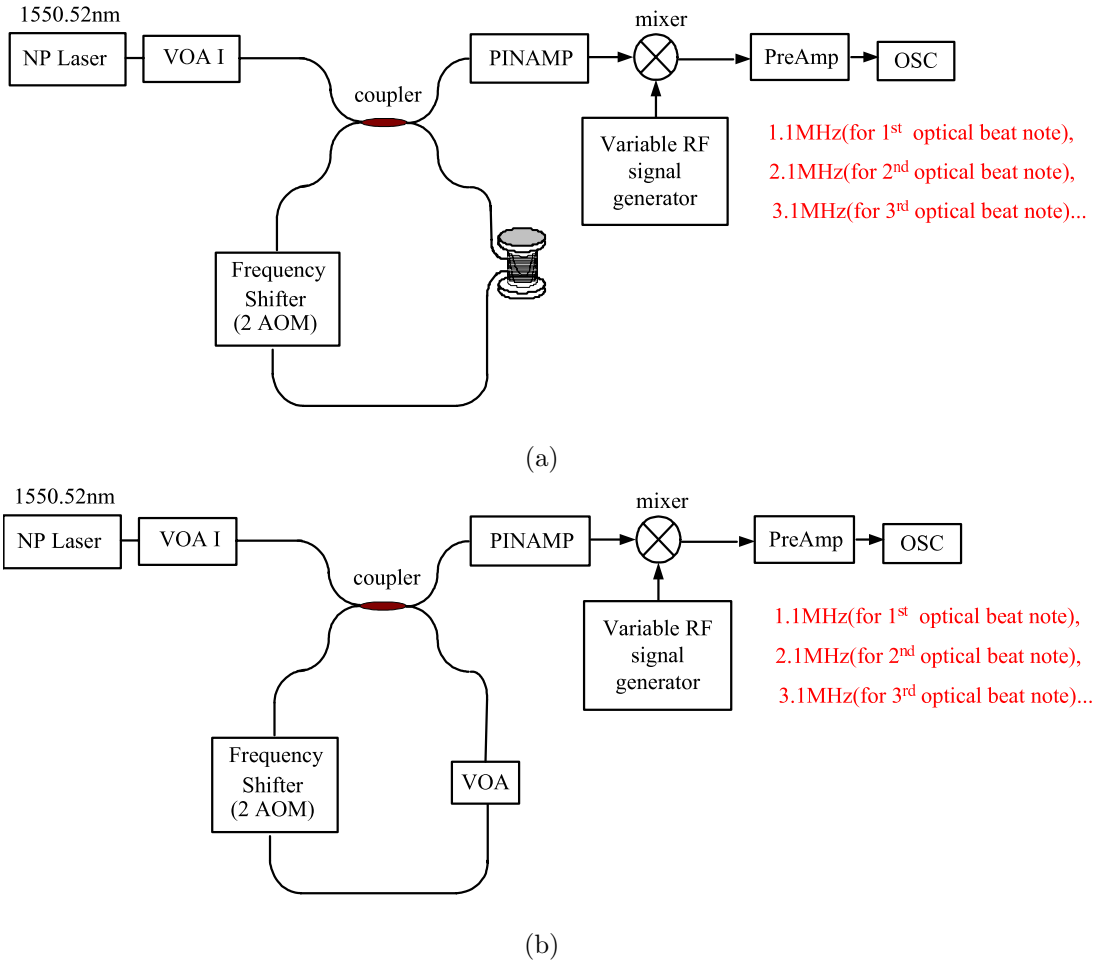

Figure 6.6: Schematic setup to verify the Kerr effect without using an EDFA

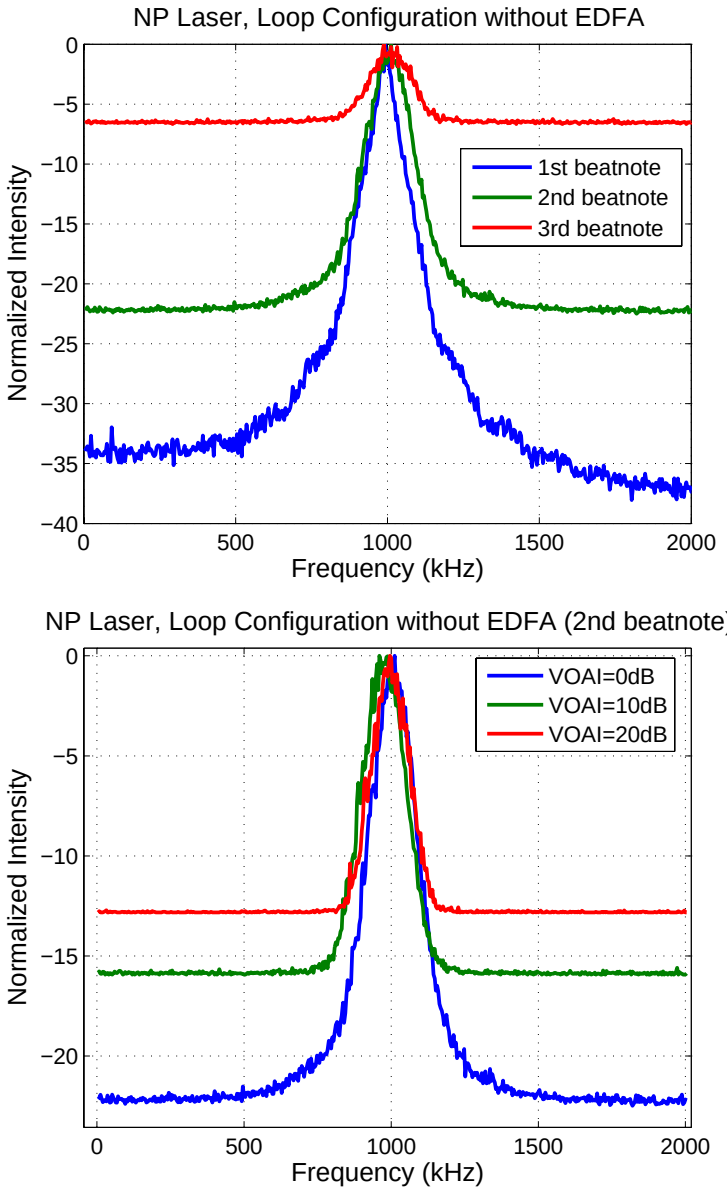

Figure 6.7: Spectrum of beat-note without EDFA in the loop

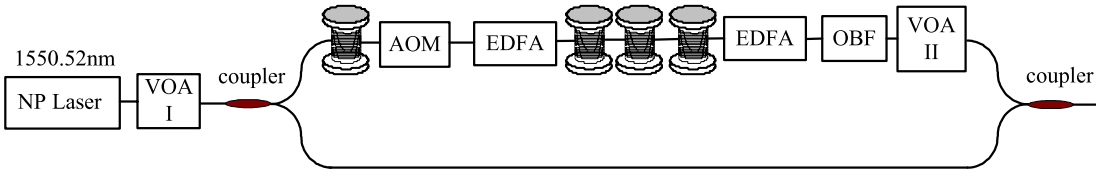

Figure 6.8: Mach-Zehnder interferometer measurement

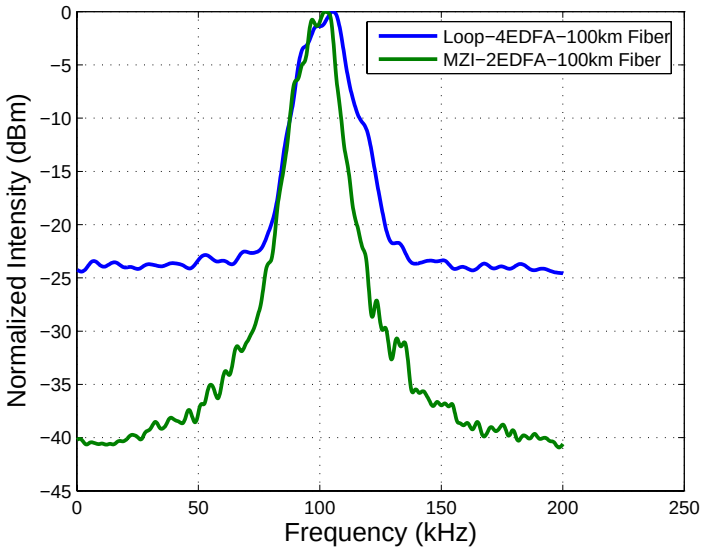

(a) 100km fiber delay

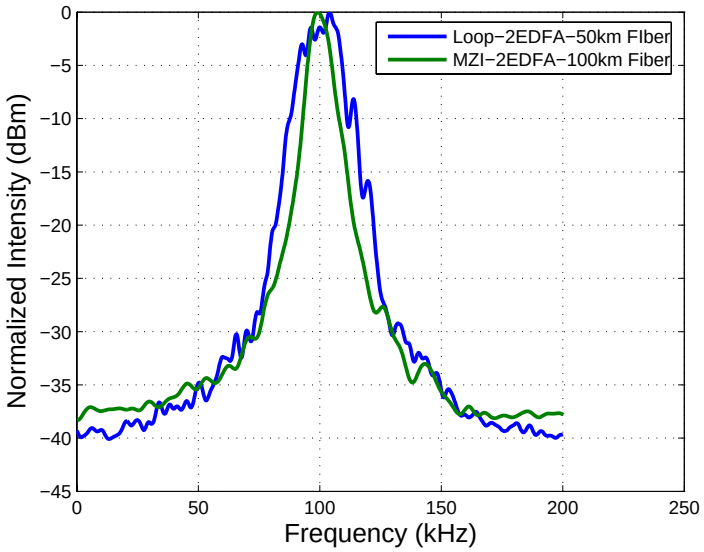

(b) 50km fiber delay

Figure 6.9: Comparison of Mach-Zehnder interferometer and LC-RDSHI

spectral lineshape and the Gaussian linewidth increases with the length increase of fiber delay line. While the Lorentzian linewidth keeps at the same value and is independent with fiber delay length. But our linewidth measurement results shown in Figure 6.10 didn't follow this rule. In Figure 6.10, the spectrum of each order of beat-note was recorded 15 times. In order to increase the reliability of the data, the spectrum capture order is randomly distributed. For example, for the first group of data, the capture order is 1st, 3rd, 6th, 9th and 12th orders of beat-note. For the second group measurement, the capture order is 11th, 8th and 4th orders of beat-notes. Four groups of measurements were conducted and a Voigt curving fitting program was used to extract the Gaussian linewidth and Lorentzian linewidth from each spectrum. It is shown that the Gaussian linewidth becomes randomly distributed and independent on fiber delay while the Lorentzian linewidth keeps broadening with the increase of the fiber delay. We attribute this phenomenon to fiber non-linearity induced phase noise.

An alternative method to measure the ultra-narrow laser linewidth is proposed to overcome the Kerr effect caused by the multiple recirculation. In this new method, we need to add two switches to control the light injection. One switch is put outside of the loop, referred to as transmitter switch. The other one is put inside the loop which is called loop switch, as shown in Figure 6.11. And the time sequence to control the switches is very critical. There must be an ultra-short overlap T (during T, both switches are closed)that makes two beams beat with each other and T must be less than τ_d. The requirements for the optical switches are ultrafast switch speed and high extinction ratio ($> 50dB$). In the time duration that the transmitter switch is open and the loop switch is close, the light circulates in the loop and is detected by the PD. Only the signal to noise ratio is going to decrease as this period of time is getting longer. But there is no intensity fluctuation caused by the recirculating if we consider the ASE noise as an additive white noise. The beat of signals from port 1 and port 3 occurs in T duration and T should be shorter than τ_d in order to avoid coupling the light to the loop while that there is still light circulating in the loop. Since there is no intensity fluctuations detected, no Kerr effect occurs.

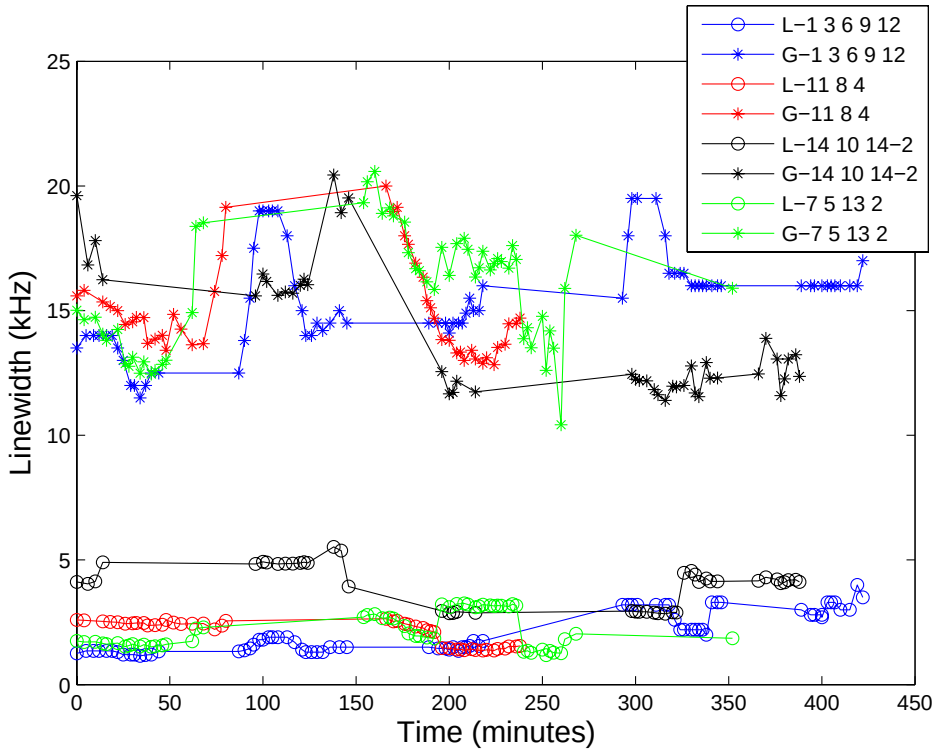

Figure 6.10: Time dependence of laser linewidth. L: Lorentzian linewidth, G: Gaussian Linewidth. Numbers represent the beat-note orders which are ordered in the time sequence of the measurements and 15 sets of data were recorded for each order of beat-note.

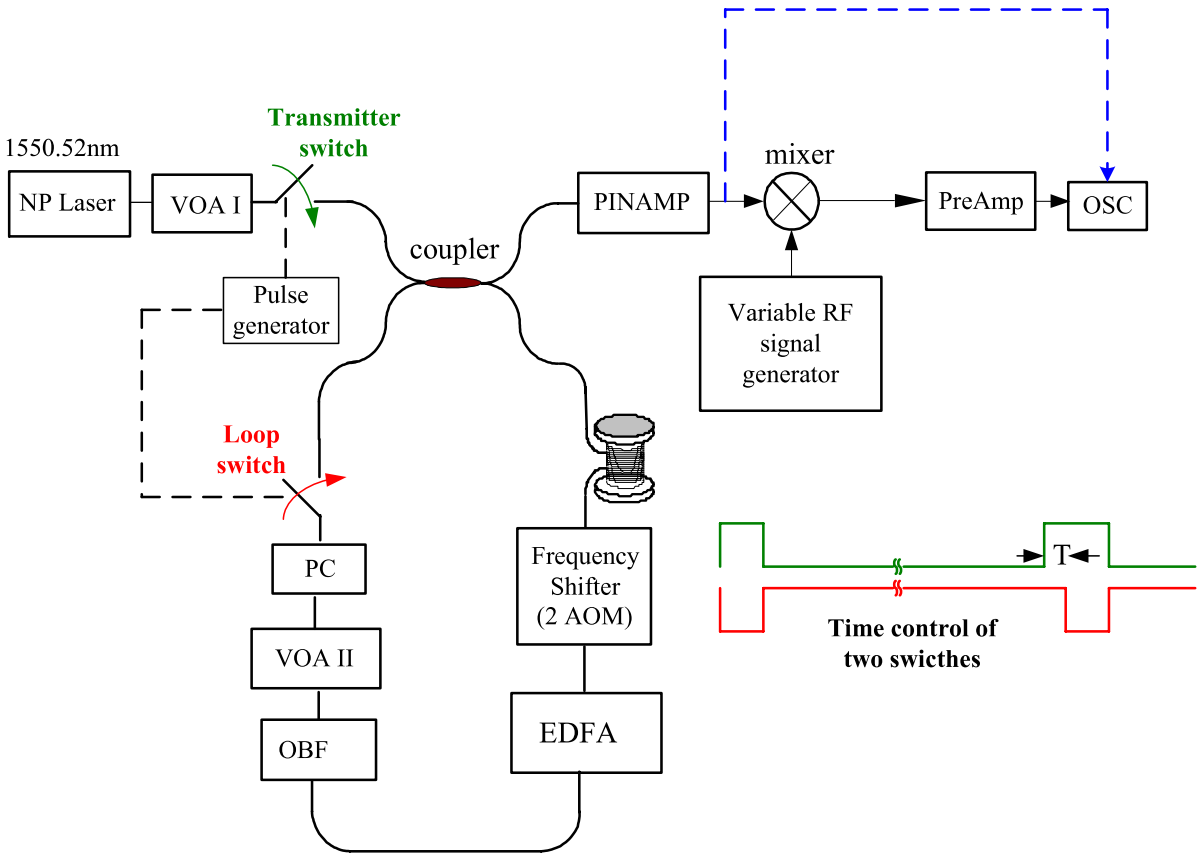

Figure 6.11: Schematic setup to control the Kerr effect

The Kerr effect caused by the ASE noise can be minimized by using a narrower optical bandpass filter to further suppress the ASE noise accumulated in the loop.

6.2 Time domain - Allan Variance

The laser linewidth can also be obtained from frequency fluctuation measurement. Frequency discriminator introduced in Section 3.2 shows that it is one of the methods that can measure the frequency fluctuation directly, but it requires calibration with many factors such as optical power and interferometer sensitivity[3, 63]. With this consideration, time domain frequency analysis of beat-note spectra is therefore used based on LC-RDSHI system. Two-sample (or Allan) variances are calculated for each order of beat-note.

6.2.1 Allan Variance

The conventional sample mean and variance formulas, as shown in Equation (6.11) and (6.12), have been widely used for 'white' noise process which is random and uncorrelated in time.

$$m = \frac{1}{N}\sum_{n=1}^{N}\bar{y}_n, \tag{6.11}$$

$$\sigma^2(N,T,\tau) = \frac{1}{N-1}\sum_{n=1}^{N}(\bar{y}-m)^2, \tag{6.12}$$

where m is the sample mean and y is the sample value. The "bar" over the y in Equation(6.11) denotes the average over a finite time interval. τ in Equation (6.12) is the measurement time of a single sample and the time T is the time interval between consecutive measurements. $T-\tau$ is called dead time.

The power spectral density (PSD) of white noise is constant with Fourier frequency. Noise models whose PSD's are power laws of the Fourier frequency but not integer exponents

are possible as well but not as common. In precise time and frequency measurement, for example, there are two quantities of great interest: instantaneous frequency and phase. If the frequency noise is white noise, the PSD of its phase noise varies as $1/f^2$ (where f is the Fourier frequency), which is commonly called random walk noise. If the PSD of the frequency noise varies as $1/f$ (flicker noise), then its phase would be the integral of the flicker noise. It would be a PSD which varies as $1/f^3$. Since the conventional sample variance fails to converge as the number of samples, N, grows for these particular types of noise, David Allan suggested to set N=2 and average many of these two-sample variances to get a convergent and stable measure of the spread of the quantity in question. This is what has come to be called the Allan variance or two sample variance[64].

Without dead time, Allan variance can be represented as $\sigma^2(2,\tau,\tau)$ and is alternatively referred to as short-hand notation $\sigma^2(2,\tau)$ or $\sigma^2(\tau)$.

$$\sigma^2(\tau) \equiv \frac{1}{2} < (\bar{y_{k+1}} - \bar{y_k})^2 >, \tag{6.13}$$

where <> denotes infinite time average, and $\bar{y_k}$ is the average over time interval of τ. In practice, $\sigma^2(\tau)$ can be well estimated from the N-times successive measurements as[3]

$$\sigma^2(\tau) \approx \frac{1}{2(N-1)} \sum_{i=1}^{N-1} (y_{i+1} - y_i)^2, \tag{6.14}$$

where y_i is the measurement over the ith time interval of τ.

6.2.2 Conversion from frequency domain to time domain

From Equation (6.13), we can rewrite the Allan variance to[4]:

$$\begin{aligned} \sigma_y^2(\tau) &= \frac{1}{2} \left\langle (\frac{1}{\tau} \left(\int_t^{t+\tau} y(t')dt' - \int_{t-\tau}^{t} y(t')dt' \right)^2 \right\rangle, \\ &= \left\langle \left(\int_{-\infty}^{\infty} y(t') h_\tau(t-t')dt' \right)^2 \right\rangle, \end{aligned} \tag{6.15}$$

by introducing the function $h_\tau(t)$ with[4]

$$h_\tau(t) = \left\{ \begin{array}{ccc} -\frac{1}{\sqrt{2\tau}} & for & -\tau < t < 0 \\ \frac{1}{\sqrt{2\tau}} & for & 0 < t < \tau \\ 0 & otherwise & \end{array} \right\} \tag{6.16}$$

The transfer function for the filter function $h_\tau(t)$ can be obtained from its Fourier transform:

$$|H(f)|^2 = 2\frac{\sin^4(\pi\tau f)}{(\pi\tau f)^2}, \tag{6.17}$$

Therefore,

$$\sigma_y^2(\tau) = 2\int_0^\infty S_y(f)\frac{\sin^4(\pi\tau f)}{(\pi\tau f)^2}df, \tag{6.18}$$

allows one to compute the Allan variance directly from (one-sided) PSD.

In noise analysis of practical oscillators, the PSD is often assumed to consist of a superposition of several power-series components resulting from independent noise processes[3]. With this assumption, one-side PSD of a laser can be approximated as[3]:

$$S_\nu(f) = \frac{k_r}{f^2} + \frac{k_f}{f} + k_w, \quad (one - side), \quad Hz^2/Hz, \tag{6.19}$$

where k_r,k_f and k_w are the coefficients used as the measurement of random-walk, flicker, and white fluctuations, respectively. The white fluctuation components expressed in Lorentzian linewidth $\Delta\nu$[Hz] is converted to k_w as

$$k_w = \frac{\Delta\nu}{\pi}, \tag{6.20}$$

Substituting Equation(6.19) into Equation(6.18) yields

$$\sigma_y^2(\tau) = k_w\frac{1}{2}\frac{1}{\tau} + k_f 2\ln 2 + k_r\frac{2\pi^2}{3}, \tag{6.21}$$

In Figure 6.12, we demonstrated two frequency fluctuation representations in frequency domain and in time domain respectively.

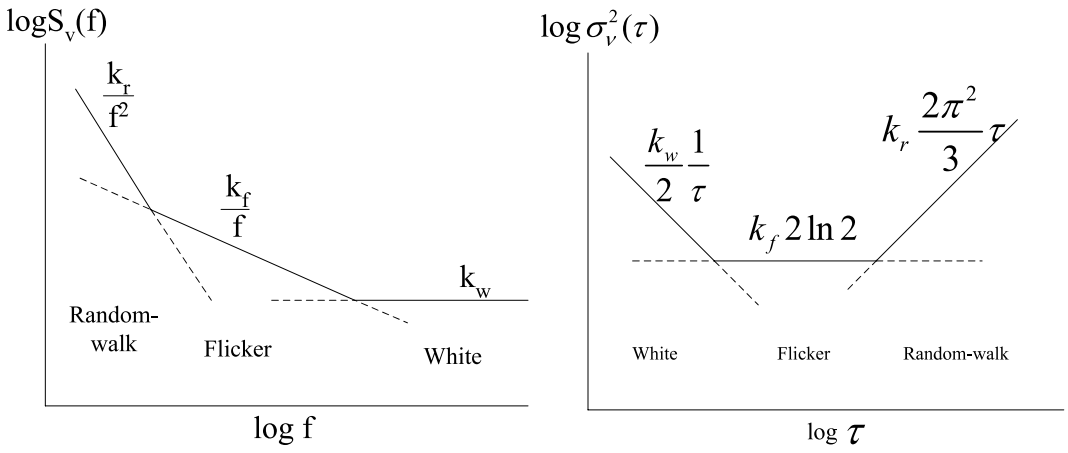

Figure 6.12: Two frequency noise representations: (a) PSD and (b) Allan Variance[3]

Note that, in the variance estimation using Equation (6.12), the uncertainty due to the finite number N depends slightly on the noise processes. The relative standard derivation on estimated $\sigma_y^2(\tau)$ is given by $KN^{1/2}$, where K is specified as 0.87, 0.77, and 0.75 for white, flicker and random walk fluctuations, respectively[3, 65, 66].

6.2.3 LC-RDSHI based time domain frequency fluctuation measurement

Multiple orders of beat-notes can be generated from the LC-RDSHI system without using the mixer circuit, as shown in Figure 6.13. The observed spectrum with 49 orders of beat-notes is thus shown in Figure 6.14

Normally, frequency noises can be easily measured by using a frequency counter. Without frequency counter available, we use oscilloscope instead. But there is dead time $T - \tau$ generated due to the data capture time (T) from the oscilloscope to computer, which is slower than the measurement time (τ). Therefore, a bias function introduced by Jame Barnes and David Allan[67] can be used in data processing.

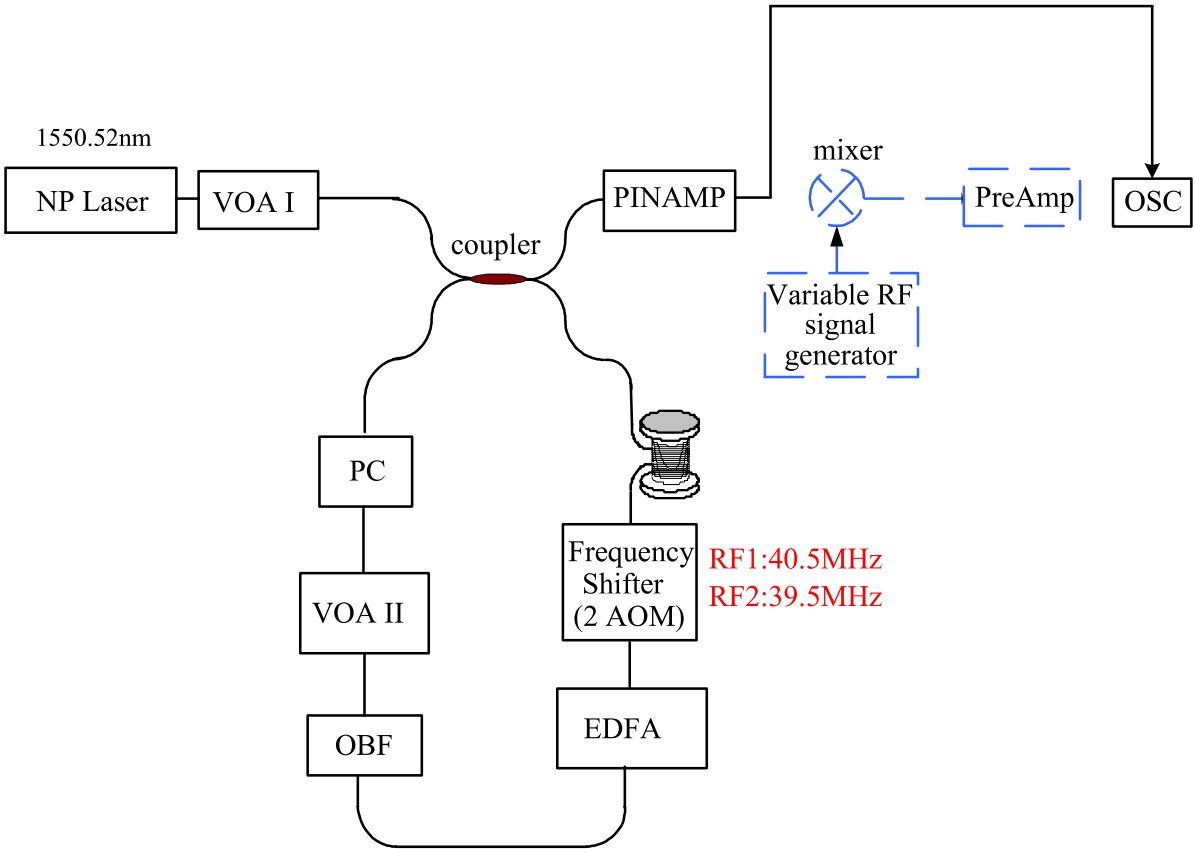

Figure 6.13: Schematic for frequency noise measurement by LC-RDSHI

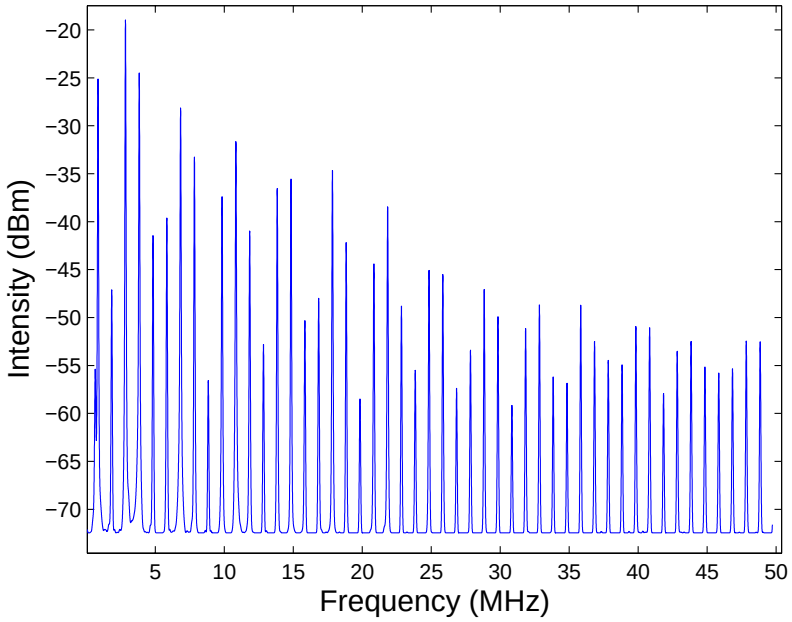

Figure 6.14: Spectrum with 49 orders of beat-note from LC-RDSHI

The bias function $B_2(r,\mu)$ is defined by[68]

$$B_2(r,\mu) = \frac{\sigma_y^2(2,T,\tau)}{\sigma_y^2(2,\tau,\tau)} = \frac{\sigma_y^2(2,T,\tau)}{\sigma_y^2(\tau)}, \tag{6.22}$$

where $r = \frac{T}{\tau}$, μ is a parameter in $\sigma_y^2(\tau) \sim \tau^\mu$ which responds to power law PSD $S_y(f) \sim f^\alpha$. In words, $B_2(r,\mu)$ is the ratio of the expected Allan variance with dead time to that without dead time. In frequency noise measurement system, $\tau = 125\mu s$ corresponds to the 25km fiber delay and $T = 40s$ for capturing the data to the computer. $B_2(r,-1) = r$ is used from [67].

Alternative methods of calculating Allan variance have been used in order to allow for the minimum measurement time necessary to retrieve the full information required[4]. If the frequency counter is used, the counter is set to the shortest gate time τ_0 where the Allan variance is to be determined and the frequency difference $\bar{y}_{i,\tau_0}$ is measured repeatedly, as shown in Figure 6.15. To derive the data from longer times, e.g., $\tau = 3\tau_0$ the consecutive values of $\bar{y}_{1,\tau} = (\bar{y}_{1,\tau_0} + \bar{y}_{2,\tau_0} + \bar{y}_{3,\tau_0})/3$,$\bar{y}_{2,\tau} = (\bar{y}_{2,\tau_0} + \bar{y}_{3,\tau_0} + \bar{y}_{4,\tau_0})/3$,... are determined in post

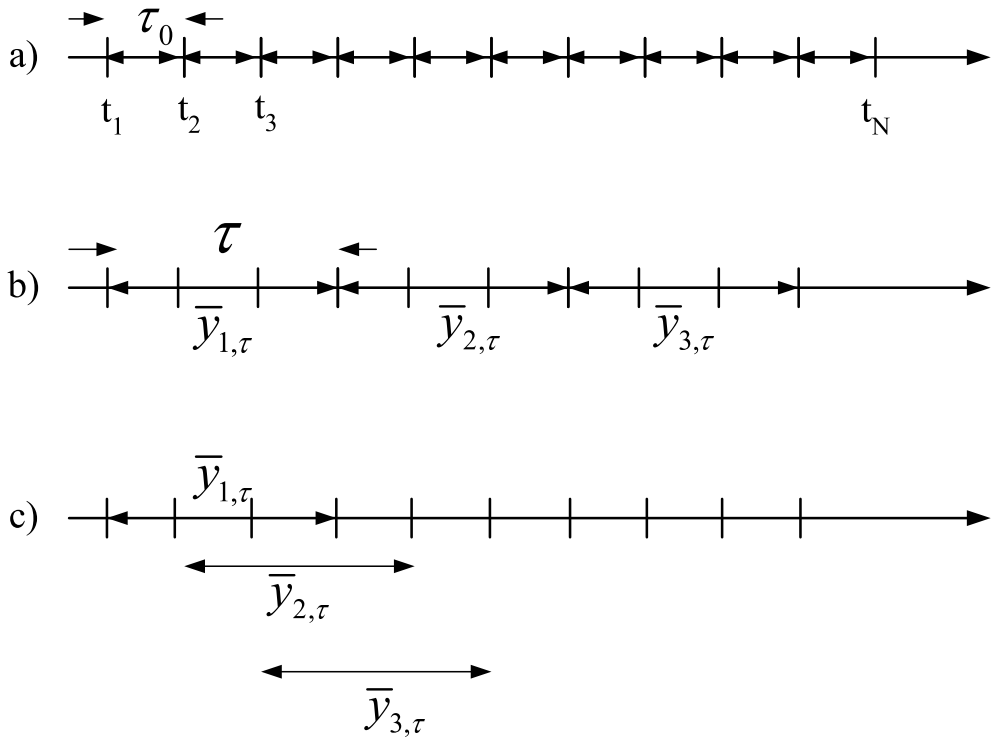

Figure 6.15: Alternative methods of calculating the Allan variance[4]

processing to estimate the Allan variance for the time $\tau = 3\tau_0$ and accordingly for all the other time τ.

In Figure 6.16, frequency noises of five orders of beat-notes are obtained. It is shown that the Lorentzian linewidth is around 700Hz for lower order beat-notes and becomes larger for higher orders of beat-notes. The Lorentzian linewidths derived from both the frequency domain and time domain methods agree with each other.

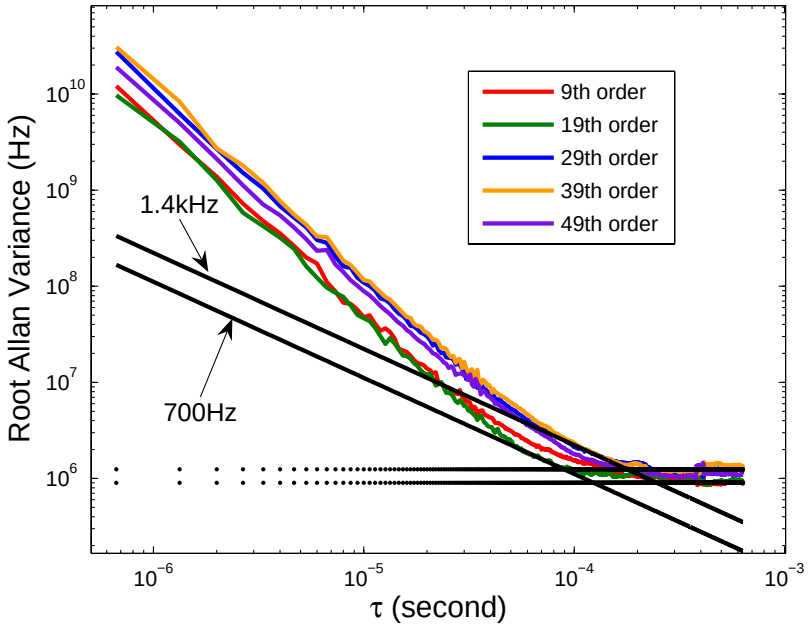

Figure 6.16: Linewidth derived from frequency noise measurement

Chapter 7

Conclusions and Future Work

As the laser spectral linewidth is getting narrower, accurately measuring the laser linewidth becomes increasingly difficult by conventional methods. The LC-RDSHI method is shown to be a good choice.

7.1 Conclusions

In this dissertation, the theoretical analysis of the LC-RDSHI has been presented. The issues of multiple recirculating effect, RIN, fiber birefringence and frequency jitter in the LC-RDSHI have been discussed. The multiple recirculating effect generates interference fringes on the spectrum of each order of beat-note. The calculation suggested that this interference effect can be eliminated by proper loop parameters in the LC-RDSHI. RIN raises the noise floor of the beat-note spectrum, but does not broaden the laser linewidth. Fiber birefringence effect causes the polarization fading without introducing additional phase noise. Frequency jitter could increase the linewidth value in the situation that the multiple beat-note spectrums must be captured at the different time and summed.

The detailed implementation of the LC-RDSHI on ultra-narrow laser linewidth measure-

ment has been described. The system was optimized to meet the requirement of accurately measuring the laser linewidth of sub-kilohertz. The multiple recirculating effect and the fiber birefringence effect raised from the theoretical analysis section were verified by the experiments. System parameters were carefully set in order to obtain the best signal. A mixer circuit was added to improve the measurement resolution. The environmental noises were minimized by adding an additional AOM and putting the whole system in a wood box with the isolation foam to isolate the thermal and acoustic perturbations.

In order to extract the Lorentzian linewidth from the Voigt profile, the Voigt curve fitting method has been used in the interpretation of the laser spectrum. In the past, most researches focused on the characterization of semiconductor lasers which have the Gaussian linewidth comparable with the Lorentzian linewidth in the presence of the $1/f$ frequency noise. The 20dB down linewidth measurement method was generally used to calculate the Lorentzian linewidth. But it was proved in this dissertation that the 20dB down direct measurement of Lorentzian linewidth over estimated the laser linewidth of ultra-narrow linewidth lasers which have a large Gaussian linewidth compared with the Lorentzian linewidth. The NP fiber laser we examined therefore has the Lorentzian linewidth of 680Hz, instead of 910Hz obtained from 20dB down direct measurement. Voigt curve fitting method also makes the Lorentzian linewidth independent from the Gaussian linewidth. In most situations, it can reduce the system sensitivity to the noises. It provides a better platform to examine the performance of any type of lasers.

It is proved in this dissertation that the LC-RDSHI is a self-calibrated system. Multiple orders of beat-notes spectrums were displayed to calibrate the linewidth measurement in the frequency domain. And Allan variance was used to calibrate the measurement in the time domain.

In order to identify the nonlinear Kerr effect in the LC-RDSHI, comprehensive experiments have been performed. The phase noise caused by the classical effect of the Kerr effect was proved to be the dominant effect in any recirculating loop. Both the Gaussian linewidth and

the Lorentzian linewidth are broadened as the number of the revolution of recirculations. The Kerr effect limits the capability of the LC-RDSHI. A two-switch LC-RDSHI structure has been proposed to eliminate the Kerr effect.

7.2 Future work

Future works are suggested to achieve the goal of conducting the accurate measurement of ultra-narrow laser linewidth.

7.2.1 Overcome the Kerr effect

As we analyzed in Section 6.1.3 that Kerr effect is serious in the LC-RDSHI system. The laser linewidth keep broadening as the light transmits along the fiber delay loop. The proposed two-switch LC-RDSHI method need experimental verification.

7.2.2 Verify the ASE noise effect through experiments

We have discussed the ASE noise effect in Chapter 4 and Chapter 6. In Chapter 4, we treat the ASE noise as an additive noise only and there is no linewidth broadening effect. And in Chapter 6, when the ASE noise induces the amplitude fluctuation, the nonlinear Kerr effect occurs. In the proposed two-switch LC-RDSHI, the Kerr effect caused by the fiber delay loop can be identified and avoided. Then we can further examine the ASE noise effect based on the two-switch LC-RDSHI. If there is still serious linewidth broadening, we conclude that the ASE noise is not only an additive white noise.

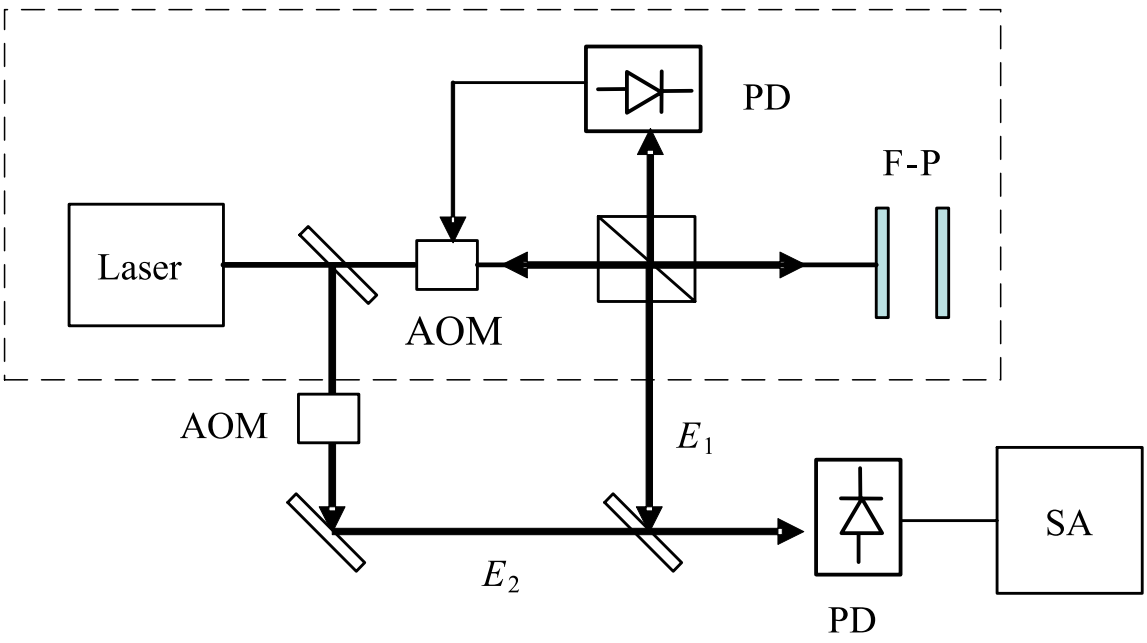

Figure 7.1: Schematic of heterodyne detection by using FP cavity

7.2.3 Calibrate LC-RDSHI measurement result by a heterodyne detection system

The LC-RDSHI measurement results should be calibrated by the heterodyne detection if a more stable and narrower linewidth laser can be available. The narrower linewidth can be obtained by stabilizing the laser frequency using the Pound-Drever-Hall technique as shown in Figure 7.1(dotted box). The stabilized linewidth is expected to be 10Hz to 100Hz.

Bibliography

[1] Shibin Jiang. Single frequency fiber lasers for defense, security and military applications. *NP Phontonics Inc.- White Paper*.

[2] Christine Spiegelberg, Jihong Geng, Yongdan Hu, Yushi Kaneda, Shibin Jiang, and N. Peyghambarian. Low-noise narrow-linewidth fiber laser at 1550nm. *Journal of Lightwave Technology*, 22(1):57–61, 2004.

[3] Osamu Ishida. Delayed-self-heterodyne measurement of laser frequency fluctuations. *IEEE Journal of Lightwave Technology*, 9(11), 1991.

[4] Fitz Riehle. *Frequency Standards Basics and Applications*. Wiley-VCH Verlag GmbH & Co. KGaA, Weinheim, Germany, 2004.

[5] Dennis Derickson. *Fiber optic test and measurement*. Upper Saddle River, N.J.: Prentice Hall PTR, 1998.

[6] Orazio Svelto. *Principles of Lasers*. Plenum Press,, New York and London, 4th ed. 1998.

[7] Amnon Yariv. *Optical Electronics in Modern Communications*. Oxford University Press,, New York, 4th ed. 1997.

[8] Philip Goldberg, Perter W. Milonni, and Bala Sundaram. Theory of the fundamental laser linewidth. *Physical Review A*, 44(3):1969–1985, 1991.

[9] Charles H. Henry. Theory of the linewidth of semiconductor lasers. *IEEE,Journal of quantum electronics*, 18(2):259–264, 1982.

[10] Philip Goldberg, Perter W. Milonni, and Bala Sundaram. Theory of the fundamental laser linewidth ii. *Physical Review A*, 44(7):4556–4563, 1991.

[11] Charles H. Henry. Phase noise in semiconductor lasers. *IEEE,Journal of lightwave technology*, 4(3):298–311, 1986.

[12] M.P. van Exter, W.A. Hamel, and J.P. Woerdman. Nonuniform phase diffusion in a laser. *Physical Review A*, 43(11):6241–6246, 1991.

[13] J. Arnaud. Classical theory of laser linewidth. *Optical and Quantum Electronics*, 28(11):1589–1615, 1996.

[14] J. Arnaud and M. Esteban. Circuit theory of laser diode modulation and noise. *IEE Proceedings-Optoelectronics*, 137(1):55–63, 1990.

[15] Rodney S. Tucker and David J. Pope. Microwave circuit models of semiconductor injection lasers. *IEEE TRANSACTIONS ON MICROWAVE THEORY AND TECHNIQUES*, 31(3):289–294, 1983.

[16] P T Greenland. Comparison between phase diffusion and random telegraph signal models of laser bandwidth. *Journal of Physics B,Atomic and molecular physics*, 17:1919–1925, 1984.

[17] Eric Alpman, Florent Munier, Thomas Eriksson, Arne Sevensson, and Herbert Airath. Estimation of phase noise for QPSK modulation over AWGN channels. *http://db.s2.chalmers.se/download/publications/munier_1371.pdf*.

[18] R. Paschotta, A. Schlatter, S.C. Zeller, H.R. Telle, and U. Keller. Optical phase noise and carrier-envelope offset noise of mode-locked lasers. *Applied Physics B: Lasers and Optics*, 82(2):265–273, 2006.

[19] Charles H. Henry. Theory of the phase noise and power spectrum of a single mode injection laser. *IEEE,Journal of quantum electronics*, 19(9):1391–1397, 1983.

[20] J. Arnaud. Detuned inhomogeneously broadened laser linewidth. *Quantum and Semiclassical Optics: Journal of the European Optical Society Part B*, 9(4):507–518, 1997.

[21] Michel J.F. Digonnet, editor. *Rare-Earth-Doped Fiber Lasers and Amplifiers*. Marcel Dekker,Inc., New York, second edition,revised and expanded edition, 2001.

[22] Rdiger Paschotta. *Encyclopedia of Laser Physics and Technology*. http://www.rp-photonics.com/encyclopedia.html, Switzerland, 2006.

[23] Elio Bava, Gianluca Galzerano, and Cesare Svelto. Frequency-noise sensitivity and amplitude-noise immunity of discriminators based on fringes-side fabry-perot cavities. *IEEE Transactions on Ultrasonics,Ferroelectrics, and Frequency Control*, 49(8):1150–1159, 2002.

[24] Ezra Ip, Joeseph M. Kahn, Doung Anthon, and Jeff Hutchins. Linewidth measurements of mems-based tunable lasers for phase-locking applications. *IEEE Photonics Technology Letters*, 17(10):2029–2031, 2005.

[25] L.D. Turner, K.P. Weber, C.J. Hawthorn, and R.E. Scholten. Frequency noise characterization of narrow linewidth diode lasers. *Optics Communications*, 201:391–397, 2002.

[26] L.B. Mercer. 1/f frequency noise effects on self-heterodyne linewidth measurements. *IEEE Journal of Lightwave Technology*, 9(4):485–493, 1991.

[27] Philippe B. Gallion and Guy Debarge. Quantum phase noise and field correlation in single frequency semiconductor laser systems. *IEEE Journal of Quantum Electronics*, QE20(4):343–349, 1984.

[28] Ming Han and Anbo Wang. Analysis of loss-compensated recirculating delayed self-heterodyne interferometer for laser linewidth measurement. *Applied Physics,B*, 81(23):53–58, 2005.

[29] Moshe Nazarathy, Wayne V. Sorin, Douglas M. Baney, and Steven A. Newton. Spectral analysis of optical mixing measurements. *IEEE Journal of Lightwave Technology*, 7(7):1083–1096, 1989.

[30] Hidemi Tsuchida. Simple technique for improving the resolution of the delayed self-heterodyne method. *Optics Letters*, 15(11):640–642, 1990.

[31] Jay W. Dawson, Namkyoo Park, and Kerry J. Vahala. An improved delay self-heterodyne interferometer for linewidth measurement. *IEEE Photonics Technology Letters*, 4(9):1063–1066, 1992.

[32] M. Groten and W. van Etten. Laser linewidth measurement in the presence of RIN and using the recirculating self-heterodyne method. *Eindhoven University of Technology Research Reports*, 92-E262, 1992.

[33] D. Wang and C.R. Menyuk. Calculation of penalties due to polarization effects in a long-haul wdm system using a strokes parameter model. *IEEE Journal of Lightwave Technology*, 19(4):487–493, 2001.

[34] M.G. Taylor. Observation of new polarization dependence effect in long haul optically amplified system. *IEEE Photonics Technology Letters*, 5(10):1244–1246, 1998.

[35] Vladimir I. Balakshy and Jamal A. Hassan. Polarization effects in acousto-optic interaction. *OPTICAL ENGINEERIN*, 32(4):746–751, 1993.

[36] Ivan P. Kaminow. Polarization in optical fibers. *IEEE Journal of Quantum Electronics*, QE-17(1):2556–2563, 1981.

[37] Scott Rashleigh. Origins and control of polarization effects in single-mode fibers. *IEEE Journal of Lightwave Technology*, LT-1(2):312–330, 1983.

[38] David W. Stone, Douglas R. Moore, and Richard G. Priest. Polarization fading in fiber interferometric sensors. *IEEE Transactions on Microwave Theory and Techniques*, MTT-30(10):1632–1635, 1982.

[39] Moshe Tur, Behzad Moslehi, and Joseph W. Goodman. Theory of laser phase noise in recirculting fiber-optic delay lines. *IEEE Journal of Lightwave Technology*, LT-3(1):20–31, 1985.

[40] Acoustic-optic modulator,instuction manual. 2005.

[41] M.P. van Exter, W.A. Hamel, J.P. Woedman, and B.R.P. Zeijlmans. Spectral signature of relaxation oscillations in semiconductor lasers. *IEEE Journal of Quantum Electronics*, 28(6):1470–1478, 1992.

[42] B.K. A. Ngoi and K. Venkatakrishnan. Techniques to eliminate error induced due to acousto-optic modulator vibration in heterodyne interferometry. *Optical Engineering*, 38(12):2050–2054, 1999.

[43] G.P. Agrawal. *Nonlinear Fiber Optics*. Academic Press, San Diega, 2001.

[44] P.R. Cowle, G.J. Morkel, R.I. Loming, and D. N. Payne. Spectral broadening due to fiber amplifier phase noise. *Electronics Letters*, 36(7):424–425, 1990.

[45] Shiro Ryu. Signal linewidth broadening due to nonlinear Kerr effect in long-haul coherent systems using cascaded optical amplifiers. *IEEE Journal of Lightwave Technology*, 10(10):1450–1457, 1992.

[46] K. Okamura and H. Iwatsuki. Spectral linewidth broadening in er-doped-fiber amplifiers measured with less than 1.4khz linewidth light source. *Electronics Letters*, 26(23):1964–1967, 1990.

[47] Dietrich Marcuse. Single-channel operation in very long nonlinear fibers with optical amplifiers at zero dispersion. *IEEE Journal of Lightwave Technology*, 9(3):356–361, 1991.

[48] S. Murakami and M. Saito. Evolution of field spectrum due to fiber-nonlinearity-induced phase noise in in-line optical amplifier systems. *IEEE Phontics Technology Letters*, 4(11):1269–1272, 1991.

[49] Lothar Möller. Novel aspects of spectral broadening due to fiber amplifier phase noise. *IEEE Journal of Quantum Electronics*, 34(9), 1998.

[50] Etienne Rochat and René Dändliker. New investigations on the effect of fiber amplifier phase noise. *IEEE Journal of Slected Topics in Quantum Electronics*, 7(1), 2001.

[51] Emmanuel Desurvire. *Erbium-doped fiber amplifiers : principles and applications*. Wiley, New York, 1994.

[52] P.C. Becker, N.A. Olsson, and J.R. Simpson. *Erbium-doped fiber amplifiers : fundamentals and technology*. Academic Press, San Diego, 1999.

[53] Claudio Vinegoni, Magnus Karlsson, Mats Petersson, and Henrik Sunnerud. The statistics of polarization-dependent loss in a recirculating loop. *IEEE Journal of Lightwave Technology*, 22(4):312–330, 2004.

[54] A. El Amari, N. Gisin, B. Perny, H. Zbinden, and C. Zimmer. Statistical prediction and experimental verification of concatenations of fiber optic components with polarization-dependent loss. *IEEE Journal of Lightwave Technology*, 16(4):332–339, 1998.

[55] A. Mecozzi and M. Shtaif. The statistics of polarization-dependent loss in optical communication systems. *IEEE Journal of phontonics Letters*, 14(4):313–315, 2002.

[56] A. Galtarossa and L. Palmieri. The exact statistics of polarization-dependent loss in fiber-optic links. *IEEE Journal of phontonics Letters*, 15(1):57–59, 2003.

[57] Gregory D. VanWiggeren and Rajarshi Roy. Transmission of linearly polarized light through a single-mode fiber with random fluctuations of birefringence. *Applied Optics*, 38(18):3888–3892, 1999.

[58] William J. Thompson. Numerous neat algorithms for the voigt profile function. *Computers in Physics*, 7(6), 1993.

[59] J.A. C. Weideman. Computation of the complex error function. *SIAM Journal on Numerical Analysis*, 31(5), 1994.

[60] Shiro Ryu. Signal linewidth broadening due to fiber nonlinearities in long-haul coherent optical fiber communication systems. *Electronics Letters*, 27(17):1527–1529, 1991.

[61] J.P. Gordon and L. F. Mollenauer. Phase noise in photonics communications systems using linear amplifiers. *Optics Letters*, 15(23):1351–1353, 1990.

[62] Tsuyoshi Satoh, Kouichi Yamazaki, and Naoyuki Ubayama. A quantum theoretical analysis of nonlinear phase noise. *IEEE Singapore ICCS/ISITA 92*, pages 244–248, 1992.

[63] Osamu Ishida. Laser frequency-fluctuation measurement employing an optical-fiber circulation loop. *IEEE Photonics Technology Letters*, 4(11):1304–1307, 1992.

[64] D.W. Allan. Statistics of atomic frequency standards. *IEEE Proceedings*, 54(3), 1966.

[65] P. Lesage and C. Audion. Characterization of frequency stability:uncertainty due to the finite number of measurements. *IEEE Transactions on Instrumentation and Measurement*, IM22(2):157–161, 1973.

[66] P. Lesage and C. Audion. Correction to: "characterization of frequency stability:uncertainty due to the finite number of measurements". *IEEE Transactions on Instrumentation and Measurement*, IM25(3), 1976.

[67] James A. Barnes and David W. Allan. Variances based on data with dead time between the measurement. *National Institute of Standards and Technology Technical Note*, 1318:1–48, 1990.

[68] James A. Barnes. Tables of bias function,b_1 and b_2, for variances based on finite samples of processes with power law spectral densities. *NBS Technical Note*, 375, 1969.